Novel Non-Covalent LSD1 Inhibitors Endowed with Anticancer Effects in Leukemia and Solid Tumor Cellular Models

Martina Menna,[a,1] Francesco Fiorentino,[a,1] Biagina Marrocco,[b] Alessia Lucidi,[a] Stefano Tomassi,[c] Domenica Cilli,[d] Mauro Romanenghi,[d] Matteo Cassandri,[e] Silvia Pomella,[e] Michele Pezzella,[e] Donatella Del Bufalo,[f] Mohammad Salik Zeya Ansari,[g,h] Nevena Tomašević,[i] Milan Mladenović,[i] Monica Viviano,[j] Gianluca Sbardella,[j] Rossella Rota,[e] Daniela Trisciuoglio,[f,h] Saverio Minucci,[d,k] Andrea Mattevi,[b] Dante Rotili,[a,**] and Antonello Mai[a,l,*]

[a]*Department of Drug Chemistry and Technologies, Sapienza University of Rome, P. le A. Moro 5, 00185 Rome, Italy.*

[b]*Department of Biology and Biotechnology, University of Pavia, Via Ferrata 9, 27100 Pavia, Italy*

[c]*Department of Pharmacy, University of Naples "Federico II", via Domenico Montesano 49, 80131 Naples, Italy*

[d]*Department of Experimental Oncology, IEO, European Institute of Oncology IRCCS, via Adamello 16, 20139 Milan, Italy*

[e]*Department of Oncohematology, Bambino Gesù Children's Hospital, IRCCS, viale di San Paolo 15, 00146, Rome, Italy*

[f]*Preclinical Models and New Therapeutic Agents Unit, IRCCS-Regina Elena National Cancer Institute, Via Elio Chianesi 53, 00144 Rome, Italy*

[g]*Department of Biology and Biotechnology "Charles Darwin", Sapienza University of Rome, P. le A. Moro 5, 00185 Rome, Italy*

[h]*Institute of Molecular Biology and Pathology, National Research Council (CNR), Via degli Apuli 4, 00185 Rome, Italy*

[i]*Kragujevac Center for Computational Biochemistry, Department of Chemistry, Faculty of Science, University of Kragujevac, Radoja Domanovića 12, 34000, Kragujevac, P.O. Box 60, Serbia*

[j]*Department of Pharmacy, University of Salerno, via Giovanni Paolo II, 132, 84084, Fisciano (SA), Italy*

[k]*Department of Biosciences, University of Milan, Via Festa del Perdono 7, 20122 Milano, Italy*

[l]*Pasteur Institute, Cenci-Bolognetti Foundation, Sapienza University of Rome, P. le A. Moro 5, 00185 Rome, Italy.*

1

* Corresponding author.

** Corresponding author.

E-mail addresses: antonello.mai@uniroma1.it (A. Mai), dante.rotili@uniroma1.it (D. Rotili).

[1]These authors contributed equally to this work.

ABSTRACT

LSD1 is a histone lysine demethylase proposed as therapeutic target in cancer. Chemical modifications applied at C2, C4 and/or C7 positions of the quinazoline core of the previously reported dual LSD1/G9a inhibitor **1** led to a series of non-covalent, highly active, and selective LSD1 inhibitors (**2**-**4** and **6**-**30**) and to the dual LSD1/G9a inhibitor **5** that was more potent than **1** against LSD1. In THP-1 and MV4-11 leukemic cells, the most potent compounds (**7**, **8**, and **29**) showed antiproliferative effects at sub-micromolar level without significant toxicity at 1 µM in non-cancer AHH-1 cells. In MV4-11 cells, the new derivatives increased the levels of the LSD1 histone mark H3K4me2 and induced the re-expression of the *CD86* gene silenced by LSD1, thereby confirming the inhibition of LSD1 at cellular level. In breast MDA-MB-231 as well as in rhabdomyosarcoma RD and RH30 cells, taken as examples of solid tumors, the same compounds displayed cell growth arrest in the same IC_{50} range, highlighting a crucial anticancer role for LSD1 inhibition and suggesting no added value for the simultaneous G9a inhibition in these tumor cell lines.

1. INTRODUCTION

The methylation status of lysine residues in both histone and non-histone proteins is regulated by the opposite activities of two families of enzymes, the lysine methyltransferases (KMTs) and the lysine demethylases (KDMs), which catalyze the addition or the removal of methyl marks at lysine residues, respectively [1, 2]. Among KDMs, lysine specific demethylase 1 (LSD1) is a FAD-dependent enzyme that removes one or two methyl groups from the lysine 4 of histone H3 (H3K4me1/2) and, in particular conditions, from H3K9me1/2, acting as either a gene silencer or activator, respectively [3]. To exert its catalytic action, LSD1 is involved in corepressor complexes containing CoREST, HDAC1/2, nuclear receptors, and other transcription factors [4]. Through these complexes, LSD1 epigenetically regulates many cellular events important in mammalian biology such as embryonic development, hematopoiesis, and neuronal development [5]. Pathologically, LSD1 is implicated in tumorigenesis and metastasis, with high levels of its expression that are associated with poor prognosis in cancer patients. Indeed, LSD1 has been found overexpressed or dysregulated in various cancer types, including acute myeloid leukemia (AML) [6], breast [7], prostate [8], small cell lung cancer [9], neuroblastoma [10], glioma [11], medulloblastoma [12] and sarcomas [13]. Moreover, since pharmacological inhibition or genetic deletion of LSD1 impairs proliferation and metastasis of diverse tumor cells [14], LSD1 has been proposed as an attractive anticancer drug target, and numerous LSD1 inhibitors, acting through either a covalent or non-covalent mechanism of action, have been developed over the last ten years [15-17]. Tranylcypromine (TCP, Figure 1) has been largely used as a template to design new irreversible LSD1 inhibitors [18-25]. due to its ability to bind the FAD cofactor. Currently, beyond the association of TCP with all-*trans*-retinoic acid [15], four TCP-based LSD1 inhibitors have reached the clinical arena alone or in combination with other drugs for the treatment of cancer; these include iadademstat (ORY-1001) [26], bomedemstat (IMG-7289) [27], INCB059872 [28], and GSK-2879552 [29] (Figure 1). Several reversible, non-covalent LSD1 inhibitors carrying different chemotypes have also been described in literature [16]. Nevertheless, only two of them, seclidemstat (SP-2577) [30] and CC-90011 [31], are

currently in clinical trials as potential anticancer agents for the treatment of both solid and hematological malignancies (Figure 1), although seclidemstat has been very recently devalidated [32]
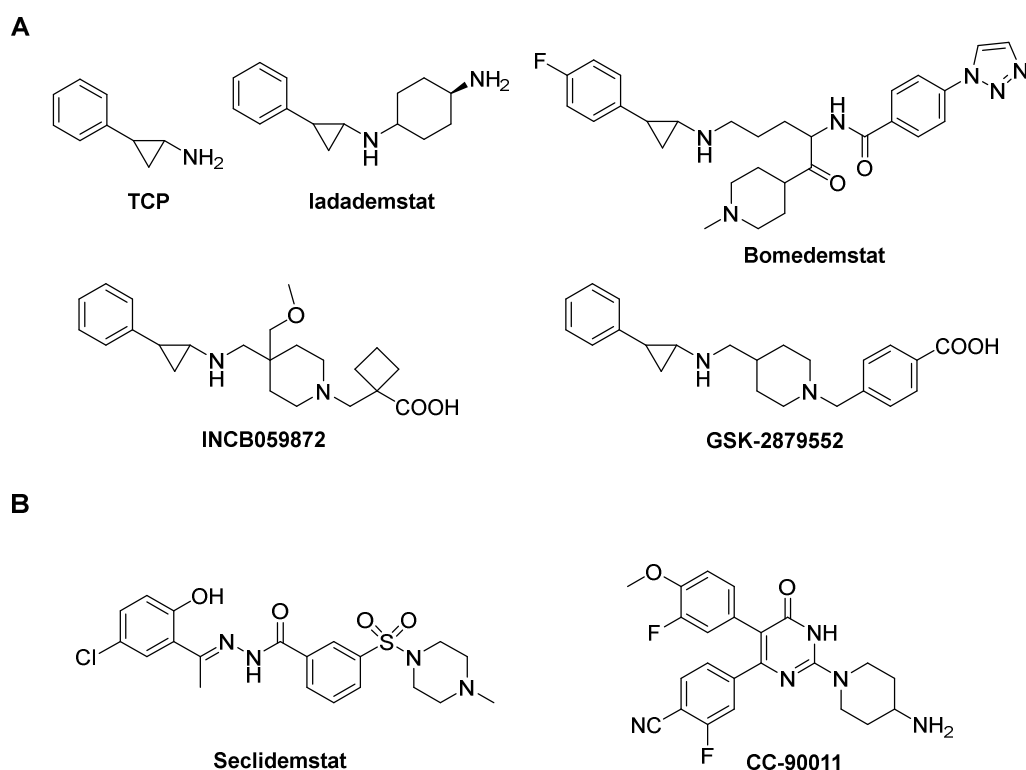

Figure 1. Covalent (**A**) and non-covalent (**B**) LSD1 inhibitors in clinical trials for cancer treatment.

TCP-based LSD1 inhibitors often show side effects that have been ascribed to their irreversible binding to FAD and to significant affinity with several other targets, including neurotransmitters metabolizing enzymes, receptors, and transporters [15, 33-35]. In addition, beyond producing long-lasting on-target effects, the covalent LSD1 inhibitors can in principle also induce prolonged off-target effects [15]. Thus, in order to study whether the safety/efficacy profile of LSD1 inhibitors can be improved the search of novel, reversible inhibitors is presently highly pursued.

Recently, we showed that E11 (MC3774, **1**) (Figure 2), previously reported as inhibitor of the histone methyltransferases G9a and G9a-like protein (GLP) [36], is also able to inhibit LSD1 in a quite unique manner. Indeed, the stacking of five copies of the molecule **1** at the entrance of the LSD1 active site leads to an efficient enzyme inhibition [37].

4

To increase its potency against LSD1, we applied chemical manipulations at the quinazoline C4, C2 or C7 position of the **1** structure and then tested the resulting analogues **2**-**30** (Figure 2) against LSD1. In parallel, we evaluated their activity against G9a, and the selectivity over a panel of histone methyltransferases (DOT1L, SETD8, EZH2 complex, and PRMT1) and MAO-A/B for two selected compounds was also determined. The crystal structure of one of the new most potent LSD1 inhibitors (**7**) in complex with LSD1-CoREST was determined and confirmed the peculiar binding mode of such compounds to this enzyme. Then, compounds **1**-**30** were tested on two AML cell lines (THP-1 and MV4-11) to assess their antiproliferative activity in a context where the anticancer target potential of LSD1 is well-known [6, 15-17]. The LSD1 inhibition in MV4-11 cells was proved through WB analysis of the H3K4me2 levels as well as the detection of increased expression levels of CD86, a monocyte/macrophage lineage differentiation marker silenced by LSD1 [38]. Finally, due to the mounting evidence suggesting the involvement of LSD1 in triple negative breast cancer (TNBC) [7] as well as in rhabdomyosarcoma (RMS) [13], selected compounds were also assayed in MDA-MB-231 cells and in two RMS cell lines (RH30 and RD).
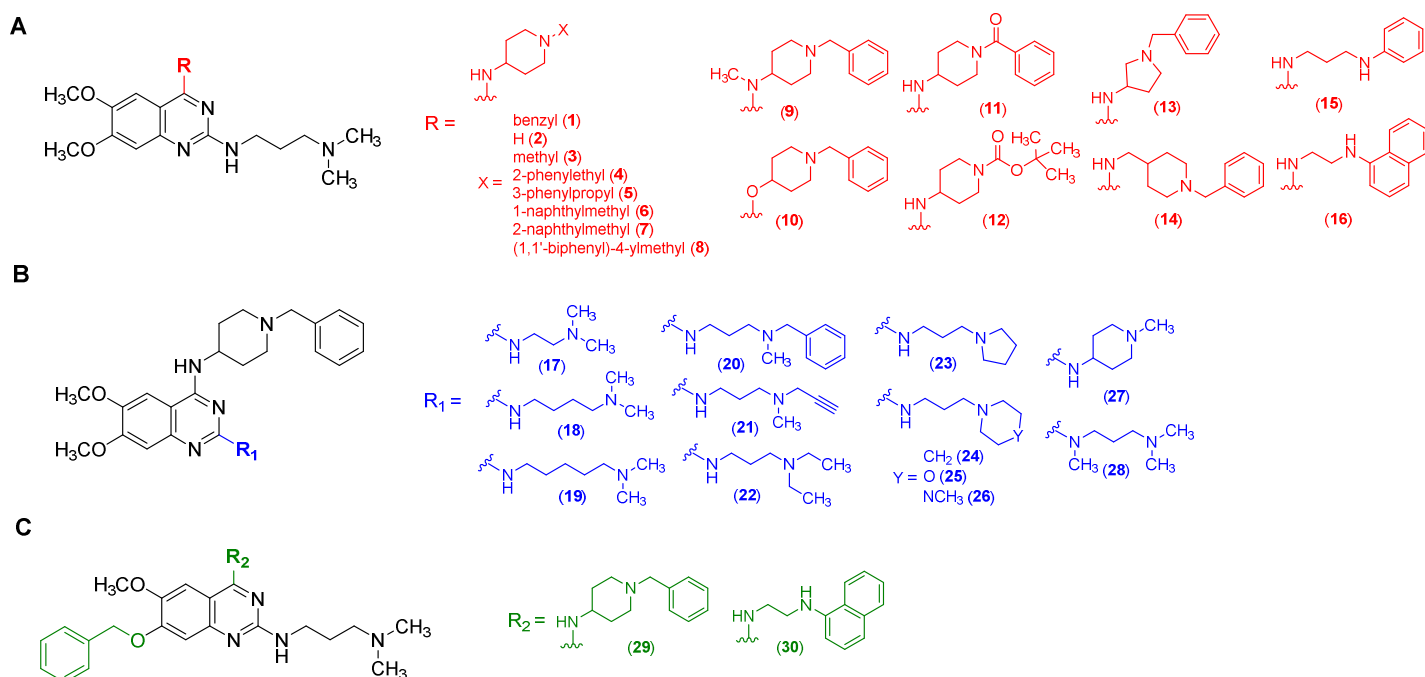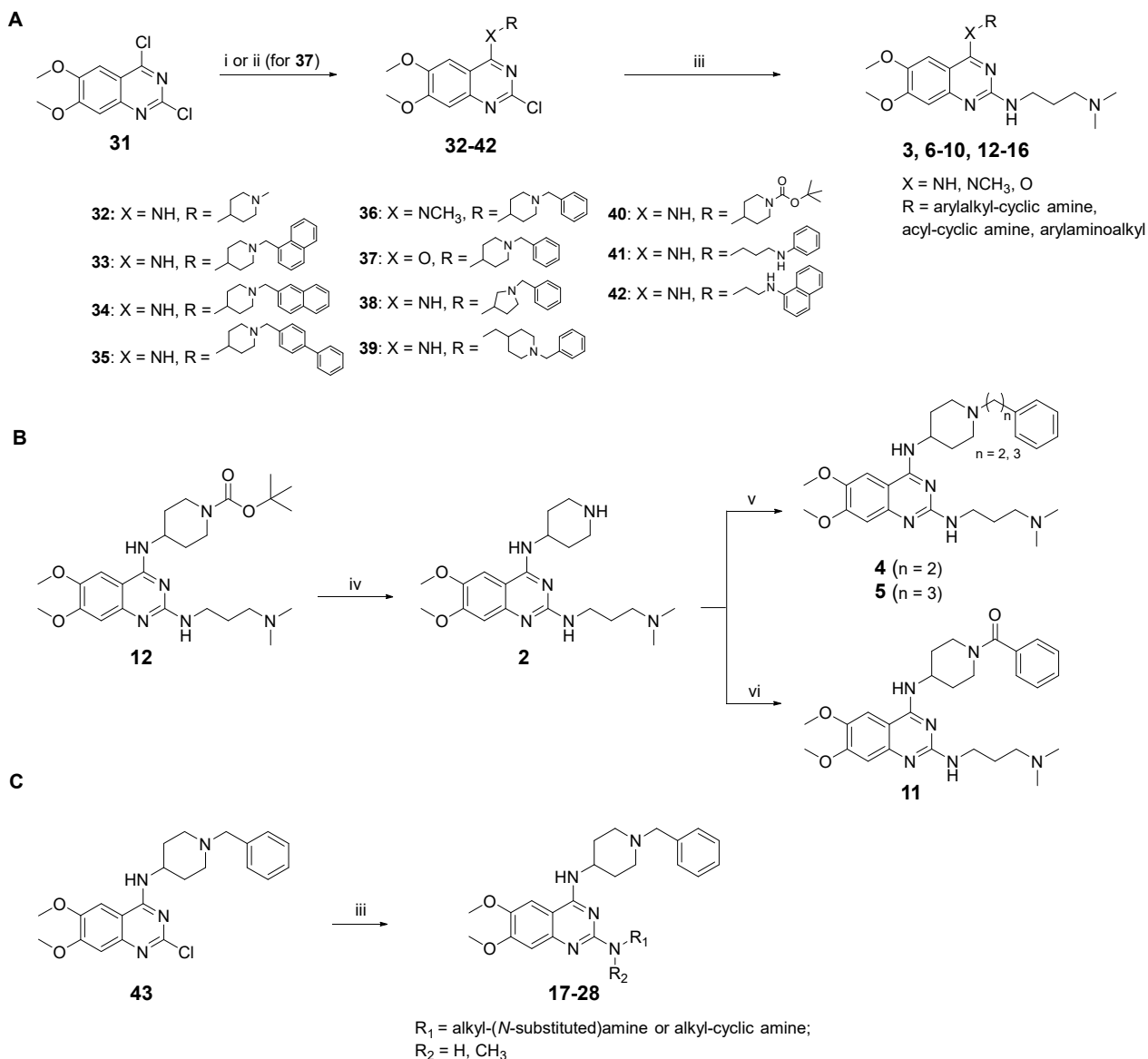

Figure 2. Quinazoline-based compounds (**2**-**30**) obtained by chemical changes applied on the structure of the dual LSD1/G9a inhibitor **1**.

2. RESULTS AND DISCUSSION

2.1. Chemistry. The synthetic routes followed for the preparation of the final derivatives **2-30** are depicted in Scheme 1. The 2,4-dichloroquinazoline **31** [39] was treated with the proper commercially available diamine in the presence of triethylamine in dry THF at room temperature (for **32**-**36**, **38**-**42**) or with 1-benzylpiperidin-4-ol in the presence of potassium *tert*-butoxide in DMSO at room temperature (for **37**) to undergo a regioselective C4 nucleophilic displacement furnishing the intermediates **32-42** (for **32** [40], **36** [41], **37** [41], **38** [42], and **40** [39] see the related references). Then, such compounds were converted into the final derivatives **3**, **6**-**10**, **13**-**16** via the C2 displacement at the quinazoline ring with the commercially available N^1,N^1-dimethylpropane-1,3-diamine under microwave irradiation at 130 °C in 2-propanol (Scheme 1A). The final compound **2** was prepared by removal of the *tert*-butoxycarbonyl protection at the piperidine moiety of **12** through acidic treatment (4 N hydrochloric acid in 1,4-dioxane) in the mixture dry THF/dry methanol. The final compounds **4** and **5** were obtained by treatment of **2** with the proper phenyl-alkyl bromide in the presence of anhydrous potassium carbonate and sodium iodide in dry DMF at room temperature, while **11** was prepared by acylation of **2** with benzoyl chloride in the presence of triethylamine in dry DCM at room temperature (Scheme 1B).

The 2-chloroquinazoline **43** [37] was subjected to C2 displacement by the appropriate commercial diamines in 2-propanol under microwave irradiation at 130 °C, leading to the final compounds **17-28** (Scheme 1C).

A

31   i or ii (for **37**) → **32-42**   iii → **3, 6-10, 12-16**

X = NH, NCH₃, O
R = arylalkyl-cyclic amine,
acyl-cyclic amine, arylaminoalkyl

32: X = NH, R =
33: X = NH, R =
34: X = NH, R =
35: X = NH, R =

36: X = NCH₃, R =
37: X = O, R =
38: X = NH, R =
39: X = NH, R =

40: X = NH, R =
41: X = NH, R =
42: X = NH, R =

B

12   iv → **2**   v → **4** (n = 2) / **5** (n = 3)   n = 2, 3

vi → **11**

C

43   iii → **17-28**

R₁ = alkyl-(*N*-substituted)amine or alkyl-cyclic amine;
R₂ = H, CH₃

Scheme 1. Synthesis of Compounds 2-28. Reagents and conditions: i) appropriate amino- or aminomethyl-(*N*-arylalkyl)cyclic amine or acyl-cyclic amine or (arylamino)alkylamine, triethylamine, dry THF, r.t.; ii) 1-benzylpiperidin-4-ol, potassium *tert*-butoxide, DMSO, r.t.; iii) appropriate (substituted or cyclic)aminoalkylamine, 2-propanol, microwave 130 °C; iv) 4 N hydrochloric acid in 1,4-dioxane, dry THF/dry methanol 1:1, 0 °C to r.t.; v) appropriate phenylalkyl bromide, anhydrous potassium carbonate, sodium iodide, dry DMF, r.t.; vi) benzoyl chloride, triethylamine, dry DCM, 0 °C to r.t.
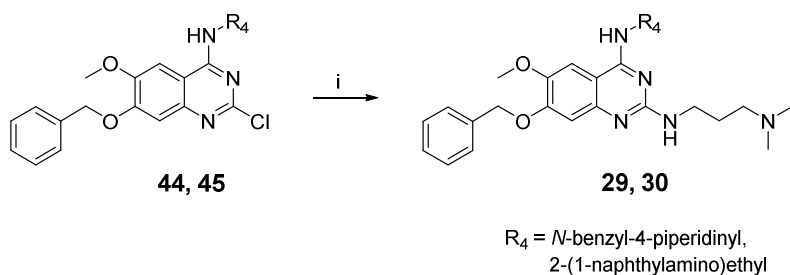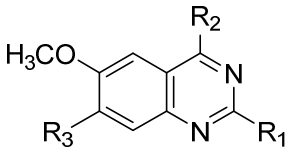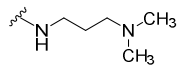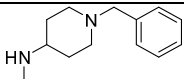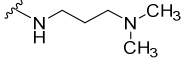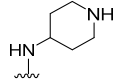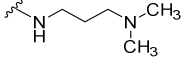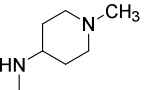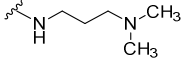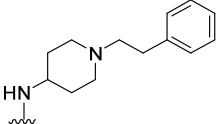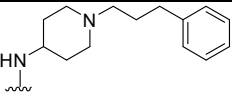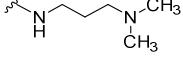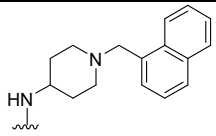
Scheme 2. Synthesis of Compounds 29 and 30. Reagents and conditions: i) N^1,N^1-dimethylpropane-1,3-diamine, 2-propanol, microwave 130 °C.
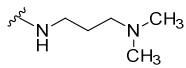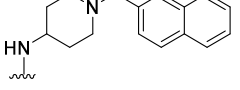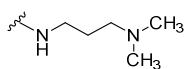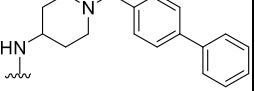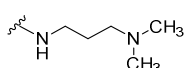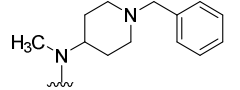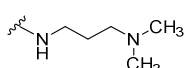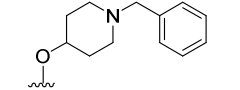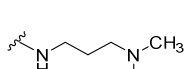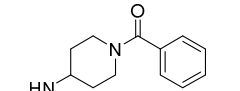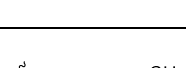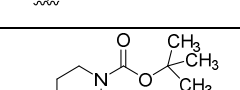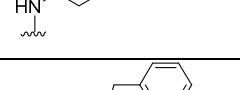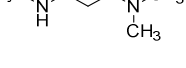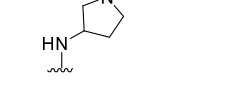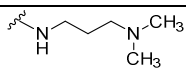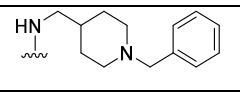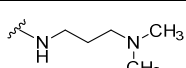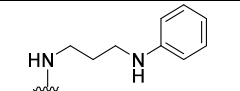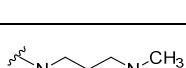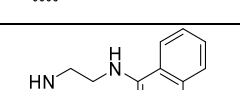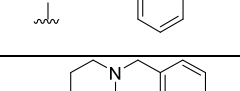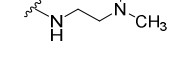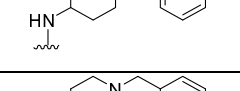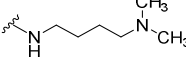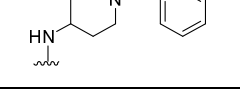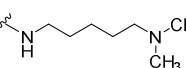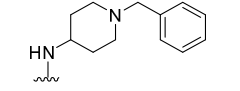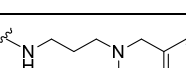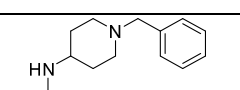
The synthesis of the compounds **29** and **30** was accomplished starting from the known C4-substituted quinazoline intermediates **44** [39] and **45** [39] by C2 nucleophilic displacement with N^1,N^1-dimethylpropane-1,3-diamine under microwave irradiation at 130 °C in 2-propanol as discussed above (Scheme 2).

The elemental analyses for the final compounds **2-30** are reported in Table S1 in Supplementary Material. ^{1}H-NMR, ^{13}C-NMR and HR-MS spectra of final compounds **2-30** are also reported in Supplementary Material.

2.2. LSD1 and G9a Inhibition Assays. The new compounds **2-30** were tested to detect their LSD1 inhibitory activity and selectivity. First, the effects of **2-30** on the thermal stability of the LSD1-CoREST complex were determined using the ThermoFAD assay [43]. The largest shifts in the T_m of the enzyme usually indicate the strongest binding capabilities (Table S2 in Suppleme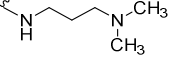ntary Material), but this correlation has always to be confirmed. Therefore, these preliminary data were verified by fluorescence polarization, demonstrating that the compounds with high thermal shift values were also able to tightly bind the LSD1-CoREST complex, with K_D values in the sub-micromolar range (Table 1).

Finally, HRP-coupled direct LSD1 inhibition detection was performed on the most effective binders and a few other selected derivatives (K_i values, Table 1). The K_D and K_i values of the prototype **1** and the reversible LSD1 inhibitor GSK-690 (**46**) [44], used as reference drug, were determined for comparison purposes (Table 1). Since **1** is a dual LSD1/G9a inhibitor, the inhibitory effects of **2**-**30** against G9a were also assessed (K_i values, Table 1). The assay was performed with 2-fold serial dilution starting from 80 μM concentration, using histone H3 (1-21) as the substrate and SAM (*S*-adenosyl-*L*-methionine) as the co-substrate. The compound UNC0638 [45] (**47**) was also tested as positive control for G9a inhibition.

Table 1. Inhibiting Activity of Compounds **2**-**30** against the KDM LSD1 and the KMT G9a.

| Compd | R₁ | R₂ | R₃ | LSD1 | | G9a |
				K_D, μM	K_i, μM	K_i, μM
1			OCH₃	0.243 ± 0.05	0.440 ± 0.05	0.68 ± 0.02
2			OCH₃	1.562 ± 0.14	NT[a]	4.83 ± 1.1
3			OCH₃	1.490 ± 0.16	NT	4.17 ± 0.7
4			OCH₃	0.147 ± 0.02	NT	3.13 ± 0.8
5			OCH₃	0.083 ± 0.01	0.149 ± 0.02	0.69 ± 0.1
6			OCH₃	0.084 ± 0.01	0.212 ± 0.02	3.10 ± 1.1

9

#						
7			OCH$_3$	0.075 ± 0.01	0.156 ± 0.02	2.93 ± 0.6
8			OCH$_3$	0.081 ± 0.01	0.146 ± 0.03	1.18 ± 0.4
9			OCH$_3$	0.356 ± 0.03	0.569 ± 0.08	>100
10			OCH$_3$	2.849 ± 0.32	NT	>100
11			OCH$_3$	0.975 ± 0.09	NT	32.9 ± 5.7
12			OCH$_3$	0.082 ± 0.01	0.205 ± 0.01	46.9 ± 8.9
13			OCH$_3$	0.251 ± 0.03	NT	8.03 ± 1.3
14			OCH$_3$	0.115 ± 0.02	NT	22.8 ± 2.2
15			OCH$_3$	0.228 ± 0.02	NT	48.3 ± 7.6
16			OCH$_3$	0.230 ± 0.03	NT	41.5 ± 6.5
17			OCH$_3$	0.237 ± 0.03	NT	5.26 ± 1.8
18			OCH$_3$	0.112 ± 0.01	NT	4.24 ± 1.2
19			OCH$_3$	0.127 ± 0.01	NT	2.79 ± 0.8
20			OCH$_3$	0.162 ± 0.02	NT	9.01 ± 1.6
21			OCH$_3$	0.064 ± 0.01	0.153 ± 0.02	26.1 ± 5.6
22			OCH$_3$	0.086 ± 0.01	0.175 ± 0.03	3.94 ± 1.4

23			OCH$_3$	0.082 ± 0.01	0.183 ± 0.02	4.01 ± 1.3
24			OCH$_3$	0.068 ± 0.01	0.170 ± 0.03	3.26 ± 0.7
25			OCH$_3$	0.369 ± 0.07	NT	22.6 ± 5.8
26			OCH$_3$	0.191 ± 0.03	NT	13.3 ± 4.2
27			OCH$_3$	0.082 ± 0.01	NT	6.33 ± 2.2
28			OCH$_3$	1.298 ± 0.14	NT	5.82 ± 2.1
29			OBn	0.067 ± 0.01	0.108 ± 0.01	39.4 ± 8.3
30			OBn	0.127 ± 0.02	NT	20.2 ± 5.4
46 (GSK-690)				0.014 ± 0.01	0.035 ± 0.002	NT
47 (UNC0638)				NT	NT	0.018 ± 0.005
^{a}NT, not tested.						

2.3. Structure-Activity Relationship of the New Anti-LSD1 Agents. Starting from the structure of the **1** prototype, a medicinal chemistry optimization study has been undertaken to increase the potency and selectivity of the quinazoline analogues against LSD1. Changes have been applied at the C4, C2, and/or C7 positions of the quinazoline ring (Figure 2). We explored the chemical space around C4 position by replacing the *N*-benzyl group of **1** with hydrogen (**2**), methyl (**3**), the longer 2-phenethyl (**4**) and 3-phenylpropyl (**5**) groups, and the bulkier 1- (**6**), 2- (**7**) naphthylmethyl, and (1,1'-biphenyl)-4-

ylmethyl (**8**) moieties. While **2** and **3** displayed a severe drop of binding affinity, **4** and mainly **5-8** exhibited a 2- or 3-fold increased binding potency, respectively. In addition, compounds **5-8** displayed 2- to 3-fold higher inhibition (compare K_i values). In compounds **9** and **10**, the C4-NH was changed into *N*-methyl (**9**) or oxygen (**10**) leading to less potent compounds; in particular, **10** was almost 12-times less effective than **1**. In compounds **11** and **12** the *N*-benzyl substituent on the piperidine at C4 was replaced with acyl functions such as benzoyl (**11**) or *tert*-butoxycarbonyl (**12**) group, with the first one showing a 4-fold decrease of binding affinity, while the latter gaining a 3-fold higher LSD1 affinity and 2-fold increased inhibitory potency. Ring contraction from piperidine to pyrrolidine led to **13**, endowed with the same binding affinity as **1**, while the replacement of the piperidine with the more flexible piperidin-4-ylmethyl group afforded **14**, that was slightly more effective than **1** in LSD1 binding. Compounds **15** and **16** in which the 4-aminopiperidine moiety of the parent compound **1** was simplified by the substitution with ω-arylaminoalkylamino groups showed no changes in LSD1 binding compared to **1** (Figure 2A) (Table 1). The *N,N*-dimethylaminopropylamino moiety at the C2 position of **1** was shortened to 2 (**17**) or lengthened to 4 (**18**) or 5 methylene units (**19**), with a little increase of binding affinity. In parallel, one of the two methyl groups of the side chain was replaced by the bulkier benzyl (**20**) or the unsaturated propynyl (**21**) group, or both the methyl groups were changed to two ethyl ones (**22**) or included into cyclic amines such as pyrrolidine (**23**), piperidine (**24**), morpholine (**25**), or *N*-methylpiperazine (**26**). While the *N*-benzyl-*N*-methyl terminal (compound **20**) afforded only a limited improvement of binding, the introduction of the *N*-methyl-*N*-propynyl group (**21**) as well as of two ethyl groups (**22**) or of some cyclic amines at the end of the C2 side chain (**23**, **24**) furnished an almost 3- to 4-fold increase of LSD1 affinity (compare K_D values), along with almost 3-fold increase in inhibitory potency (compare K_i values). In contrast, the morpholine (**25**) and *N*-methylpiperazine (**26**) analogues showed decreased or only slightly improved LSD1 binding, respectively. An improvement in terms of LSD1 binding compared to **1** was also obtained with **27**, a constrained analogue in which the *N,N*-dimethylaminopropylamine side chain at C2 was replaced with the 1-methylpiperidin-4-ylamine.

In contrast, the methylation of the NH function at the C2 side chain was detrimental for LSD1 interaction (compare **28** with **1**, Table 1).

Finally, the replacement of the methoxy group at the C7 quinazoline ring position with a benzyloxy moiety (**29** and **30**; Figure 2C) improved up to 4-fold LSD1 binding as well as inhibitory potency (compare, in particular, **29** with **1**, Table 1).

Overall, many of the new described quinazolines displayed 3- to 4-fold improved inhibition of LSD1 compared to **1**, with K_D values ranging from 64 to 86 nM and K_i values from 108 to 212 nM (see **5-8**, **12**, **21-24**, **27**, **29**).

Very interesting were the results regarding G9a inhibition. Indeed, all newly prepared compounds displayed a G9a inhibitory potency 1.7- to >147-fold lower than **1**, with the only exception of **5**, which showed almost the same activity. Therefore, in contrast to **1**, some of the new most potent LSD1 inhibitors such as **12**, **21** and **29** (LSD1 K_i values = 108-205 nM) can be regarded also as selective over G9a (K_i values = 26-47 μM). Differently, **5** confirmed the dual LSD1/G9a inhibition of **1** with an increased potency against LSD1.

2.4. Effects of Selected Quinazolines 5 and 29 Against a Panel of Histone Methyltransferases, MAO-A and MAO-B. Compounds **5** and **29** were also tested against a panel of histone lysine and arginine methyltransferases (HMTs) to assess their selectivity towards LSD1 or LSD1/G9a (for **5**) (Table 2). The substrates used for the assays were the nucleosomes for DOT1L and SETD8, the core histones for the EZH2 complex, and the histone H4 for PRMT1. For each HMT were determined the percentage of inhibition by **5** and **29** at 100 μM in duplicate and the IC_{50} values in 10-dose mode with 3-fold serial dilution starting at 100 μM. SAH (*S*-(5'-adenosyl)-L-homocysteine) and ryuvidine [46] were tested as positive controls for the inhibition of DOT1L/EZH2 complex/PRMT1 and SETD8, respectively. In the assays, both compounds displayed very low inhibition against the tested HMTs, with IC_{50} values always >100 μM under the experimental conditions (Table 2). In addition, **5** and **29**

13

were tested against the FAD-dependent enzymes MAO-A and -B at 100 μM in duplicate and the IC_{50} values in 10-fold serial dilution at 100 μM, using *p*-tyramine as the substrate. Clorgyline and pargyline were tested as reference drugs for MAO-A and -B, respectively. In these assays, both compounds exerted negligible inhibition of MAOs, with IC_{50} values always >100 μM under the experimental conditions.

Table 2. Inhibitory Activity of **5** and **29** Against DOT1L, SETD8, EZH2 Complex, PRMT1, MAO-A and MAO-B.

Compd	% Inhibition @ 100 μM/*IC₅₀, μM*					
	DOT1L	**SETD8**	**EZH2 complex**	**PRMT1**	**MAO-A**	**MAO-B**
5	30.3%/*>100*	13.9%/*>100*	2.9%/*>100*	0%/*>100*	7.4%/*>100*	0.3%/*>100*
29	22.6%/*>100*	0%/*>100*	1.8%/*>100*	0%/*>100*	0.8%/*>100*	0.5%/*>100*
SAH	100%/*0.14*	ND[a]	84.2%/*23.7*	100%/*0.25*	ND	ND
Ryuvidine	ND	91.6%/*0.37*	ND	ND	ND	ND
Clorgyline	ND	ND	ND	ND	*0.043*	ND
Pargyline	ND	ND	ND	ND	ND	*0.048*
[a]ND, not detected.						

2.5. Structural Studies. Compound **7**, 3-fold more potent than **1** against LSD1, was crystallized in complex with LSD1-CoREST. The X-ray structure, solved at 2.6 Å resolution (PDB: 6TUY; Table S2), displays an unusual mode of inhibition of **7** with three copies of the inhibitor bound to LSD1 (Figure 3), similarly to what previously observed for **1** [37]. The extensive stacking of the three quinazoline rings is at the heart of this binding mode. These interactions are further extended by the 2-naphthylmethyl and 3-(*N*,*N*-dimethylamino)propylamino moieties of the inhibitor molecules bound in the innermost segment of the active site. Here, the inhibitor substituents point towards the FAD and extensively interact with each other as well as with the flavin ring (Figure 3). To exclude the possibility of crystallization artifacts determined by ligand concentration we performed different soaking experiments

14

in a concentration range of 0.8 to 5 mM. In all tested cases, compound **7** possesses the same conformation, forming a stacked pile comprising three copies of the molecule. The active site pocket is thereby filled by the inhibitor molecules blocking the accessibility to the flavin. The presence of these extensive interactions between the inhibitor molecules and the flavin rationalizes the potency and the high-affinity binding featured by **7**.
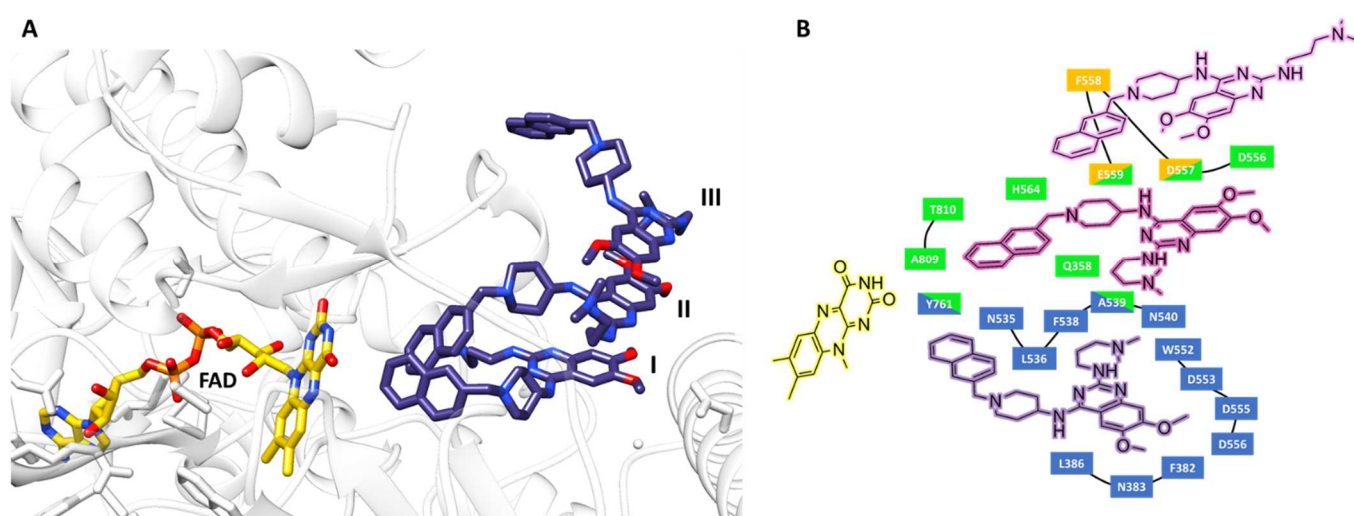
Figure 3. A) Crystal structure of **7** in complex with LSD1-CoREST (PDB: 6TUY). Compound **7** is represented as dark blue sticks; FAD is represented as yellow sticks. B) Key interactions of **7** into the LSD1-CoREST binding site; FAD is represented in yellow.

2.6. Determination of Growth Arrest in THP-1 Cells.

Selected compounds **1**, **5**, **7-9**, **12**, **21**, and **29** were tested for their effects on the proliferation of THP-1 acute monocytic leukemia cells using increasing doses (0.025, 0.05, 0.1, 0.2, 0.5, 1, 2.5, and 5 µM) of each inhibitor for 24, 72, and 144 h (Figure 4). For comparison purposes we also evaluated the activity on THP-1 cells of **46** and **47**, chosen as reference drugs for reversible LSD1 and G9a inhibition, respectively. Because of the scarce potency shown by **46** in THP-1 cells at the various tested doses,

maybe due to cell permeability and/or metabolic issues, the relative IC_{50} values (Table 3) were not determined.
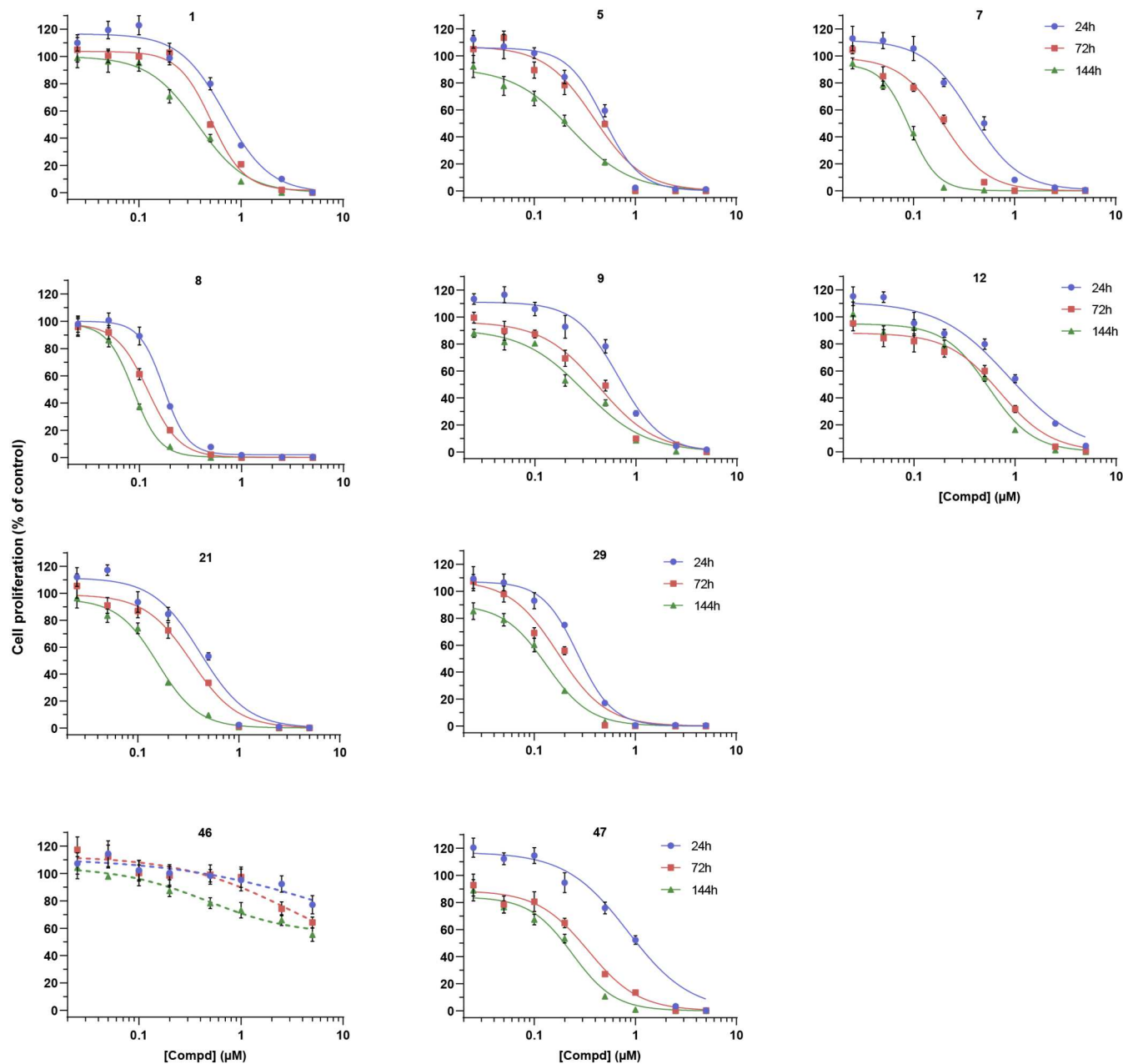
Figure 4. Antiproliferative activity of derivatives **1**, **5**, **7-9**, **12**, **21**, and **29** tested at 0.025, 0.05, 0.1, 0.2, 0.5, 1, 2.5, and 5 µM for 24, 72, and 144 h in the THP-1 cell line. Compounds **46** and **47** were used as reference drugs for reversible LSD1 and G9a inhibition, respectively. Control cells were treated with vehicle (DMSO).

The compounds were selected for the assay on THP-1 cells based on their enzyme inhibition profile. Indeed, **5** was included because it is a dual LSD1/G9a inhibitor like **1**, though 3-fold more potent against LSD1 [K_i values, μM: 0.149 (**5**) and 0.440 (**1**)] and equipotent against G9a [K_i values, μM: 0.69 (**5**) and 0.68 (**1**)], while **7** and **8** because they display similar LSD1 inhibition as **5**, but with less potency against G9a [K_i values, μM: 2.93 (**7**) and 1.18 (**8**)]. In contrast, compounds **9**, **12**, **21**, and **29** were tested because they are all potent LSD1 inhibitors with great selectivity over G9a. Indeed, **9** is almost 4-fold less effective than **5**, **7** and **8** against LSD1, but totally inactive against G9a, while compounds **12**, **21**, and **29** show high inhibition against LSD1 (K_i from 0.108 to 0.205 μM) with a very low residual activity against G9a (K_i values from 26 to 47 μM).

All compounds showed high, time- and dose-dependent decrease of cell viability and proliferation in THP-1 cells and were generally more effective than **1** as well as than the positive controls for LSD1 (**46**) and G9a (**47**) inhibition (Figure 4). Similarly to **1**, the dual LSD1/G9a inhibitor **5** exerted lower antiproliferative effects than the compounds endowed with a preferential LSD1 inhibition such as **7-9**, **12**, **21**, and **29**. Therefore, LSD1 inhibition seems to play a crucial role in triggering the block of THP-1 proliferation, while the concomitant G9a inhibition does not seem to be essential. Compound **8** exhibited the strongest antiproliferative activity, with a huge arrest of proliferation at 0.2 μM after 24 h and a total suppression after 72 and 144 h of treatment, followed by **7** and **29** (Figure 4). The highest potency displayed in inhibiting THP-1 cell proliferation by **7**, **8** and **29** was also confirmed by the corresponding IC$_{50}$ values (Table 3).

Table 3. IC$_{50}$ values (μM) of 1, 5, 7-9, 12, 21, and 29 after 24, 72, and 144 h treatment in THP-1 cells.			
Compd	**THP-1, IC$_{50}$ (μM)**		
	24 h	**72 h**	**144 h**

1	0.69 ± 0.07	0.51 ± 0.03	0.38 ± 0.03
5	0.49 ± 0.04	0.39 ± 0.05	0.22 ± 0.03
7	0.30 ± 0.03	0.16 ± 0.01	0.092 ± 0.004
8	0.17 ± 0.01	0.12 ± 0.02	0.087 ± 0.002
9	0.67 ± 0.06	0.43 ± 0.05	0.30 ± 0.04
12	0.87 ± 0.19	0.71 ± 0.09	0.55 ± 0.05
21	0.42 ± 0.05	0.34 ± 0.03	0.16 ± 0.01
29	0.27 ± 0.02	0.17 ± 0.02	0.13 ± 0.01
47[a]	0.84 ± 0.18	0.34 ± 0.04	0.24 ± 0.03
[a]Data for **47** were included as a reference drug for G9a inhibition.			

Compounds **7**, **8** and **29** (IC_{50}^{THP-1} values at 72 h: 0. 12-0.17 µM) were also tested at 1 µM in non-cancer peripheral blood B lymphocyte AHH-1 cells to assess their differential toxicities. After 72 h treatment, they only modestly affected the proliferation of normal cells (81.5%, 79.1%, and 90% residual viability, respectively), thus being less effective in normal than in THP-1 leukemia cells as antiproliferative agents (Figure S1).

2.7. Anticancer Effects in MV4-11 Cells. The quinazolines **1**, **5**, **7-9**, **21** and **29** were then tested at 0.2, 1.0, and 2.5 µM for 72 and 144 h against human MV4-11 AML cells to determine their effects on proliferation (Figure 5). The reversible LSD1 inhibitor **46** and the G9a inhibitor **47** were also tested for comparison. Among the tested compounds, **29** was the most potent with cell growth inhibitory effects starting from 0.2 µM concentration and abolishing it at 2.5 (after 72 h) or 1 µM (after 144 h). Compounds **7**, **8** and **21** abrogated cell proliferation at 2.5 µM at the same time points. As for the THP-1 cells, G9a inhibition appears to be less important than LSD1 inhibition. In fact, the known G9a inhibitor **47** displayed a modest effect under these conditions, and the dual LSD1/G9a inhibitors **1** and **5** were less effective than preferential LSD1 inhibitors **7**, **8**, and **21**, and the reference LSD1 inhibitor **46**.

Compound **9**, almost 4-fold less potent against LSD1 than **5**, **7**, **8**, **21** and **29** in vitro, exerted only a very low activity in this cell line, thereby further supporting the important role for LSD1 inhibition to trigger the block of proliferation in MV4-11 cells.
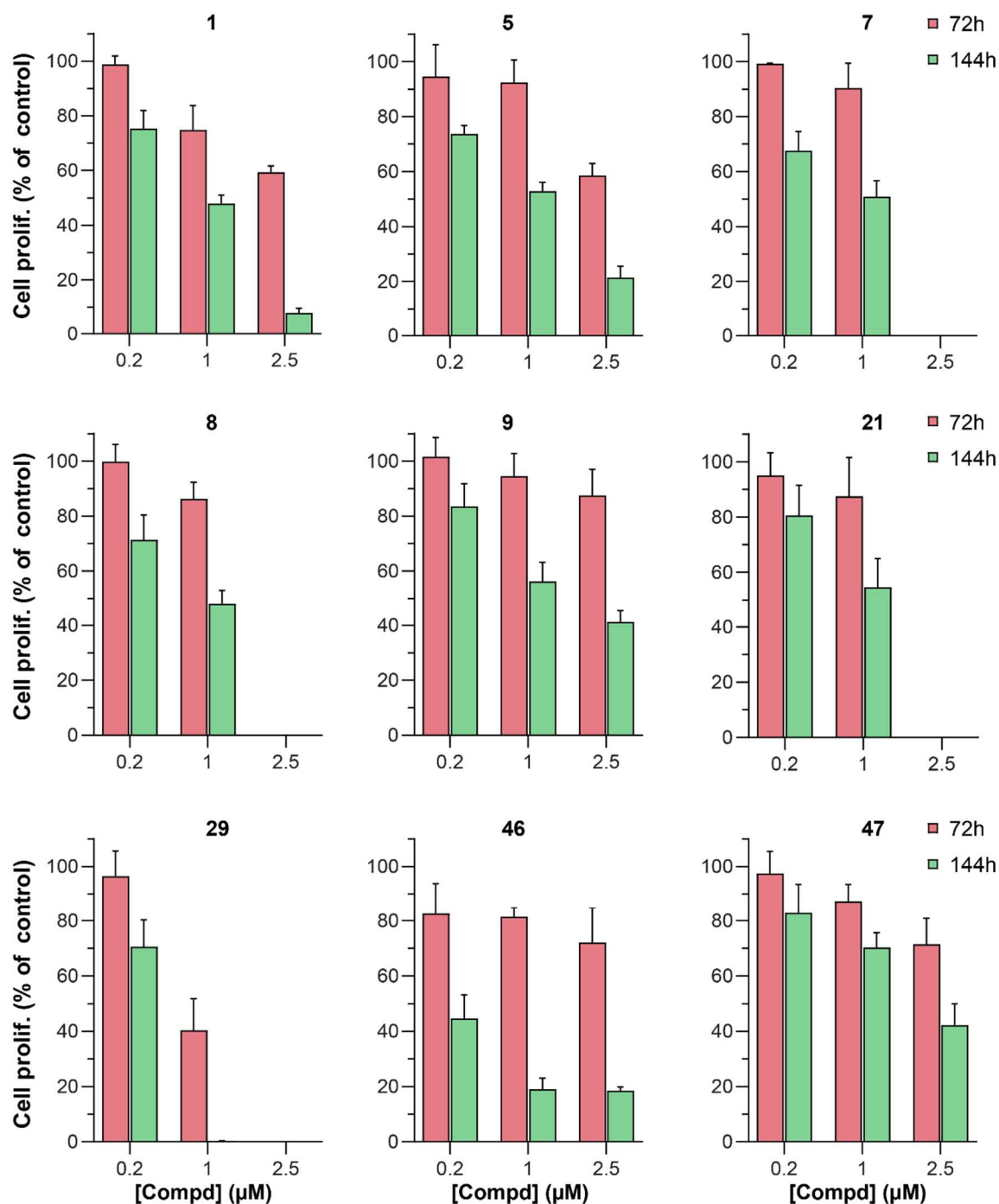
Figure 5. Antiproliferative activity of **1**, **5**, **7**-**9**, **21**, and **29** tested at 0.2, 1.0, and 2.5 µM in MV4-11 cells for 72 and 144 h. Compounds **46** and **47** were tested for comparison purposes. Control cells were treated with vehicle (DMSO).

To shed light on the causal link between the phenotypic effects observed in MV4-11 cells with the quinazoline compounds and LSD1 inhibition, we carried out western blot analyses to detect the levels of H3K4me2 after treatment with **1**, **5**, **7**-**9**, **21** and **29** for 24 h at 0.2, 1.0 and 2.5 µM (Figure 6A). Moreover, the expression level of the monocyte/macrophage lineage differentiation marker *CD86* [38], a gene known to be silenced by LSD1, was determined after treatment of MV4-11 cells with the same inhibitors at 0.2 and 1.0 µM for 24 h (Figure 6B).
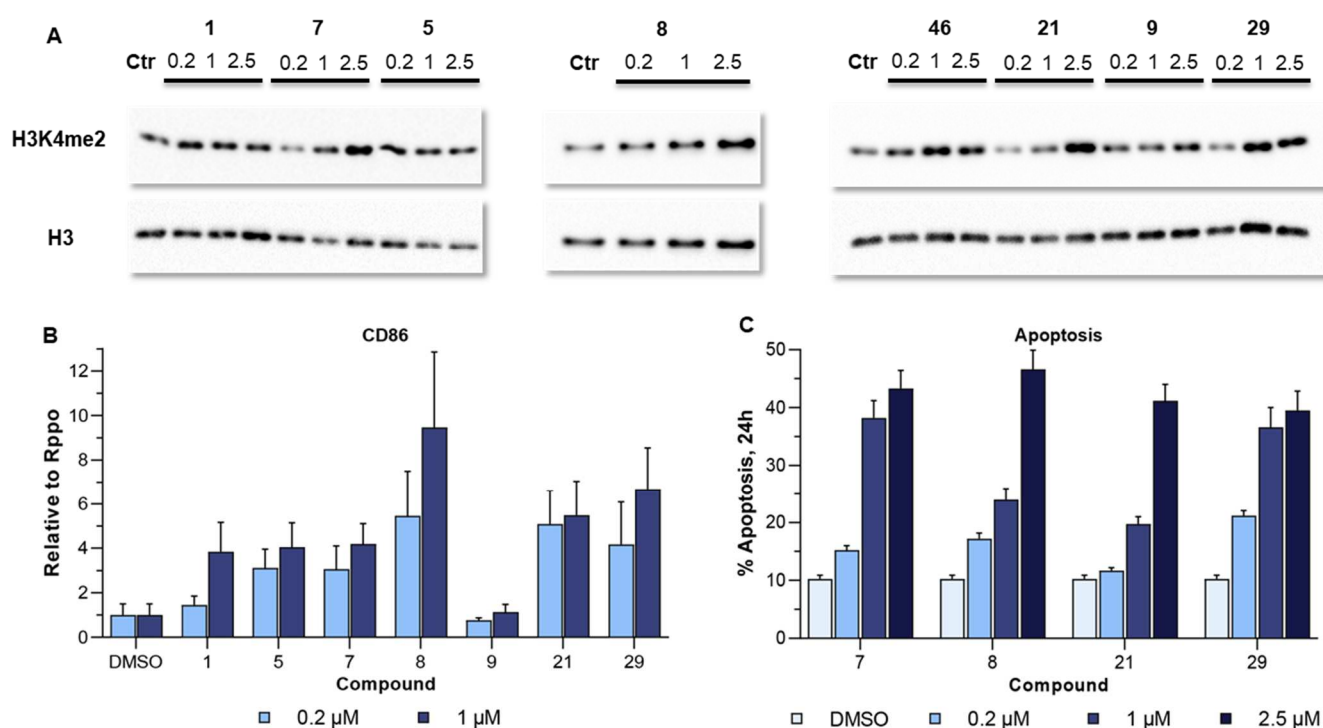
Figure 6. A) Western blot analyses performed on MV4-11 cells treated with **1**, **5**, **7**-**9**, **21**, and **29** at 0.2, 1.0, and 2.5 µM for 24 h. The known reversible LSD1 inhibitor **46** was used as positive control. Antibody anti-H3K4me2 has been used. Histone H3 has been used as loading control. B) Expression

levels of *CD86* in MV4-11 cells after 24 h treatment with compounds **1**, **5**, **7-9**, **21**, and **29** at 0.2 and 1.0

µM. C) Apoptosis induction in MV4-11 cells treated with **7**, **8**, **21** and **29** at 0.2, 1.0, and 2.5 µM for 24

h.

Western blot analyses performed on MV4-11 cells using an anti-H3K4me2 antibody confirmed the

inhibition of LSD1 by the new quinazolines at cellular level. Indeed, all tested inhibitors increased the

H3K4me2 levels respect to the control (DMSO), with **5** (dual LSD1/G9a inhibitor) and **9** (least potent

LSD1 inhibitor) being the least effective compounds (Figure 6A).

Treatment of MV4-11 cells for 24 h with the same inhibitors at 0.2 and 1.0 µM also showed a dose-

dependent increase of the expression level of *CD86*, more evident with **8**, **21** and **29** (Figure 6B).

Cell cycle analysis performed on MV4-11 cells after 24 h treatment with selected compounds **7**, **8**, **21**

and **29** at 0.2, 1.0, and 2.5 µM showed an arrest at the G1 phase of the cell cycle similar for all tested

compounds (Figure S2). Quantification of the sub-G1 peaks highlighted a dose-dependent induction of

apoptosis by all four tested LSD1 inhibitors (Figure 6C).

2.8. Antiproliferative Activity in MDA-MB-231 Breast Cancer Cells. To evaluate the effects of

the new quinazolines in solid tumor models, selected compounds **1**, **5**, **7-9**, **21** and **29** were also tested in

the MDA-MB-231 TNBC cell line at 0.05, 0.1, 0.25, 0.5, 1, 2.5, and 5 µM for 72 h (Figure 7).

Compounds **46** and **47** were added for comparison, as done before. The IC_{50} values determined for all

tested compounds are reported in Table 4. Due to the scarce potency shown by **46** in this cell system,

the corresponding IC_{50} value was not determined.
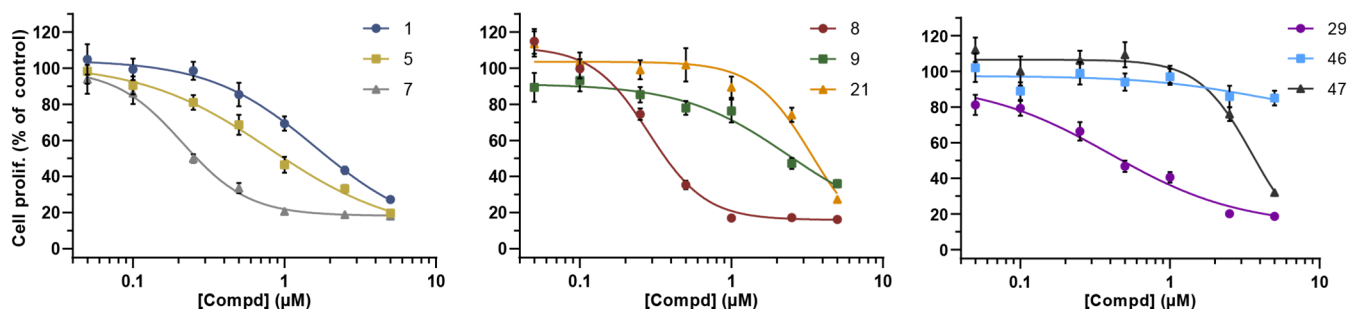
Figure 7. Antiproliferative activities of compounds **1**, **5**, **7-9**, **21** and **29** tested at 0.05, 0.1, 0.25, 0.5, 1.0, 2.5, and 5 µM for 72 h in the MDA-MB-231 TNBC cell line. Compounds **46** and **47** were used as reference drugs for reversible LSD1 and G9a inhibition, respectively. Control cells were treated with vehicle (DMSO).

Among the tested compounds, the potent LSD1 inhibitors **7**, **8** and **29** were the most effective as antiproliferative agents in this cell line. The dual LSD1/G9a inhibitors **1** and **5** as well as **9**, the least potent LSD1 inhibitor, displayed the lowest potency. Surprisingly, the highly potent and selective LSD1 inhibitor **21** failed in inducing growth arrest at the lowest doses, while at the highest tested dose (5 µM), **21** displayed a huge decrease of proliferation, in contrast to the reference LSD1 inhibitor **46** which was essentially inactive in this context at the same concentration (Figure 7, Table 4).

Table 4. IC$_{50}$ values (µM) of **1**, **5**, **7-9**, **21** and **29** after 72 h in the MDA-MB-231 TNBC cell line. Data for **47** were added for comparison.	
Compd	**IC$_{50}$ (µM), 72 h**
1	1.60 ± 0.46
5	0.80 ± 0.16
7	0.21 ± 0.02
8	0.29 ± 0.02

9	2.38 ± 1.63
21	3.40 ± 1.66
29	0.40 ± 0.09
47	3.56 ± 1.77

When tested in human mammary epithelial (HME) normal cells for 72 h to determine their effects on proliferation, **7** and **8** (IC_{50}^{MDA} values: 0.21 and 0.29 μM, respectively) showed 96.5% and 88.1% of residual viability at 1 μM, respectively, while **29** (IC_{50}^{MDA}: 0.42 μM) was slightly more toxic (76% residual viability at 1 μM), but no substantial toxicity was detected at 0.5 μM (93% of residual viability) (Figure S3).

2.9. Effects on RD and RH30 Rhabdomyosarcoma Cells. RMS is a highly aggressive pediatric cancer derived by the failure of differentiation of mesenchymal into skeletal muscle cells. The two most frequent subtypes are the embryonal, devoid of any fusion gene (fusion-negative RMS, FN-RMS), but with specific mutations of the RAS and RTK pathways, and the alveolar subtype, characterized by the expression of the PAX3/PAX7-FOXO1 oncogenic fusion proteins (fusion-positive RMS, FP-RMS) and poor prognosis [47]. Selected compounds **1**, **7**, **21** and **29** were tested in the range 0.01-20 μM at 24, 72, and 144 h against the two most representative RMS cell lines, RD and RH30, belonging to the FN-RMS and FP-RMS subtype, respectively [48], to determine their effect on cell proliferation (Figure 8A). The LSD1 inhibitor **46** and the G9a inhibitor **47** were included in the analysis for comparison purposes. The IC_{50} values of the tested compounds for the two RMS cell lines at 24, 72 and 144 h are reported in Table 5. Western blot analysis of the levels of H3K4me2 after treatment for 48 h with **1**, **7**, **21** and **29** at doses around their IC_{50} values was performed as a readout of LSD1 inhibition in RMS cells (Figure 8B). Calcein AM staining of RD and RH30 cells treated with selected inhibitors at 24 and 72 h allowed

the quantification of live cells (green: Calcein AM positive cells) (Figure 9A-B). Furthermore, caspase-3/7 activity in both the RMS cell lines treated with selected LSD1 inhibitors for 24 h was evaluated and quantified as index of apoptosis induction (Figure 9C).

A

RD

RH30

B
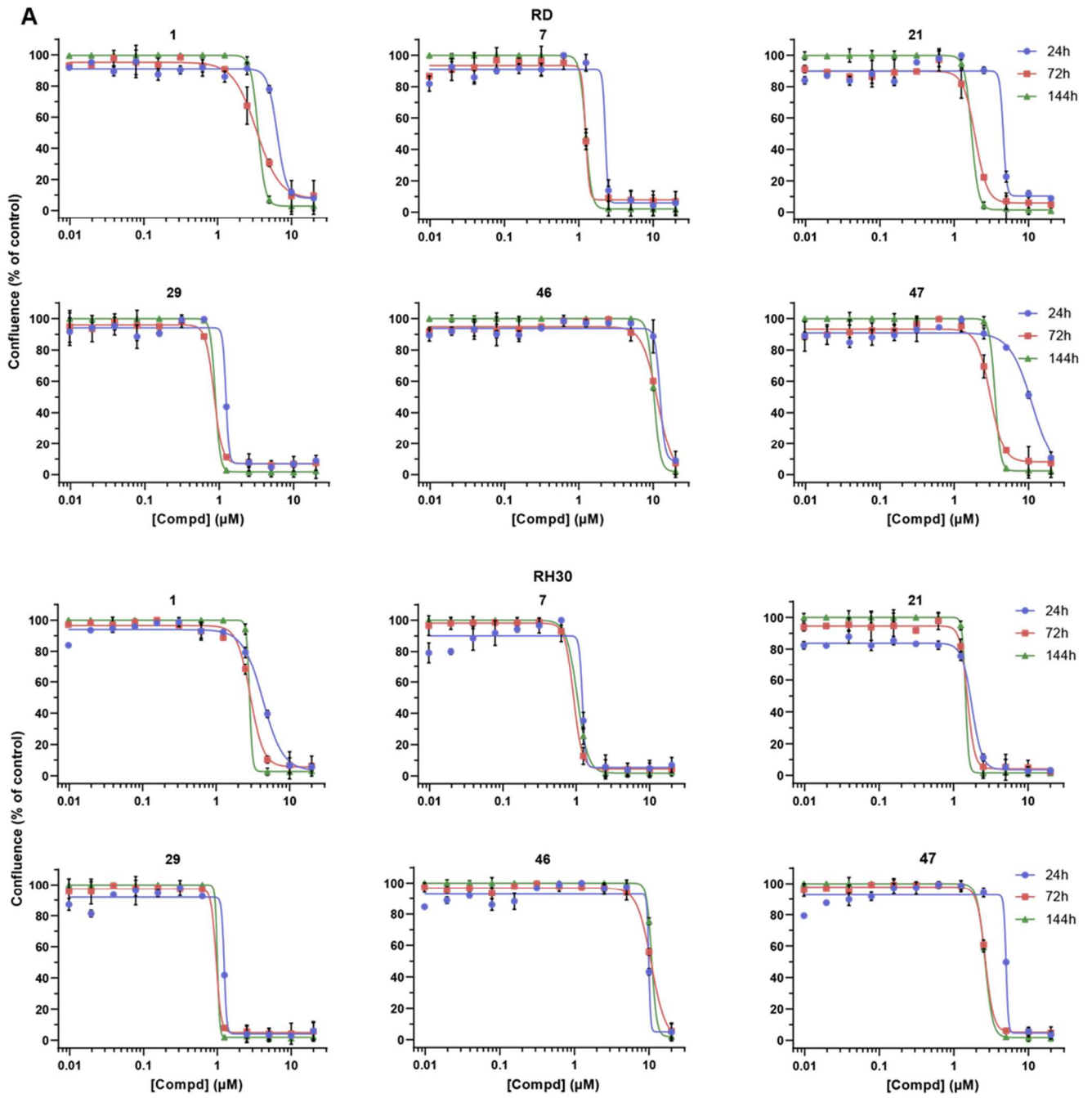
Figure 8. A) Dose-response curves of selected inhibitors **1**, **7**, **21**, and **29** at 24, 72 and 144 h tested on RD (FN-RMS) and RH30 (FP-RMS) cells. The LSD1 inhibitor **46** and the G9a inhibitor **47** were used for comparison purposes. Control cells were treated with vehicle (DMSO). B) Western blot depicting H3K4me2 protein levels in RD (left) and RH30 (right) cells treated with reported doses of tested compounds for 48 h. Histone H3 protein levels were detected as loading control.

Table 5. Calculated IC_{50} values for **1**, **7**, **21** and **29** at the indicated time points in RD and RH30 RMS cells. Data for the inhibitors **46** and **47** were added for comparison.

Compd	RD, IC_{50} (μM)			RH30, IC_{50} (μM)		
	24 h	72 h	144 h	24 h	72 h	144 h
1	6.40 ± 0.39	3.36 ± 0.21	2.82 ± 0.05	4.33 ± 0.18	2.92 ± 0.10	2.57 ± 0.04
7	2.28 ± 0.81	1.23 ± 0.19	0.90 ± 0.01	1.21 ± 0.31	0.91 ± 0.03	0.69 ± 0.01
21	4.56 ± 0.61	1.92 ± 0.08	1.42 ± 0.04	1.76 ± 0.06	1.53 ± 0.16	1.42 ± 0.04
29	1.23 ± 0.43	0.85 ± 0.05	0.73 ± 0.02	1.24 ± 0.28	0.96 ± 0.23	0.68 ± 0.05
46	12.35 ± 1.18	11.43 ± 1.21	10.2 ± 0.49	9.93 ± 0.54	10.7 ± 0.40	10.3 ± 0.67
47	11.17 ± 1.42	3.05 ± 0.16	2.91 ± 0.11	5.01 ± 1.25	2.64 ± 0.08	2.48 ± 0.02
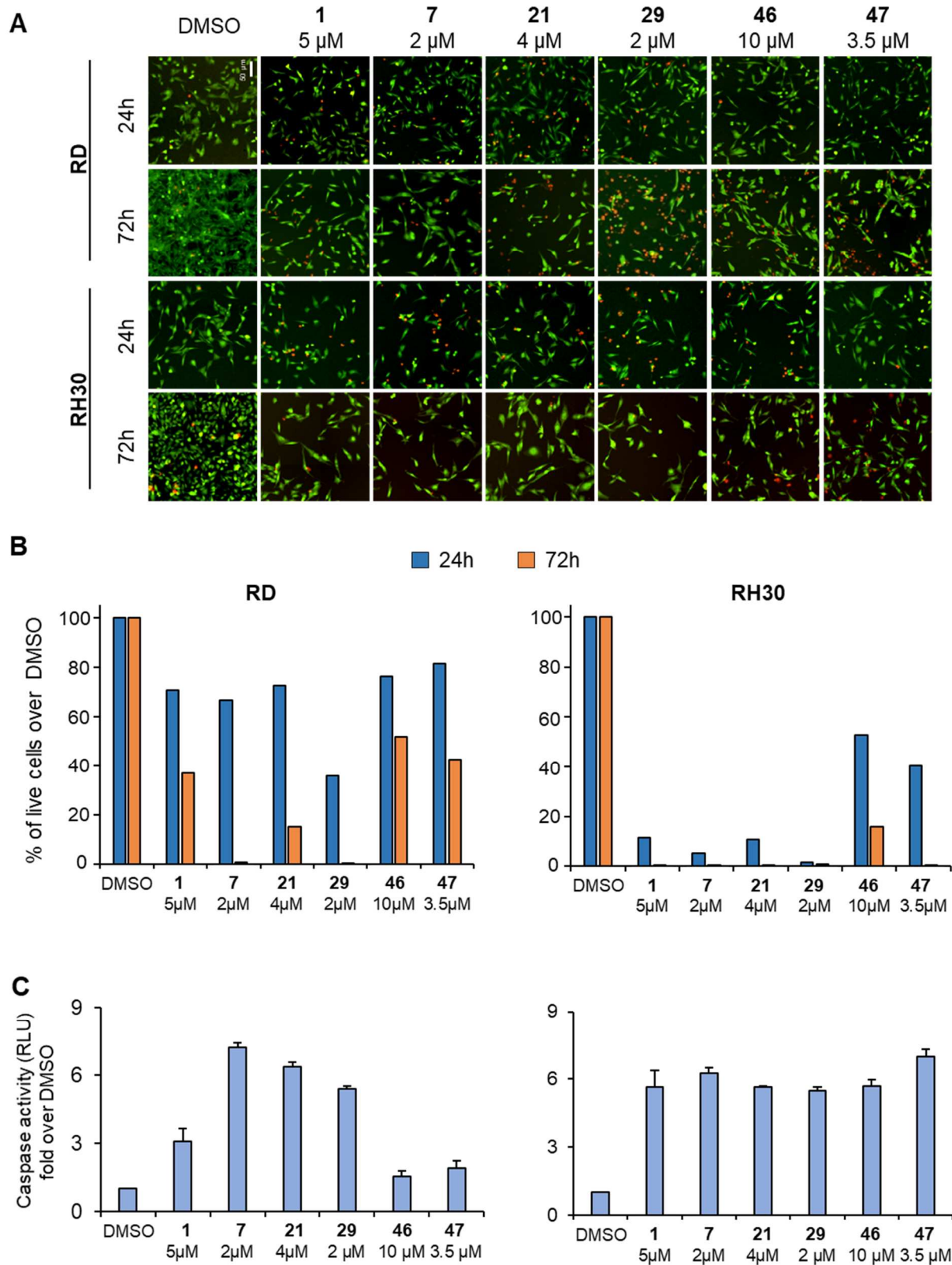
Figure 9. A) Representative images of Calcein AM (green) staining of RD and RH30 RMS cells treated

with selected inhibitors at the reported doses for 24 and 72 h. Propidium Iodide (red) staining indicates

remnants of dead cells. Scale bar = 50 μm. B) Quantification of live cells (green: Calcein AM positive cells) in RD (left) and RH30 (right) treated with selected inhibitors at the reported doses for 24 and 72 h. C) Histograms depicting caspase-3/7 activity in RD (left) and RH30 (right) cells treated with selected inhibitors at the reported doses for 24 h.

All tested compounds **1**, **7**, **21** and **29** induced arrest of proliferation in both RMS cell lines, with the new more potent LSD1 inhibitors **7**, **21** and **29** being more effective than the prototype **1**. Indeed, LSD1 inhibitors **7**, **21** and **29** showed lower IC_{50} values compared to the prototype **1**. The evidence that **7**, **21** and **29** are LSD1 inhibitors endowed with selectivity over G9a, while **1** is a dual LSD1/G9a inhibitor, suggests that the simultaneous inhibition of LSD1 and G9a does not provide any added value in terms of antiproliferative effects in this solid cancer model.

Since human-derived mesenchymal stem cells are the normal precursors of RMS cells, **1**, **7**, **21** and **29** were also tested in these cells for 72 h at around their IC_{50} values in RMS lines (2.5 μM for **1**, and 1.25 μM for **7**, **21** and **29**) to assess a potential cancer-selective action. In accordance with what previously observed in other normal cell lines, all tested compounds exhibited very low cytotoxicity [percentage of residual viability: 85% (**1**), 96% (**7** and **21**), and 92% (**29**)] in mesenchymal stem cells (data not shown). The increased levels of the H3K4me2 histone mark detected by Western blot analysis in the two RMS cell lines treated with the selected compounds confirmed the LSD1 inhibition in cells. The effect is more evident in RH30 FP-RMS cells and is consistent with the higher sensitivity of this cell line to epigenetic drugs [49]. Accordingly, Calcein AM staining in RMS cells showed in Figure 9A,B confirmed that treatment with **7**, **21** and **29** in RH30 results in a decreased amount of live cells (green) as early as 24 h. Conversely, RD cells showed live cells decrease only after 72 h of treatment with the selected compounds. Regarding the apoptosis induction after 24 h treatment, in RD FN-RMS cells the most potent LSD1 inhibitors **7**, **21** and **29** exhibited the highest activity among the tested compounds, as

highlighted by the enhancement of caspase-3/7 activity, while in RH30 FP-RMS cells all evaluated molecules reached almost the same level of induction.

3. CONCLUSION

For its ability to mimic specific peptide sequences of histone substrates the quinazoline scaffold is considered a privileged structure in the epi-drug discovery field. Indeed, over the past years, the decoration of the quinazoline ring with appropriate substituents at the C2, C4, C6 and/or C7 positions led to the medicinal chemistry development of selective epi-drugs targeting different epi-targets, including KMTs [36, 40, 45, 50-56], KDMs [57], DNMTs [58, 59], HDACs [60-64], acetyl- and methyl-readers [65-68], and various epigenetic multi-target modulators [69-73].

During our studies on LSD1 inhibitors [17-25, 37, 74, 75], we selected from our in-house library some quinazolines bearing potential lysine mimetic chains and identified **1** as a dual non-covalent LSD1/G9a inhibitor endowed with antiproliferative activity in MV4-11 leukemia cells. To obtain more potent and specific LSD1 inhibitors we performed some chemical modifications at the C2, C4, and/or C7 positions of the **1** quinazoline scaffold and prepared compounds **2-30**. Compared to **1**, many new derivatives increased their inhibitory potency against LSD1 and some of them (in particular, **12**, **21**, and **29**) also showed a concomitant loss or at least significant reduction of activity versus G9a. The structural analysis showed that **7**, one of the most potent LSD1 inhibitors, bind deeply into the active site of LSD1 forming a stacking pile of three copies and extensively interact with the flavin and nearby protein residues. Among the compounds tested against THP-1 cells **7**, **8** and **29** were the most effective as antiproliferative agents, with 0.12-0.17 µM IC$_{50}$ values after 72 h and 0.087-0.13 µM after 144 h treatment, without displaying significant cytotoxicity in non-cancer blood cells. The same compounds were the most potent in reducing the proliferation of MV4-11 cells, with **29** being the most effective one. Interestingly, the dual LSD1/G9a inhibitors **1** and **5** as well as the specific but less potent LSD1 inhibitor **9**

showed weaker effects on the proliferation of both AML cell lines than the most potent and specific LSD1 inhibitors **7**, **8**, and **29**, suggesting a pivotal role for LSD1 inhibition and a negligible importance of the simultaneous G9a inhibition in this leukemia context. Analyses carried out in MV4-11 cells showed a dose-dependent increase of the levels of H3K4me2, a well-known marker of anti-LSD1 activity, and an induction of *CD86*, a gene under control of LSD1, thus suggesting that the observed phenotypic effects may likely be ascribed to LSD1 inhibition. Moreover, selected compounds induced dose-dependent apoptosis in MV4-11 cells.

To evaluate the effects of such compounds in solid cancer models, selected inhibitors **1**, **5**, **7-9**, **21** and **29** were tested against MDA-MB-231 TNBC cells. After 72 h treatment, once again **7**, **8** and **29** were the most potent in reducing cell proliferation with 0.21-0.40 μM IC_{50} values, without cytotoxicity in non-cancer HME cells. Compounds **1**, **7**, **21** and **29** were also tested in RD and RH30 RMS cells at 24, 72 and 144 h, with **7** and **29** being the most effective. Interestingly, RH30 cell line was the most sensitive to LSD1 inhibition, accordingly to the high sensitivity of the FP-RMS subtype to epigenetic drugs. In the RMS cell lines the two quinazoline derivatives displayed IC_{50} values between 0.85 and 1.23 μM at 72 h and between 0.68 and 0.90 μM at 144 h, without showing major cytotoxicity in human-derived mesenchymal stem cells at the same doses. The increase of caspase-3/7 activity assay was clearly indicative of apoptosis in the same cell line and western blot analyses confirmed the LSD1 inhibition in RMS cells.

As already seen in AML cells, in breast and in RMS cancer cell models specific LSD1 inhibition is more effective than dual LSD1/G9a inhibition in reducing proliferation, suggesting no added value for the simultaneous G9a inhibition in these contexts.

Further in-depth investigation of the best prototypes identified in the present study (**7**, **8**, and **29**) will likely allow to assess their potential as lead compounds for the development of new generation therapeutics for the management of hematological and solid tumors.

4. EXPERIMENTAL SECTION

4.1. Chemistry. Melting points were determined on a Buchi 530 melting point apparatus and are uncorrected. ^{1}H-NMR spectra were recorded at 400 MHz on a Bruker AC 400 spectrometer, while ^{13}C-NMR spectra were recorded at 700 MHz on a Bruker AC 700 spectrometer. HRMS spectra were recorded on ThermoFisher Scientific Orbitrap XL mass spectrometer in electrospray positive ionization modes (ESI-MS). Chemical shifts are reported in δ (ppm) units relative

to the internal reference tetramethylsilane (Me$_4$Si). Microwave-assisted reactions were performed with a Biotage Initiator (Uppsala, Sweden) high-frequency microwave synthesizer working at 2.45 GHz, fitted with magnetic stirrer and sample processor; reaction vessels were Biotage microwave glass vials sealed with applicable cap; temperature was controlled through the internal IR sensor of the microwave apparatus. Low-resolution mass spectra of final and intermediate compounds were recorded on an API-TOF Mariner by Perspective Biosystem (Stratford, Texas, USA), samples were injected by a Harvard pump using a flow rate of 5-10 µL/min, infused in the Electrospray system. All compounds were routinely checked by TLC and ^{1}H-NMR; all final compounds were also checked by ^{13}C-NMR. TLC was performed on aluminum backed silica gel plates (Merck DC, Alufolien Kieselgel 60 F$_{254}$) with spots visualized by UV light. All solvents were reagent grade and, when necessary, were purified and dried by

standard methods. Concentration of solutions after reactions and extractions involved the use of a rotary evaporator operating at reduced pressure of ca. 20 Torr. Organic solutions were dried over anhydrous sodium sulphate. Elemental analysis has been used to determine the purity of all final compounds, that is > 95%. Analytical results are within ± 0.40% of the theoretical values. All chemicals were purchased from Sigma Aldrich s.r.l, Milan (Italy), or from TCI Europe N.V., Zwijndrecht (Belgium), and were of the highest purity.

Procedure for the Synthesis of N^2-(3-(dimethylamino)propyl)-6,7-dimethoxy-N^4-(piperidin-4-yl)quinazoline-2,4-diamine trihydrochloride (2). A 4N hydrochloric acid solution in 1,4-dioxane (24.87 mmol, 45 eq.) was added dropwise to a cooled solution of **12** (0.55 mmol, 1 eq.) in a mixture of dry THF/dry methanol 1:1 (2.15 mL:2.15 mL), and the mixture was stirred at room temperature for about 5 h. Then, the reaction mixture was filtered under vacuum and washed over filter in sequence with dry THF and dry diethyl ether to afford the final compound **2** as a white powder. Yield, 57%; mp 282-283 °C. ^{1}H-NMR (400 MHz; DMSO-d_6) δ 1.98-2.11 (m, 6H, 4 × C*H* piperidine ring and NHCH$_2$C*H*$_2$CH$_2$N(CH$_3$)$_2$), 2.72 (s, 3H, N(C*H*$_3$)CH$_3$·HCl), 2.73 (s, 3H, N(CH$_3$)C*H*$_3$·HCl), 3.12 (br m, 2H, 2 × C*H* piperidine ring), 3.38 (br m, 2H, NHCH$_2$CH$_2$C*H*$_2$N(CH$_3$)$_2$), 3.57 (br m, 4H, NHCH$_2$CH$_2$C*H*$_2$N(CH$_3$)$_2$ and 2 × C*H* piperidine ring), 3.89 (s, 3H, OC*H*$_3$), 3.90 (s, 3H, OC*H*$_3$), 4.43-4.55 (br s, 1H, C$_4$-*H* piperidine), 6.99 (br s, 1H, C$_8$-*H* quinazoline ring), 8.01 (s, 1H, C$_5$-*H* quinazoline ring), 8.11 (br s, 1H, N*H*CH$_2$CH$_2$CH$_2$N(CH$_3$)$_2$), 9.14-9.19 (br m, 2H, piperidine N1-*H*·*H*Cl), 9.32 (br s,1H, quinazoline-C4-N*H*), 10.84 (br, s, 1H, *H*Cl), 12.73 (br, s, 1H, *H*Cl). ^{13}C-NMR (176 MHz; DMSO-d_6) δ 24.63, 28.19 (2C), 38.42, 42.38 (2C), 42.67, 47.37 (2C), 54.61, 56.53, 57.17, 98.62, 102.47, 105.85, 135.91, 147.01, 152.83, 155.76, 159.13. MS (ESI) *m/z:* 389 [M + H]$^+$. HR-MS (ESI) *m/z*: calcd for C$_{20}$H$_{33}$N$_6$O$_2$$^+$ [M + H]$^+$, 389.2660; found, 389.2651.

*General Procedure for the Synthesis of **3,6-10,12-30***. The properly substituted 2-chloroquinazolines **32-45** (for **32** [40], **36** [41], **37** [41], **38** [42], **40** [39], **43** [37], **44** [39], and **45** [39] see the related references) (0.24 mmol, 1 eq.) were poured in a microwave glass vial and dissolved in 2-propanol (1 mL). The appropriate commercial amine (0.53 mmol, 2.2 eq.) was then added, and the resulting mixture was heated to 130 °C by microwave irradiation for a variable time from 3 h to 4.5 h. Upon completion of the reaction, the solvent was removed under vacuum, and the remaining residue was poured into water (7 mL) and extracted with ethyl acetate (6 × 10 mL). The organic phases were then washed with saturated sodium chloride solution (30 mL), dried over anhydrous sodium sulfate, and finally concentrated under vacuum to furnish a crude residue which was purified by alumina gel column chromatography by eluting with the proper mixture ethyl acetate/methanol to provide the final compounds.

N^2-(3-(dimethylamino)propyl)-6,7-dimethoxy-N^4-(1-methylpiperidin-4-yl)quinazoline-2,4-diamine (3). Yield, 65%; mp 91-93 °C. ^{1}H-NMR (400 MHz; DMSO-d_6) δ 1.57-1.69 (m, 4H, 2 x C*H* piperidine ring and NHCH$_2$C*H*$_2$CH$_2$N(CH$_3$)$_2$), 1.91-1.98 (m, 4H, 4 × C*H* piperidine ring), 2.19 (s, 6H, N(C*H*$_3$)$_2$), 2.23 (s, 3H, NC*H*$_3$), 2.25 (t, *J*=7 Hz, 2H, NHCH$_2$CH$_2$C*H*$_2$N(CH$_3$)$_2$), 2.835 (br d, 2H, 2 × C*H* piperidine ring), 3.24-3.27 (m, 2H, NHC*H*$_2$CH$_2$CH$_2$N(CH$_3$)$_2$), 3.80 (s, 3H, OC*H*$_3$), 3.81 (s, 3H, OC*H*$_3$), 4.05-4.08 (br m, 1H, C$_4$-*H* piperidine), 6.16 (br t, 1H, N*H*CH$_2$CH$_2$CH$_2$N(CH$_3$)$_2$), 6.66 (s, 1H, C$_8$-*H* quinazoline ring), 7.17-7.18 (br d, 1H, N*H*-piperidine), 7.42 (s, 1H, C$_5$-*H* quinazoline ring). ^{13}C-NMR (176 MHz; DMSO-d_6) δ 24.71, 28.69 (2C), 38.51, 42.39 (2C), 42.90, 47.10, 52.71, 54.57, 56.55 (2C), 57.04, 98.66, 102.44, 105.53, 135.92, 147.05, 152.83, 155.80, 159.24. MS (ESI) *m/z:* 403 [M + H]$^+$. HR-MS (ESI) *m/z*: calcd for C$_{21}$H$_{35}$N$_6$O$_2$$^+$ [M + H]$^+$, 404.2816; found, 403.2807.

N²-(3-(dimethylamino)propyl)-6,7-dimethoxy-N⁴-(1-(naphthalen-1-ylmethyl)piperidin-4-yl)quinazoline-2,4-diamine (6). Yield, 70%; mp 97-100 °C. ^{1}H-NMR (400 MHz; DMSO-d_6) δ 1.56-1.69 (m, 4H, NHCH$_2$C*H$_2$*CH$_2$N(CH$_3$)$_2$ and 2 × C*H* piperidine ring), 1.88-1.91 (br d, 2H, 2 × C*H* piperidine ring), 2.09 (m, 2H, 2 × C*H* piperidine ring), 2.14 (s, 6H, N(C*H$_3$*)$_2$), 2.26 (t, *J*=7 Hz, 2H, NHCH$_2$CH$_2$C*H$_2$*N(CH$_3$)$_2$), 2.94-2.97 (br d, 2H, 2 × C*H* piperidine ring), 3.24-3.29 (m, 2H, NHC*H$_2$*CH$_2$CH$_2$N(CH$_3$)$_2$), 3.77 (s, 3H, OC*H$_3$*), 3.80 (s, 3H, OC*H$_3$*), 3.91 (s, 2H, NC*H$_2$*-naphthalene), 4.16-4.18 (br m, 1H, C$_4$-*H* piperidine), 6.17 (br t, 1H, N*H*CH$_2$CH$_2$CH$_2$N(CH$_3$)$_2$), 6.65 (s, 1H, C$_8$-*H* quinazoline ring), 7.16-7.18 (br d, 1H, N*H*-piperidine), 7.38 (s, 1H, C$_5$-*H* quinazoline ring), 7.45-7.51 (m, 2H, C*H* naphthalene ring), 7.52-7.56 (m, 2H, C*H* naphthalene ring), 7.84-7.87 (t, 1H, C*H* naphthalene ring) 7.91-7.94 (d, 1H, C*H* naphthalene ring), 8.34-8.36 (d, 1H, C*H* naphthalene ring). ^{13}C-NMR (176 MHz; DMSO-d_6) δ 24.84, 28.50 (2C), 38.61, 42.43 (2C), 47.71, 51.15 (2C), 54.60, 55.46, 56.52, 57.16, 98.63, 102.47, 105.83, 124.70, 125.87, 126.70, 126.79, 127.54, 129.24, 130.75, 132.15, 132.76, 133.88, 135.90, 147.02, 152.81, 155.78, 159.27. MS (ESI) *m/z:* 529 [M + H]$^+$. HR-MS (ESI) *m/z*: calcd for C$_{31}$H$_{41}$N$_6$O$_2^+$ [M + H]$^+$, 529.3286; found, 529.3275.

N²-(3-(dimethylamino)propyl)-6,7-dimethoxy-N⁴-(1-(naphthalen-2-ylmethyl)piperidin-4-yl)quinazoline-2,4-diamine (7). Yield, 40%; mp 96-98 °C. ^{1}H-NMR (400 MHz; DMSO-d_6) δ 1.63-1.68 (m, 4H, NHCH$_2$C*H$_2$*CH$_2$N(CH$_3$)$_2$ and 2 × C*H* piperidine ring), 1.90-1.94 (m, 2H, 2 × C*H* piperidine ring), 2.08 (m, 2H, 2 × C*H* piperidine ring), 2.11 (s, 6H, N(C*H$_3$*)$_2$), 2.25 (t, *J*=7 Hz, 2H, NHCH$_2$CH$_2$C*H$_2$*N(CH$_3$)$_2$), 2.92-2.95 (br d, 2H, 2 × C*H* piperidine ring), 3.25-3.34 (m, 2H, NHC*H$_2$*CH$_2$CH$_2$N(CH$_3$)$_2$), 3.68 (s, 2H, NC*H$_2$*-naphthalene), 3.80 (s, 3H, OC*H$_3$*), 3.81 (s, 3H, OC*H$_3$*), 4.12-4.15 (br m, 1H, C$_4$-*H* piperidine), 6.14 (br t, 1H, N*H*CH$_2$CH$_2$CH$_2$N(CH$_3$)$_2$), 6.66 (s, 1H, C$_8$-*H* quinazoline ring), 7.17-7.19 (br d, 1H, N*H*-piperidine), 7.41 (s, 1H, C$_5$-*H* quinazoline

ring), 7.47-7.53 (m, 3H, C*H* naphthalene ring), 7.81 (s, 1H, C*H* naphthalene ring), 7.88-7.90 (m, 3H, C*H* naphthalene ring). ^{13}C-NMR (176 MHz; DMSO-d_6) δ 24.37, 28.50 (2C), 38.61, 42.43 (2C), 47.96, 51.15 (2C), 54.60, 55.40, 56.52, 57.16, 98.63, 102.47, 105.83, 124.80, 125.87, 126.85, 127.60, 129.19, 130.75, 131.64, 132.48, 132.76, 133.88, 135.93, 147.02, 152.81, 155.78, 159.27. MS (ESI) *m/z:* 529 [M + H]$^+$. HR-MS (ESI) *m/z:* calcd for $C_{31}H_{41}N_6O_2{}^+$ [M + H]$^+$, 529.3286; found, 529.3278.

N^4-(1-([1,1'-biphenyl]-4-ylmethyl)piperidin-4-yl)-N^2-(3-(dimethylamino)propyl)-6,7-dimethoxyquinazoline-2,4-diamine (8). Yield, 48%; mp 100-102 °C. ^{1}H-NMR (400 MHz; DMSO-d_6) δ 1.65-1.68 (m, 4H, NHCH$_2$C*H$_2$*CH$_2$N(CH$_3$)$_2$ and 2 x C*H* piperidine ring), 1.91-1.94 (m, 2H, 2 × C*H* piperidine ring), 2.05-2.10 (br t, 2H, 2 × C*H* piperidine ring), 2.16 (s, 6H, N(C*H$_3$*)$_2$), 2.29 (t, *J*=7 Hz, 2H, NHCH$_2$CH$_2$C*H$_2$*N(CH$_3$)$_2$), 2.92 (br d, 2H, 2 × C*H* piperidine ring), 3.24-3.29 (m, 2H, NHC*H$_2$*CH$_2$CH$_2$N(CH$_3$)$_2$), 3.56 (s, 2H, C*H$_2$*-biphenyl ring), 3.80 (s, 3H, OC*H$_3$*), 3.81 (s, 3H, OC*H$_3$*), 4.11-4.14 (br m, 1H, C$_4$-*H* piperidine), 6.21 (br t, 1H, N*H*CH$_2$CH$_2$CH$_2$N(CH$_3$)$_2$), 6.66 (s, 1H, C$_8$-*H* quinazoline ring), 7.22-7.24 (br d, 1H, N*H*-piperidine) 7.34-7.49 (m, 6H, C$_5$-*H* quinazoline ring and 5 × C*H* biphenyl ring) 7.62-7.68 (m, 4H, C*H* biphenyl ring). ^{13}C-NMR (176 MHz; DMSO-d_6) δ 24.73, 28.38 (2C), 38.61, 42.42 (2C), 47.77, 50.82 (2C), 54.60, 56.53, 57.07, 58.91, 98.61, 102.44, 105.60, 127.26 (2C), 127.41 (2C), 128.35 (2C), 129.51 (2C), 132.14, 132.65, 135.92, 139.80, 141.56, 147.04, 152.80, 155.79, 159.27. MS (ESI) *m/z:* 555 [M + H]$^+$. HR-MS (ESI) *m/z:* calcd for $C_{33}H_{43}N_6O_2{}^+$ [M + H]$^+$, 555.3442; found, 555.3436.

N^4-(1-benzylpiperidin-4-yl)-N^2-(3-(dimethylamino)propyl)-6,7-dimethoxy-N^4-methyl quinazoline-2,4-diamine (9). Yield, 73%; mp 115-117 °C. ^{1}H-NMR (400 MHz; DMSO-d_6) δ 1.62-1.69 (m, 2H, NHCH$_2$C*H$_2$*CH$_2$N(CH$_3$)$_2$), 1.75-1.78 (m, 2H, 2 × C*H* piperidine ring), 1.86-

1.93 (m, 2H, 2 × CH piperidine ring), 1.87-2.04 (m, 2H, 2 × CH piperidine ring), 2.12 (s, 6H, N(CH_3)$_2$), 2.25 (t, J=7 Hz, 2H, NHCH$_2$CH$_2$CH_2N(CH$_3$)$_2$), 2.91 (br d, 2H, 2 × CH piperidine ring), 2.98 (br s, 3H, NCH_3), 3.25-3.28 (m, 2H, NHCH_2CH$_2$CH$_2$N(CH$_3$)$_2$), 3.47 (s, 2H, NCH_2Ph), 3.77 (s, 3H, OCH_3), 3.84 (s, 3H, OCH_3), 4.02 (br m, 1H, C$_4$-H piperidine), 6.38 (t, J=6 Hz, 1H, NHCH$_2$CH$_2$CH$_2$N(CH$_3$)$_2$), 6.75 (s, 1H, C$_8$-H quinazoline ring), 6.99 (s, 1H, C$_5$-H quinazoline ring), 7.23-7.27 (m, 1H, CH benzene ring), 7.30-7.35 (m, 4H, CH benzene ring). ^{13}C-NMR (176 MHz; DMSO-d_6) δ 24.63, 24.91 (2C), 35.55, 38.73, 42.43 (2C), 50.70, 54.60 (2C), 56.43, 56.62, 59.09, 65.39, 98.72, 102.85, 108.48, 129.24 (2C), 129.85 (2C), 130.57, 131.85, 138.45, 145.65, 151.42, 155.63, 162.62. MS (ESI) *m/z:* 493 [M + H]$^+$. HR-MS (ESI) *m/z*: calcd for C$_{28}$H$_{41}$N$_6$O$_2$$^+$ [M + H]$^+$, 493.3286; found, 493.3263.

N^1-(4-((1-benzylpiperidin-4-yl)oxy)-6,7-dimethoxyquinazolin-2-yl)-N^3,N^3-dimethyl propane-1,3-diamine (10). Yield, 63%; mp 132-133 °C. ^{1}H-NMR (400 MHz; DMSO-d_6) δ 1.63-1.70 (m, 2H, NHCH$_2$CH_2CH$_2$N(CH$_3$)$_2$), 1.77-1.82 (m, 2H, 2 × CH piperidine ring), 1.91-2.02 (m, 2H, 2 × CH piperidine ring), 2.12 (s, 6H, N(CH_3)$_2$), 2.23-2.29 (m, 4H, 2 × CH piperidine ring and NHCH$_2$CH$_2$CH_2N(CH$_3$)$_2$), 2.66-2.72 (m, 2H, 2 × CH piperidine ring), 3.27-3.32 (m, 2H, NHCH_2CH$_2$CH$_2$N(CH$_3$)$_2$), 3.53 (s, 2H, NCH_2Ph), 3.79 (s, 3H, OCH_3), 3.86 (s, 3H, OCH_3), 5.23-5.25 (m, 1H, OC$_4$-H piperidine), 6.78-6.81 (m, 2H, C$_8$-H quinazoline ring and NHCH$_2$CH$_2$CH$_2$N(CH$_3$)$_2$), 7.09 (s, 1H, C$_5$-H quinazoline ring), 7.23-7.31 (m, 2H, CH benzene ring), 7.33-7.34 (m, 3H, CH benzene ring). ^{13}C-NMR (176 MHz; DMSO-d_6) δ 26.56, 29.62 (2C), 42.36, 46.95 (2C), 54.42 (2C), 56.57, 56.83, 56.92, 64.78, 72.63, 98.63, 103.84, 104.76, 129.18 (2C), 129.91, 131.98 (2C), 132.11, 138.58, 147.67, 153.44, 157.75, 165.55. MS (ESI) *m/z:* 480 [M + H]$^+$. HR-MS (ESI) *m/z*: calcd for C$_{27}$H$_{38}$N$_5$O$_3$$^+$ [M + H]$^+$, 480.2969; found, 480.2953.

Tert-butyl 4-((2-((3-(dimethylamino)propyl)amino)-6,7-dimethoxyquinazolin-4-yl)amino)piperidine-1-carboxylate (12). Yield, 71%; mp 106-107 °C. ^{1}H-NMR (400 MHz; DMSO-d_6) δ 1.43 (s, 9H, COO(CH_3)$_3$), 1.46-1.48 (m, 2H, 2 × CH piperidine ring), 1.58-1.67 (m, 2H, NHCH$_2$CH_2CH$_2$N(CH$_3$)$_2$), 1.91-1.94 (br d, 2H, 2 × CH piperidine ring), 2.13 (s, 6H, N(CH_3)$_2$), 2.25 (t, J=8 Hz, 2H, NHCH$_2$CH$_2$CH_2N(CH$_3$)$_2$), 2.82 (br m, 2H, 2 × CH piperidine ring), 3.25-3.28 (m, 2H, NHCH_2CH$_2$CH$_2$N(CH$_3$)$_2$), 3.80 (s, 3H, OCH_3), 3.81 (s, 3H, OCH_3), 4.01-4.04 (br m, 2H, 2 × CH piperidine ring), 4.25-4.33 (br m, 1H, C$_4$-H piperidine), 6.14-6.17 (br t, 1H, NHCH$_2$CH$_2$CH$_2$N(CH$_3$)$_2$), 6.67 (s, 1H, C$_8$-H quinazoline ring), 7.15-7.17 (br d, 1H, NH-piperidine), 7.38 (s, 1H, C$_5$-H quinazoline ring). ^{13}C-NMR (176 MHz; DMSO-d_6) δ 28.05, 28.58 (3C), 32.01 (2C), 43.10, 43.90 (2C), 45.76 (2C), 47.59, 55.78, 56.49, 57.72, 79.11, 103.78, 103.91, 105.66, 144.78, 149.33, 154.19, 154.33, 158.67, 159.39. MS (ESI) *m/z:* 489 [M + H]$^+$. HR-MS (ESI) *m/z:* calcd for C$_{25}$H$_{41}$N$_6$O$_4^+$ [M + H]$^+$ 489.3184; found, 489.3166 .

N^4-(1-benzylpyrrolidin-3-yl)-N^2-(3-(dimethylamino)propyl)-6,7-dimethoxyquinazoline-2,4-diamine (13). Yield, 61%; mp 58-61 °C. ^{1}H-NMR (400 MHz; DMSO-d_6) δ 1.60-1.65 (m, 2H, NHCH$_2$CH_2CH$_2$N(CH$_3$)$_2$), 1.84-1.93 (m, 1H, CH pyrrolidine ring), 2.12 (s, 6H, N(CH_3)$_2$), 2.22-2.26 (m, 3H, NHCH$_2$CH$_2$CH_2N(CH$_3$)$_2$ and CH pyrrolidine ring), 2.44-2.47 (m, 1H, CH pyrrolidine ring), 2.67-2.68 (m, 1H, CH pyrrolidine ring), 2.87-2.91 (br t, 1H, CH pyrrolidine ring), 3.22-3.28 (m, 3H, NHCH_2CH$_2$CH$_2$N(CH$_3$)$_2$ and CH pyrrolidine ring), 3.61 (s, 1H, NCHHPh), 3.64 (s, 1H, NCHHPh), 3.80 (s, 3H, OCH_3), 3.81 (s, 3H, OCH_3), 4.60-4.66 (br m, 1H, NHC$_3$-H pyrrolidine), 6.16 (br t, 1H, NHCH$_2$CH$_2$CH$_2$N(CH$_3$)$_2$), 6.66 (s, 1H, C$_8$-H quinazoline ring), 7.22-7.26 (m, 1H, CH benzene ring), 7.29-7.32 (m, 4H, CH benzene ring), 7.39-7.41 (br d, 1H, NH-pyrrolidine), 7.46 (s, 1H, C$_5$-H quinazoline ring). ^{13}C-NMR (176 MHz; DMSO-d_6) δ 24.59, 30.31, 37.33, 42.43 (2C), 50.18, 52.14, 54.51, 56.54, 56.84, 57.21, 57.54,

98.60, 102.57, 106.48, 129.21 (2C), 129.71, 131.05 (2C), 131.65, 135.91, 147.08, 152.73, 155.90, 159.72. MS (ESI) *m/z:* 465 [M + H]$^+$. HR-MS (ESI) *m/z*: calcd for C$_{26}$H$_{37}$N$_6$O$_2^+$ [M + H]$^+$, 465.2973; found, 465.2954.

N^4-((1-benzylpiperidin-4-yl)methyl)-N^2-(3-(dimethylamino)propyl)-6,7-dimethoxyquinazoline-2,4-diamine (14). Yield, 71%; mp 185-186 °C. ^{1}H-NMR (400 MHz; DMSO-*d$_6$*) *δ* 1.16-1.27 (m, 2H, 2 × C*H* piperidine ring), 1.63-1.71 (m, 5H, NHCH$_2$C*H$_2$*CH$_2$N(CH$_3$)$_2$, 2 × C*H* piperidine ring and C$_4$-*H*-piperidine), 1.87-1.92 (br t, 2H, 2 × C*H* piperidine ring), 2.12 (s, 6H, N(C*H$_3$*)$_2$), 2.25 (m, *J*=8 Hz, 2H, NHCH$_2$CH$_2$C*H$_2$*N(CH$_3$)$_2$), 2.79-2.82 (br d, 2H, 2 × C*H* piperidine ring), 3.23-3.41 (m, 4H, NHC*H$_2$*-piperidine and NHC*H$_2$*CH$_2$CH$_2$N(CH$_3$)$_2$ and 3.43 (s, 2H, NC*H$_2$*Ph), 3.78 (s, 3H, OC*H$_3$*), 3.80 (s, 3H, OC*H$_3$*), 6.12 (br t, 1H, N*H*CH$_2$CH$_2$CH$_2$N(CH$_3$)$_2$), 6.59 (s, 1H, C$_8$-*H* quinazoline ring), 7.21-7.23 (m, 1H, C*H* benzene ring), 7.27-7.33 (m, 4H, C*H* benzene ring), 7.40 (s, 1H, C$_5$-*H* quinazoline ring), 7.52 (br s, 1H, N*H*CH$_2$-piperidine). ^{13}C-NMR (176 MHz; DMSO-*d$_6$*) *δ* 24.54, 27.16 (2C), 34.03, 42.42 (2C), 46.15, 51.48 (2C), 54.59, 56.53, 57.04, 59.29, 65.39, 98.51, 102.58, 105.58, 129.15 (2C), 129.80, 130.44, 131.91 (2C), 135.64, 147.03, 152.82, 155.67, 159.87. MS (ESI) *m/z:* 493 [M + H]$^+$. HR-MS (ESI) *m/z*: calcd for C$_{28}$H$_{41}$N$_6$O$_2^+$ [M + H]$^+$, 493.3286; found, 493.3271.

N^2-(3-(dimethylamino)propyl)-6,7-dimethoxy-N^4-(3-(phenylamine)propyl)quinazolin-2,4-diamine (15). Yield, 71%; mp 102-105 °C. ^{1}H-NMR (400 MHz; DMSO-*d$_6$*) *δ* 1.68-1.75 (m, 2H, NHCH$_2$C*H$_2$*CH$_2$N(CH$_3$)$_2$), 1.93-2.00 (m, 2H, NHCH$_2$C*H$_2$*CH$_2$NHPh), 2.18 (s, 6H, N(C*H$_3$*)$_2$), 2.31 (t, *J*=8 Hz, 2H, NHCH$_2$CH$_2$C*H$_2$*N(CH$_3$)$_2$), 3.12-3.17 (m, 2H, NHCH$_2$CH$_2$C*H$_2$*NHPh), 3.31-3.36 (m, 2H, NHC*H$_2$*CH$_2$CH$_2$N(CH$_3$)$_2$), 3.57-3.63 (m, 2H, NHC*H$_2$*CH$_2$CH$_2$NHPh), 3.84 (s, 3H, OC*H$_3$*), 3.87 (s, 3H, OC*H$_3$*), 5.63 (t, *J*=5 Hz, 1H, CH$_2$CH$_2$CH$_2$N*H*Ph), 6.18 (br t, 1H, N*H*CH$_2$CH$_2$CH$_2$N(CH$_3$)$_2$), 6.54-6.58 (m, 1H, C*H* benzene ring), 6.62-6.64 (m, 2H, 2 × C*H*

benzene ring), 6.73 (s, 1H, C_8-*H* quinazoline ring), 7.09-7.13 (m, 2H, C*H* benzene ring), 7.45 (s, 1H, C_5-*H* quinazoline ring), 7.60 (br m, 1H, N*H*CH$_2$CH$_2$CH$_2$NHPh). ^{13}C-NMR (176 MHz; DMSO-d_6) δ 24.53, 25.94, 38.34, 39.02, 42.48 (2C), 47.40, 54.64, 56.52, 57.01, 98.63, 99.85, 102.64, 105.56, 121.62, 130.11 (2C), 135.56 (2C), 146.95, 147.01, 152.90, 155.61, 159.66. MS (ESI) *m/z:* 439 [M + H]$^+$. HR-MS (ESI) *m/z:* calcd for $C_{24}H_{35}N_6O_2^+$ [M + H]$^+$, 439.2816; found, 439.2805.

N^2-(3-(dimethylamino)propyl)-6,7-dimethoxy-N^4-(2-(naphthalen-1-ylamino)ethyl)quinazoline-2,4-diamine (16). Yield, 68%; mp 109-110 °C. ^{1}H-NMR (400 MHz; DMSO-d_6) δ 1.68-1.75 (m, 2H, NHCH$_2$C*H$_2$*CH$_2$N(CH$_3$)$_2$), 2.12 (s, 6H, N(C*H$_3$*)$_2$), 2.27-2.30 (t, *J*=8 Hz, 2H, NHCH$_2$CH$_2$C*H$_2$*N(CH$_3$)$_2$), 3.34-3.39 (m, 2H, NHC*H$_2$*CH$_2$CH$_2$N(CH$_3$)$_2$), 3.48-3.51 (m, 2H, NHCH$_2$C*H$_2$*NH-naphthalene), 3.79 (s, 3H, OC*H$_3$*), 3.82-3.86 (m, 5H, OC*H$_3$* and NH-C*H$_2$*CH$_2$NH-naphthalene), 6.26 (t, *J*=6 Hz, 1H, NHCH$_2$CH$_2$N*H*-naphthalene), 6.38-6.41 (br t, 1H, N*H*CH$_2$CH$_2$CH$_2$N(CH$_3$)$_2$), 6.64 (d, 1H, C*H* naphthalene ring), 6.71(s, 1H, C_8-*H* quinazoline ring), 7.10 (d, 1H, C*H* naphthalene ring), 7.28-7.44 (m, 4H, C_5-*H* quinazoline ring and 3 x C*H* naphthalene ring), 7.75 (d, 1H, C*H* naphthalene ring), 7.81 (br t, 1H, N*H*-CH$_2$CH$_2$-NH-naphthalene), 8.06 (d, 1H, C*H* naphthalene ring). ^{13}C-NMR (176 MHz; DMSO-d_6) δ 24.48, 38.28, 42.41 (2C), 43.39, 54.61, 56.51, 57.12, 65.39, 98.71, 102.76, 105.76, 118.19, 122.49, 123.91, 124.93, 125.38, 126.34, 127.07, 128.49, 134.57, 135.58, 142.61, 147.02, 152.95, 155.68, 159.86. MS (ESI) *m/z:* 475 [M + H]$^+$. HR-MS (ESI) *m/z:* calcd for $C_{27}H_{35}N_6O_2^+$ [M + H]$^+$ 475.2816; found, 475.2808.

N^4-(1-benzylpiperidin-4-yl)-N^2-(2-(dimethylamino)ethyl)-6,7-dimethoxyquinazoline-2,4-diamine (17). Yield, 63%; mp 95-97 °C. ^{1}H-NMR (400 MHz; DMSO-d_6) δ 1.58-1.68 (m, 2H, 2 × C*H* piperidine ring), 1.88-1.92 (br d, 2H, 2 × C*H* piperidine ring), 1.99-2.06 (br t, 2H, 2 × C*H*

piperidine ring), 2.17 (s, 6H, N(CH_3)$_2$), 2.39 (t, J=7 Hz, 2H, NHCH$_2$CH_2N(CH$_3$)$_2$), 2.86-2.89 (br

d, 2H, 2 × CH piperidine ring), 3.27-3.31 (m, 2H, NHCH_2CH$_2$N(CH$_3$)$_2$), 3.50 (s, 2H, NCH_2Ph),

3.80 (s, 3H, OCH_3), 3.81 (s, 3H, OCH_3), 4.08-4.15 (br m, 1H, C$_4$-H piperidine), 5.89 (br s, 1H,

NHCH$_2$CH$_2$N(CH$_3$)$_2$), 6.66 (s, 1H, C$_8$-H quinazoline ring), 7.20 (br d, 1H, NH), 7.23-7.24 (m,

1H, CH benzene ring), 7.26-7.34 (m, 4H, benzene ring protons), 7.42 (s, 1H, C$_5$-H quinazoline

ring). ^{13}C-NMR (176 MHz; DMSO-d_6) δ 28.47 (2C), 36.21, 42.82 (2C), 47.30, 50.70 (2C),

55.37, 56.55, 57.09, 59.51, 98.69, 102.58, 105.60, 129.26 (2C), 129.35 (2C), 129.92, 131.48,

135.91, 147.16, 152.66, 155.81, 159.18. MS (ESI) *m/z:* 465 [M + H]$^+$. HR-MS (ESI) *m/z*: calcd

for C$_{26}$H$_{37}$N$_6$O$_2^+$ [M + H]$^+$, 465.2973; found, 465.2954.

N^4-(1-benzylpiperidin-4-yl)-N^2-(4-(dimethylamino)butyl)-6,7-dimethoxyquinazoline-2,4-

diamine (18). Yield, 65%; mp 78-80 °C. ^{1}H-NMR (400 MHz; DMSO-d_6) δ 1.39-1.51 (m, 4H,

NHCH$_2$CH_2CH_2CH$_2$N(CH$_3$)$_2$), 1.55-1.68 (m, 2H, 2 × CH piperidine ring), 1.90-1.92 (br d, 2H, 2

× CH piperidine ring), 2.01-2.06 (br t, 2H, 2 × CH piperidine ring), 2.10 (s, 6H, N(CH_3)$_2$), 2.19

(t, J=7 Hz, 2H, NHCH$_2$CH$_2$CH$_2$CH_2N(CH$_3$)$_2$), 2.87-2.90 (br d, 2H, 2 × CH piperidine ring),

3.22-3.25 (m, 2H, NHCH_2CH$_2$CH$_2$CH$_2$N(CH$_3$)$_2$), 3.50 (s, 2H, NCH_2Ph), 3.80 (s, 3H, OCH_3),

3.81 (s, 3H, OCH_3), 4.10-4.12 (br m, 1H, C$_4$-H piperidine), 6.20 (br t, 1H,

NHCH$_2$CH$_2$CH$_2$CH$_2$N(CH$_3$)$_2$), 6.65 (s, 1H, C$_8$-H quinazoline ring), 7.18-7.19 (br d, 1H, NH),

7.2-7.25 (m, 1H, CH benzene ring), 7.26-7.36 (m, 4H, CH benzene ring), 7.41 (s, 1H, C$_5$-H

quinazoline ring). ^{13}C-NMR (176 MHz; DMSO-d_6) δ 21.95, 26.74, 28.25 (2C), 42.29 (2C),

42.42, 48.05, 50.80 (2C), 56.47, 56.53, 57.06, 59.03, 98.62, 102.33, 105.66, 129.19 (2C), 129.85,

130.67, 132.01 (2C), 135.91, 146.99, 152.75, 155.79, 159.25. MS (ESI) *m/z:* 493 [M + H]$^+$. HR-

MS (ESI) *m/z*: calcd for C$_{28}$H$_{41}$N$_6$O$_2^+$ [M + H]$^+$, 493.3286; found, 493.3263.

N⁴-(1-benzylpiperidin-4-yl)-N²-(5-(dimethylamino)pentyl)-6,7-dimethoxyquinazoline-2,4-

diamine (19). Yield, 40%; mp 158-161 °C. ^{1}H-NMR (400 MHz; DMSO-d_6) δ 1.35-1.39 (m, 2H, NHCH₂CH₂CH_2CH₂CH₂N(CH₃)₂), 1.43-1.49 (m, 2H, NHCH₂CH₂CH₂CH_2CH₂N(CH₃)₂), 1.50-1.56 (m, 2H, NHCH₂CH_2CH₂CH₂CH₂N(CH₃)₂), 1.58-1.64 (m, 2H, 2 × C*H* piperidine ring), 1.89-1.96 (br d, 2H, 2 × C*H* piperidine ring), 2.06-2.12 (m, 2H, 2 × C*H* piperidine ring), 2.14 (s, 6H, NHCH₂CH₂CH₂CH₂CH₂N(CH_3)₂), 2.22 (t, *J*=7 Hz, 2H, NHCH₂CH₂CH₂CH₂CH_2N(CH₃)₂), 2.92-2.95 (m, 2H, 2 × C*H* piperidine ring), 3.27-3.32 (m, 2H, NHCH_2CH₂CH₂CH₂CH₂N(CH₃)₂), 3.56 (s, 2H, NCH_2Ph), 3.85 (s, 3H, OCH_3), 3.86 (s, 3H, OCH_3), 4.15-4.18 (br m, 1H, C₄-*H* piperidine), 6.18 (br t, 1H, N*H*(CH₂)₅N(CH₃)₂), 6.70 (s, 1H, C₈-*H* quinazoline ring), 7.22-7.24 (br d, 1H, N*H*), 7.29-7.31 (m, 1H, C*H* benzene ring), 7.33-7.38 (m, 4H, C*H* benzene ring), 7.46 (s, 1H, C₅-*H* quinazoline ring). ^{13}C-NMR (176 MHz; DMSO-d_6) δ 23.82, 28.23, 28.96 (2C), 31.78, 40.77, 42.39 (2C), 47.96, 50.79 (2C), 56.53, 56.75, 57.05, 59.11, 98.09, 102.75, 105.66, 129.22 (2C), 129.91, 131.55, 132.04 (2C), 135.87, 146.98, 152.83, 155.78, 159.27. MS (ESI) *m/z:* 507 [M + H]⁺. HR-MS (ESI) *m/z*: calcd for $C_{29}H_{43}N_6O_2^+$ [M + H]⁺, 507.3442; found, 507.3416 [M + H]⁺.

N²-(3-(benzyl(methyl)amino)propyl)-N⁴-(1-benzylpiperidin-4-yl)-6,7-dimethoxy quinazoline-

2,4-diamine (20). Yield, 69%; mp 79-82 °C. ^{1}H-NMR (400 MHz; DMSO-d_6) δ 1.56-1.69 (m, 2H, 2 × C*H* piperidine ring), 1.70-1.76 (m, 2H, NHCH₂CH_2CH₂N), 1.84-1.95 (br d, 2H, 2 × C*H* piperidine ring), 1.95-2.06 (br t, 2H, 2 × C*H* piperidine ring), 2.09 (s, 3H, NCH_3), 2.39 (t, *J*=7 Hz, 2H, NHCH₂CH₂CH_2N), 2.85-2.88 (m, 2H, CH_2 piperidine ring), 3.25-3.31 (m, 2H, NHCH_2CH₂CH₂N), 3.46 (s, 2H, N(CH₃)CH_2Ph), 3.49 (s, 2H, NCH_2Ph), 3.77 (s, 3H, OCH_3), 3.79 (s, 3H, OCH_3), 4.02-4.12 (br m, 1H, C₄-*H* piperidine), 6.16 (br t, 1H, N*H*CH₂CH₂CH₂N), 6.63 (s, 1H, C₈-*H* quinazoline ring), 7.17-7.21 (br d, 1H, N*H*), 7.22-7.25 (m, 2H, C*H* benzene

ring), 7.26-7.36 (m, 8H, CH benzene rings), 7.41 (s, 1H, C$_5$-H quinazoline ring). ^{13}C-NMR (176 MHz; DMSO-d_6) δ 24.31, 28.36 (2C), 38.53, 39.08, 47.84, 50.80 (2C), 52.65, 56.54, 57.08, 58.46, 59.29, 98.72, 102.44, 105.62, 129.13, 129.20 (2C), 129.32, 129.76 (2C), 129.86, 130.64, 131.75 (2C), 131.99 (2C), 135.90, 147.04, 152.77, 155.80, 159.22. MS (ESI) *m/z:* 555 [M + H]$^+$. HR-MS (ESI) *m/z*: calcd for C$_{33}$H$_{43}$N$_6$O$_2^+$ [M + H]$^+$, 555.3442; found, 555.3428.

N^4-(1-benzylpiperidin-4-yl)-6,7-dimethoxy-N^2-(3-(methyl(prop-2-yn-1-yl)amino)propyl) quinazoline-2,4-diamine (21). Yield, 64%; mp 85-88 °C. ^{1}H-NMR (400 MHz; DMSO-d_6) δ 1.59-1.68 (m, 4H, 2 × CH piperidine ring and NHCH$_2$CH_2CH$_2$N), 1.87-1.92 (m, 2H, 2 × CH piperidine ring), 1.99-2.07 (br t, 2H, 2 × CH piperidine ring), 2.19 (s, 3H, NCH_3), 2.38 (t, *J*=7 Hz, 2H, NHCH$_2$CH$_2$CH_2N(CH$_3$)$_2$), 2.87-2.89 (br d, 2H, 2 × CH piperidine ring), 3.10 (t, *J*=2 Hz, 1H, CH$_2$-C≡CH), 3.23-3.27 (m, 2H, NHCH_2CH$_2$CH$_2$N(CH$_3$)$_2$), 3.31 (d, *J*=2 Hz, 2H, CH_2-C≡CH), 3.51 (s, 2H, NCH_2Ph), 3.78 (s, 3H, OCH_3), 3.81 (s, 3H, OCH_3), 4.10-4.13 (br m, 1H, C$_4$-H piperidine), 6.15 (br t, 1H, NHCH$_2$CH$_2$CH$_2$N(CH$_3$)$_2$), 6.66 (s, 1H, C$_8$-H quinazoline ring), 7.18 (br d, 1H, NH), 7.25-7.28 (m, 1H, CH benzene ring), 7.29-7.34 (m, 4H, CH benzene ring), 7.41 (s, 1H, C$_5$-H quinazoline ring). ^{13}C-NMR (176 MHz; DMSO-d_6) δ 27.95, 32.19 (2C), 40.49, 41.76, 45.43, 47.85, 53.02 (2C), 53.54, 55.76, 56.52, 62.61, 76.09, 79.61, 103.90, 105.51, 108.06, 127.32, 128.63 (2C), 129.19 (2C), 139.10, 144.75, 149.22, 154.13, 158.81, 159.40. MS (ESI) *m/z:* 503 [M + H]$^+$. HR-MS (ESI) *m/z*: calcd for C$_{29}$H$_{39}$N$_6$O$_2^+$ [M + H]$^+$, 503.3129; found, 503.3120.

N^4-(1-benzylpiperidin-4-yl)-N^2-(3-(diethylamino)propyl)-6,7-dimethoxyquinazoline-2,4-diamine (22). Yield, 75%; mp 89-91 °C. ^{1}H-NMR (400 MHz; DMSO-d_6) δ 0.93-1.00 (t, *J*=7 Hz, 6H, N(CH$_2$CH_3)$_2$), 1.58-1.66 (m, 4H, 2 × CH piperidine ring e NHCH$_2$CH_2CH$_2$N), 1.91-1.93 (br d, 2H, 2 × CH piperidine ring), 2.03 (br t, 2H, 2 × CH piperidine ring), 2.43-2.50 (m, 6H,

N(CH_2CH$_3$)$_2$ and NHCH$_2$CH$_2$CH_2N), 2.88 (br d, 2H, 2 × CH piperidine ring), 3.23-3.29 (m, 2H,

NHCH_2CH$_2$CH$_2$N), 3.50 (s, 2H, NCH_2Ph), 3.80 (s, 3H, OCH_3), 3.81 (s, 3H, OCH_3), 4.06-4.11

(br m, 1H, C$_4$-H piperidine), 6.23 (t, J=6 Hz, 1H, NHCH$_2$CH$_2$CH$_2$N), 6.65 (s, 1H, C$_8$-H

quinazoline ring), 7.18 (br d, 1H, NH), 7.24-7.28 (m, 1H, CH benzene ring), 7.31-7.36 (m, 4H,

CH benzene ring), 7.41 (s, 1H, C$_5$-H quinazoline ring). ^{13}C-NMR (176 MHz; DMSO-d_6) δ 15.64

(2C), 24.03, 28.34 (2C), 38.62, 46.43 (2C), 48.75, 50.80 (2C), 56.53, 57.06, 59.34, 65.39, 98.62,

102.41, 105.60, 129.21 (2C), 129.89 (2C), 130.46, 131.99, 135.90, 147.04, 152.85, 155.78,

159.27. MS (ESI) m/z: 507 [M + H]$^+$. HR-MS (ESI) m/z: calcd for C$_{29}$H$_{43}$N$_6$O$_2$$^+$ [M + H]$^+$,

507.3442; found, 507.3417.

N^4-(1-benzylpiperidin-4-yl)-6,7-dimethoxy-N^2-(3-(pyrrolidin-1-yl)propyl)quinazoline-2,4-

diamine (23). Yield, 72%; mp 90-92 °C. ^{1}H-NMR (400 MHz; DMSO-d_6) δ 1.54-1.71 (m, 8H, 2

× CH piperidine ring, 4 × CH pyrrolidine ring and NHCH$_2$CH_2CH$_2$N), 1.84-1.91 (m, 2H, 2 × CH

piperidine ring), 1.96-2.05 (br t, 2H, 2 × CH piperidine ring), 2.36-2.43 (m, 6H, 4 × CH

pyrrolidine ring and NHCH$_2$CH$_2$CH_2N), 2.86 (br d, 2H, 2 × CH piperidine ring), 3.22-3.26 (m,

2H, NHCH_2CH$_2$CH$_2$N), 3.48 (s, 2H, NCH_2Ph), 3.77 (s, 3H, OCH_3), 3.78 (s, 3H, OCH_3), 4.07 (br

m, 1H, C$_4$-H piperidine), 6.19 (t, J=8 Hz, 1H, NHCH$_2$CH$_2$CH$_2$-pyrrolidine), 6.63 (s, 1H, C$_8$-H

quinazoline ring), 7.15-7.18 (br d, 1H, NH), 7.22-7.26 (m, 1H, CH benzene ring), 7.28-7.35 (m,

4H, CH benzene ring), 7.39 (s, 1H, C$_5$-H quinazoline ring). ^{13}C-NMR (176 MHz; DMSO-d_6) δ

23.21 (2C), 25.97, 28.38 (2C), 38.69, 47.76, 50.80, 51.87 (2C), 53.22 (2C), 56.53, 57.06, 59.35,

98.68, 102.42, 105.59, 129.22 (2C), 129.34 (2C), 129.89, 132.00, 135.92, 147.04, 152.77,

155.80, 159.27. MS (ESI) m/z: 505 [M + H]$^+$. HR-MS (ESI) m/z: calcd for C$_{29}$H$_{41}$N$_6$O$_2$$^+$ [M +

H]$^+$, 505.3286; found, 505.3278.

N^4-(1-benzylpiperidin-4-yl)-6,7-dimethoxy-N^2-(3-(piperidin-1-yl)propyl)quinazoline-2,4-diamine (24). Yield, 70%; mp 91-93 °C. ^{1}H-NMR (400 MHz; DMSO-d_6) δ 1.44-1.45 (m, 2H, 2 x C*H* piperidine ring), 1.55-1.58 (m, 4H, 4 × C*H* piperidine ring), 1.64-1.75 (m, 4H, 2 × C*H* piperidine ring and NHCH$_2$C*H$_2$*CH$_2$-piperidine), 1.96-1.99 (br d, 2H, 2 × C*H* piperidine ring), 2.05-2.11 (br t, 2H, 2 × C*H* piperidine ring), 2.35-2.38 (m, 6H, 4 × C*H* piperidine ring and NHCH$_2$CH$_2$C*H$_2$*N), 2.94 (br d, 2H, 2 × C*H* piperidine ring), 3.30-3.35 (m, 2H, NHC*H$_2$*CH$_2$CH$_2$-piperidine), 3.56 (s, 2H, NC*H$_2$*Ph), 3.85 (s, 3H, OC*H$_3$*), 3.86 (s, 3H, OC*H$_3$*), 4.13-4.15 (br m, 1H, C$_4$-*H* piperidine), 6.41 (br m, 1H, N*H*CH$_2$CH$_2$CH$_2$R), 6.72 (s, 1H, C$_8$-*H* quinazoline ring), 7.22 (br d, 1H, N*H*), 7.29-7.31 (m, 1H, C*H* benzene ring), 7.33-7.41 (m, 4H, benzene ring), 7.47 (s, 1H, C$_5$-*H* quinazoline ring). ^{13}C-NMR (176 MHz; DMSO-d_6) δ 21.78, 22.79 (2C), 24.05, 28.33 (2C), 38.46, 47.52, 50.84 (2C), 52.39, 53.93, 56.58 (2C), 57.06, 59.36, 98.67, 102.27, 105.46, 129.28 (2C), 130.00, 130.31, 131.95 (2C), 135.74, 147.09, 152.54, 155.87, 159.20. MS (ESI) *m/z:* 519 [M + H]$^+$. HR-MS (ESI) *m/z*: calcd for C$_{30}$H$_{43}$N$_6$O$_2$$^+$ [M + H]$^+$, 519.3442; found, 519.3433.

N^4-(1-benzylpiperidin-4-yl)-6,7-dimethoxy-N^2-(3-morpholinopropyl)quinazoline-2,4-diamine (25). Yield, 60%; mp 98-100 °C. ^{1}H-NMR (400 MHz; DMSO-d_6) δ 1.60-1.71 (m, 4H, 2 × C*H* piperidine ring and NHCH$_2$C*H$_2$*CH$_2$-morpholine), 1.91 (br d, 2H, 2 × C*H* piperidine ring), 2.03 (br t, 2H, 2 × C*H* piperidine ring) 2.32-2.35 (m, 6H, 2 × C*H$_2$* morpholine ring and NHCH$_2$CH$_2$C*H$_2$*-morpholine), 2.88 (br d, 2H, 2 × C*H* piperidine ring), 3.26-3.31 (m, 2H, NHC*H$_2$*CH$_2$CH$_2$-morpholine), 3.51 (s, 2H, NC*H$_2$*Ph), 3.58 (t, 4H, 2 × C*H$_2$* morpholine ring), 3.80 (s, 3H, OC*H$_3$*), 3.81 (s, 3H, OC*H$_3$*), 4.02-4.11 (br m, 1H, C$_4$-*H* piperidine), 6.24 (t, *J*=6 Hz, 1H, N*H*CH$_2$CH$_2$CH$_2$-morpholine), 6.65 (s, 1H, C$_8$-*H* quinazoline ring), 7.17 (br d, 1H, N*H*), 7.24-7.25 (m, 1H, C*H* benzene ring), 7.31-7.36 (m, 4H, C*H* benzene ring), 7.41 (s, 1H, C$_5$-*H*

quinazoline ring). ^{13}C-NMR (176 MHz; DMSO-d_6) δ 23.71, 28.36 (2C), 38.59, 47.81, 50.84 (2C), 51.48, 54.06, 56.54 (2C), 57.06, 59.34, 63.62 (2C), 98.72, 102.45, 105.56, 129.24 (2C), 129.92, 131.51 (2C), 131.99, 135.95, 147.07, 152.72, 155.82, 159.27. MS (ESI) *m/z:* 521 [M + H]$^+$. HR-MS (ESI) *m/z*: calcd for C$_{29}$H$_{41}$N$_6$O$_3^+$ [M + H]$^+$, 521.3235; found, 521.3231.

N^4-(1-benzylpiperidin-4-yl)-6,7-dimethoxy-N^2-(3-(4-methylpiperazin-1-yl)propyl)quinazoline-2,4-diamine (26). Yield, 63%; mp 94-97 °C. ^{1}H-NMR (400 MHz; DMSO-d_6) δ 1.64-1.79 (m, 4H, 2 × C*H* piperidine ring and NHCH$_2$C*H$_2$*CH$_2$-piperazine), 1.90-1.93 (br d, 2H, 2 × C*H* piperidine ring), 2.05 (br t, 2H, NHCH$_2$CH$_2$C*H$_2$*-piperazine), 2.16 (s, 3H, NC*H$_3$*), 2.30-2.36, (m, 10H, 8 × C*H* piperazine ring and NHCH$_2$CH$_2$C*H$_2$*-piperazine), 2.88 (br d, 2H, 2 × C*H* piperidine ring), 3.25-3.30 (m, 2H, 2 × C*H* piperidine ring), 3.51 (s, 2H, NC*H$_2$*Ph), 3.80 (s, 3H, OC*H$_3$*), 3.81 (s, 3H, OC*H$_3$*), 4.09-4.13 (br m, 1H, C$_4$-*H* piperidine), 6.26 (t, *J*=5 Hz, 1H, N*H*CH$_2$CH$_2$CH$_2$-piperazine), 6.66 (s, 1H, C$_8$-*H* quinazoline ring), 7.19 (br d, 1H, N*H*), 7.24-7.28 (m, 1H, C*H* benzene ring), 7.30-7.36 (m, 4H, C*H* benzene ring), 7.41 (s, 1H, C$_5$-*H* quinazoline ring). ^{13}C-NMR (176 MHz; DMSO-d_6) δ 23.98, 28.35 (2C), 38.58, 42.51, 47.84, 48.49, 50.07, 50.87 (2C), 54.06, 56.53 (2C), 57.07 (2C), 59.39, 98.64, 102.43, 105.63, 129.21 (2C), 129.86, 131.50, 132.04 (2C), 135.90, 147.02, 152.81, 155.78, 159.26. MS (ESI) *m/z:* 534 [M + H]$^+$. HR-MS (ESI) *m/z*: calcd for C$_{30}$H$_{44}$N$_7$O$_2^+$ [M + H]$^+$, 534.3551; found, 534.3541.

N^4-(1-benzylpiperidin-4-yl)-6,7-dimethoxy-N^2-(1-methylpiperidin-4-yl)quinazoline-2,4-diamine (27). Yield, 43%; mp 103-106 °C. ^{1}H-NMR (400 MHz; DMSO-d_6) δ 1.43-1.58 (m, 2H, 2 × C*H* methylpiperidine ring), 1.59-1.64 (m, 2H, 2 × C*H* piperidine ring), 1.65-1.67 (m, 2H, 2 × C*H* methylpiperidine ring), 1.81-1.95 (m, 4H, 2 × C*H* piperidine and 2 × C*H* methylpiperidine ring), 2.06-2.09 (m, 2H, 2 × C*H* piperidine ring), 2.16 (s, 3H, NC*H$_3$*), 2.73 (br d, 2H, 2 × C*H* methylpiperidine ring), 2.88 (br d, 2H, 2 × C*H* piperidine ring), 3.51 (s, 2H, NC*H$_2$*Ph), 3.68-3.79

(br m, 1H, C$_4$-H methylpiperidine), 3.79 (s, 3H, OCH_3), 3.81 (s, 3H, OCH_3), 4.02-4.10 (br m, 1H, C$_4$-H piperidine), 5.97 (br d, J=7 Hz, 1H, NH-methylpiperidine), 6.64 (s, 1H, C$_8$-H quinazoline ring), 7.19-7.24 (br m, 1H, NH), 7.25-7.28 (m, 1H, CH benzene ring), 7.31-7.36 (m, 4H, CH benzene ring), 7.41 (s, 1H, C$_5$-H quinazoline ring). ^{13}C-NMR (176 MHz; DMSO-d_6) δ 28.42 (2C), 29.24 (2C), 42.83, 47.94, 49.29, 50.66, 52.53, 56.14 (2C), 57.02 (2C), 59.08, 98.93, 102.44, 105.57, 129.21, 129.92 (2C), 130.73, 132.68 (2C), 138.37, 147.13, 152.09, 155.98, 159.12. MS (ESI) m/z: 491 [M + H]$^+$. HR-MS (ESI) m/z: calcd for C$_{28}$H$_{39}$N$_6$O$_2^+$ [M + H]$^+$, 491.3129; found, 491.3129.

N^4-(1-benzylpiperidin-4-yl)-N^2-(3-(dimethylamino)propyl)-6,7-dimethoxy-N2-methyl

quinazoline-2,4-diamine (28). Yield, 66%; mp 78-81 °C. ^{1}H-NMR (400 MHz; DMSO-d_6) δ 1.58-1.69 (m, 4H, 2 × CH piperidine ring and N(CH$_3$)CH$_2$CH_2CH$_2$N(CH$_3$)$_2$), 1.97 (br d, 2H, 2 × CH piperidine ring), 2.06 (br t, 2H, 2 × CH piperidine ring), 2.11 (s, 6H, N(CH$_3$)CH$_2$CH$_2$CH$_2$N(CH_3)$_2$), 2.20 (t, J=7 Hz, 2H, N(CH$_3$)CH$_2$CH$_2$CH_2N(CH$_3$)$_2$), 2.89 (br d, 2H, 2 × CH piperidine ring), 3.06 (s, 3H, N(CH_3)CH$_2$CH$_2$CH$_2$N(CH$_3$)$_2$), 3.51 (s, 2H, NCH_2Ph), 3.56 (t, J=7 Hz, 2H, N(CH$_3$)CH_2CH$_2$CH$_2$N(CH$_3$)$_2$), 3.80 (s, 3H, OCH_3), 3.82 (s, 3H, OCH_3), 3.99-4.06 (br m, 1H, C$_4$-H piperidine), 6.69 (s, 1H, C$_8$-H quinazoline ring), 7.25 (br d, 1H, NH), 7.27-7.29 (m, 1H, CH benzene ring), 7.31-7.36 (m, 4H, CH benzene ring), 7.42 (s, 1H, C$_5$-H quinazoline ring). ^{13}C-NMR (176 MHz, DMSO) δ 25.95, 32.08 (2C), 35.27, 45.76 (2C), 47.47, 48.67, 53.09 (2C), 55.78, 56.50, 57.53, 62.69, 103.20, 103.75, 105.73, 127.34, 128.63 (2C), 129.23 (2C), 139.03, 144.83, 149.38, 154.20, 158.58, 158.81. MS (ESI) m/z: 493 [M + H]$^+$. HR-MS (ESI) m/z: calcd, for C$_{28}$H$_{41}$N$_6$O$_2^+$ [M + H]$^+$ 493.3286; found, 493.3263.

7-(benzyloxy)-N^4-(1-benzylpiperidin-4-yl)-N^2-(3-(dimethylamino)propyl)-6-methoxy

quinazoline-2,4-diamine (29). Yield, 78%; mp 149-152 °C. ^{1}H-NMR (400 MHz; DMSO-d_6) δ

1.55-1.65 (m, 4H, 2 x C*H* piperidine ring and NHCH$_2$C*H*$_2$CH$_2$N(CH$_3$)$_2$), 1.91 (br d, 2H, 2 × C*H*

piperidine ring), 1.92-2.01-2.03 (br t, 2H, 2 × C*H* piperidine ring), 2.11 (s, 6H, N(C*H*$_3$)$_2$), 2.23 (t,

J=7 Hz, 2H, NHCH$_2$CH$_2$C*H*$_2$N(CH$_3$)$_2$), 2.88 (br d, 2H, 2 × C*H* piperidine ring), 3.22-3.27 (m,

2H, NHC*H*$_2$CH$_2$CH$_2$N(CH$_3$)$_2$), 3.52 (s, 2H, NC*H*$_2$Ph), 3.81 (s, 3H, OC*H*$_3$), 4.10-4.12 (br m, 1H,

C$_4$-*H* piperidine), 5.16 (s, 2H, OC*H*$_2$Ph), 6.17 (br t, 1H, N*H*CH$_2$CH$_2$CH$_2$N(CH$_3$)$_2$), 6.75 (s, 1H,

C$_8$-*H* quinazoline ring), 7.19-7.21 (br d, 1H, N*H*-piperidine), 7.24-7.28 (m, 1H, C*H* benzene

ring), 7.31-7.36 (m, 5H, C*H* benzene ring), 7.39-7.47 (m, 5H, C*H* benzene ring and C$_5$-*H*

quinazoline ring). ^{13}C-NMR (176 MHz; DMSO-d_6) δ 28.11, 32.17 (2C), 40.49, 45.75 (2C),

48.00, 53.02 (2C), 56.61, 57.72, 62.62, 69.93, 104.16, 105.70, 106.92, 127.33, 128.23, 128.34

(2C), 128.63 (2C), 128.91 (2C), 129.19 (2C), 137.31, 139.08, 144.89, 149.16, 153.08, 158.80,

159.43. MS (ESI) *m/z:* 555 [M + H]$^+$. HR-MS (ESI) *m/z*: calcd for C$_{33}$H$_{43}$N$_6$O$_2$$^+$ [M + H]$^+$,

555.3442; found, 555.3423.

7-(benzyloxy)-N^2-(3-(dimethylamino)propyl)-6-methoxy-N^4-(2-(naphthalen-1-

ylamino)ethyl)quinazoline-2,4-diamine (30). Yield, 61%; mp 117-118 °C. ^{1}H-NMR (400 MHz;

DMSO-d_6) δ 1.66-1.71 (m, 2H, NHCH$_2$C*H*$_2$CH$_2$N(CH$_3$)$_2$), 2.10 (s, 6H, N(C*H*$_3$)$_2$), 2.26 (t, *J*=8

Hz, 2H, NHCH$_2$CH$_2$C*H*$_2$N(CH$_3$)$_2$), 3.32-3.38 (m, 2H, NHC*H*$_2$CH$_2$CH$_2$N(CH$_3$)$_2$), 3.46-3.50 (m,

2H, NHCH$_2$C*H*$_2$NH-naphthalene), 3.79-3.83 (m, 5H, OC*H*$_3$ and NHC*H*$_2$CH$_2$NH-naphthalene),

5.16 (s, 2H, OC*H*$_2$Ph), 6.23-6.25 (br t, 1H, NHCH$_2$CH$_2$N*H*-naphthalene), 6.39 (br t, 1H,

N*H*CH$_2$CH$_2$CH$_2$N(CH$_3$)$_2$), 6.61 (d, 1H, C*H* naphthalene ring), 6.79 (s, 1H, C$_8$-*H* quinazoline

ring), 7.07-7.10 (d, 1H C*H* naphthalene ring), 7.26-7.41 (m, 9H, 5 × C*H* benzene ring, C$_5$-*H*

quinazoline ring and 3 × C*H* naphthalene ring), 7.72-7.75 (m, 1H, C*H* naphthalene ring), 7.82 (br

t, 1H, N*H*-CH$_2$CH$_2$-NH-naphthalene), 8.03-8.06 (br d, 1H, C*H* naphthalene ring). ^{13}C-NMR (176 MHz; DMSO-*d$_6$*) δ 24.46, 31.78, 38.28, 42.42 (2C), 42.99, 54.62, 57.13, 70.66, 99.90, 102.91, 104.79, 105.91, 117.14, 122.43, 123.76, 124.74, 126.27, 127.14, 128.46, 128.61, 128.78 (2C), 129.03 (2C), 134.58, 135.42, 136.14, 143.30, 147.22, 152.96, 154.51, 159.85. MS (ESI) *m/z:* 551 [M + H]$^+$. HR-MS (ESI) *m/z*: calcd for C$_{33}$H$_{39}$N$_6$O$_2^+$ [M + H]$^+$, 551.3129; found, 551.3112.

General Procedure for the Synthesis of 4 and 5. The proper phenylalkyl bromide (0.28 mmol, 1.4 eq.), anhydrous potassium carbonate (0.81 mmol, 4 eq.), and sodium iodide (0.22 mmol, 1.1 eq.) were added in sequence to a solution of **2** (0.20 mmol, 1 eq.) in dry DMF (1.2 mL). The resulting mixture was stirred at room temperature for 48 h. Upon conclusion of the reaction, the solvent was concentrated under vacuum and the resulting crude was poured into a saturated sodium chloride solution (10 mL) and extracted with ethyl acetate (4 × 15 mL). The organic phases were dried over sodium sulphate and concentrated under vacuum to furnish a crude that was purified on alumina column chromatography by eluting with a mixture ethyl acetate/methanol 15:1 to obtain the final compounds **4** and **5**.

N^2-(3-(dimethylamino)propyl)-6,7-dimethoxy-N^4-(1-phenethylpiperidin-4-yl)quinazoline-2,4-diamine (4). Yield, 68%; mp 82-85 °C. ^{1}H-NMR (400 MHz; DMSO-*d$_6$*) δ 1.69-1.75 (m, 4H, 2 × C*H* piperidine ring and NHCH$_2$C*H$_2$*CH$_2$N(CH$_3$)$_2$), 1.99 (br d, 2H, 2 × C*H* piperidine ring), 2.10 (br t, 2H, 2 × C*H* piperidine ring), 2.19 (s, 6H, N(C*H$_3$*)$_2$), 2.31 (t, *J*=7 Hz, 2H, NHCH$_2$CH$_2$C*H$_2$*N(CH$_3$)$_2$), 2.60 (t, *J*=7 Hz, 2H, NCH$_2$C*H$_2$*Ph), 2.81 (t, *J*=7 Hz, 2H, NC*H$_2$*CH$_2$Ph), 3.07 (br d, 2H, 2 × C*H* piperidine ring), 3.29-3.33 (m, 2H, NHC*H$_2$*CH$_2$CH$_2$N(CH$_3$)$_2$), 3.85 (s, 3H, OC*H$_3$*), 3.87 (s, 3H, OC*H$_3$*), 4.15-4.19 (br m, 1H, C$_4$-*H* piperidine), 6.21 (br t, 1H, N*H*CH$_2$CH$_2$CH$_2$N(CH$_3$)$_2$), 6.72 (s, 1H, C$_8$-*H* quinazoline ring), 7.19-7.27 (m, 2H, quinazoline-C$_4$-N*H* and C*H* benzene ring), 7.30-7.36 (m, 4H, C*H* benzene ring),

7.47 (s, 1H, C$_5$-H quinazoline ring). ^{13}C-NMR (176 MHz; DMSO-d_6) δ 24.72, 28.60, 29.98 (2C), 38.52, 42.44 (2C), 47.58, 51.08, 54.60 (2C), 56.56, 57.03, 57.08, 98.71, 102.46, 105.57, 127.29, 129.15 (2C), 129.22 (2C), 135.95, 137.72, 147.07, 152.80, 155.83, 159.28. MS (ESI) *m/z*: 493 [M+H]$^+$. HR-MS (ESI) *m/z*: calcd for C$_{28}$H$_{41}$N$_6$O$_2^+$ [M + H]$^+$, 493.3286; found, 493.3279.

N^2-(3-(dimethylamino)propyl)-6,7-dimethoxy-N^4-(1-(3-phenylpropyl)piperidin-4-yl) *quinazoline-2,4-diamine (5).* Yield, 70%; mp 75-78 °C. ^{1}H-NMR (400 MHz; DMSO-d_6) δ 1.57-1.67 (m, 4H, 2 × CH piperidine ring and NHCH$_2$CH_2CH$_2$N(CH$_3$)$_2$), 1.69-1.74 (m, 2H, CH$_2$CH_2CH$_2$Ph), 1.82-1.92 (m, 4H, 4 × CH piperidine ring), 2.09 (s, 6H, N(CH_3)$_2$), 2.24 (t, *J*=7 Hz, 2H, NHCH$_2$CH$_2$CH_2N(CH$_3$)$_2$), 2.29 (t, *J*=7 Hz, 2H, NCH_2CH$_2$CH$_2$Ph), 2.61 (t, *J*=7 Hz, 2H, CH$_2$CH$_2$CH_2Ph), 2.92 (br d, 2H, 2 × CH piperidine ring), 3.23-3.28 (m, 2H, NHCH_2CH$_2$CH$_2$N(CH$_3$)$_2$), 3.80 (s, 3H, OCH_3), 3.81 (s, 3H, OCH_3), 4.09-4.11 (br m, 1H, C$_4$-H piperidine), 6.16 (br t, 1H, NHCH$_2$CH$_2$CH$_2$N(CH$_3$)$_2$), 6.66 (s, 1H, C$_8$-H quinazoline ring), 7.16-7.23 (m, 4H, quinazoline-C$_4$-NH and 3 x CH benzene ring), 7.27-7.36 (m, 2H, CH benzene ring), 7.42 (s, 1H, C$_5$-H quinazoline ring). ^{13}C-NMR (176 MHz; DMSO-d_6) δ 24.72, 28.53, 29.98 (2C), 31.78, 38.52, 42.54 (2C), 47.58 (2C), 51.07, 54.60, 56.56, 57.03, 57.08, 98.72, 102.47, 105.58, 127.29, 129.15 (2C), 129.18 (2C), 135.95, 137.72, 147.07, 152.77, 155.81, 159.24. MS (ESI) *m/z:* 507 [M + H]$^+$. HR-MS (ESI) *m/z*: calcd for C$_{29}$H$_{43}$N$_6$O$_2^+$ [M + H]$^+$, 507.3442; found, 507.3433.

Procedure for the Synthesis of (4-((2-((3-(dimethylamino)propyl)amino)-6,7-dimethoxyquinazolin-4-yl)amino)piperidin-1-yl)(phenyl)methanone (11). Triethylamine (1.21 mmol, 6 eq.) and benzoyl chloride (0.23 mmol, 1.15 eq.) were added in sequence to a cooled solution of **2** (0.20 mmol, 1 eq.) in dry DCM (1.6 mL), and the resulting mixture was stirred at room temperature for 3.5 h. Upon conclusion of the reaction, the resulting mixture was poured

into water (10 mL) and extracted with DCM (4 × 10 mL). The organic phases were washed with saturated sodium bicarbonate solution (2 × 20 mL) and saturated sodium chloride solution (30 mL), dried over anhydrous sodium sulphate and concentrated under vacuum to furnish a crude residue that was purified by silica gel column chromatography by eluting with a mixture chloroform/methanol/ammonia 18:1:0.1 to afford the final compound **11**. Yield, 45%; mp 192-194 °C. ^{1}H-NMR (400 MHz; DMSO-d_6) δ 1.48-1.57 (br m, 2H, 2 × CH piperidine ring), 1.65-1.68 (m, 2H, NHCH$_2$CH_2CH$_2$N(CH$_3$)$_2$), 1.91 (br m, 1H, CH piperidine ring), 2.06-2.09 (br m, 1H, CH piperidine ring), 2.16 (s, 6H, N(CH_3)$_2$), 2.29 (t, J=7 Hz, 2H, NHCH$_2$CH$_2$CH_2N(CH$_3$)$_2$), 2.89 (br m, 1H, CH piperidine ring), 3.17 (br m, 1H, CH piperidine ring), 3.25-3.30 (m, 2H, NHCH_2CH$_2$CH$_2$N(CH$_3$)$_2$), 3.67 (m, 1H, CH piperidine ring), 3.80 (s, 3H, OCH_3), 3.81 (s, 3H, OCH_3), 4.38-4.41 (br m, 1H, CH piperidine ring), 4.55 (br m, 1H, C$_4$-H piperidine), 6.22 (br t, 1H, NHCH$_2$CH$_2$CH$_2$N(CH$_3$)$_2$), 6.68 (s, 1H, C$_8$-H quinazoline ring), 7.23-7.25 (br d, 1H, NH-piperidine), 7.40-7.42 (m, 3H, 2 x CH benzene ring and C$_5$-H quinazoline ring), 7.47-7.49 (m, 3H, CH benzene ring). ^{13}C-NMR (176 MHz; DMSO-d_6) δ 24.54, 31.11, 31.85, 42.43 (2C), 46.72, 49.38, 54.64 (2C), 56.53 (2C), 57.11, 98.72, 102.55, 105.52, 127.12 (2C), 129.01 (2C), 130.03, 135.86, 136.60, 147.05, 152.87, 155.71, 158.90, 169.58. MS (ESI) m/z: 493 [M + H]$^+$. HR-MS (ESI) m/z: calcd for C$_{27}$H$_{37}$N$_6$O$_3^+$ [M + H]$^+$, 493.2922; found, 493.2913 [M + H]$^+$.

General Procedure for the Synthesis of the Intermediates 33-35,39,41,42. The specific commercially available amine (2.89 mmol, 3 eq.) was added to a solution of the 2,4-dichloroquinazoline **31**[39] (0.96 mmol, 1 eq.) in dry THF (5.5 mL) in the presence of triethylamine (0.40 mL, 3 eq.), and the resulting suspension was left stirring at room temperature for about 24 h. Upon completion of the reaction, the salt was filtered under vacuum, and the

filtrate was concentrated in vacuo. The resulting crude product was triturated with petroleum ether, collected by filtration, and finally purified by silica gel column chromatography by eluting with the appropriate mixture chloroform/methanol to provide the intermediates **33-35,39,41,42**.

2-chloro-6,7-dimethoxy-N-(1-(naphthalen-1-ylmethyl)piperidin-4-yl)quinazolin-4-amine (33). Yield, 65%; mp 121-123 °C. ^{1}H-NMR (400 MHz; DMSO-d_6) δ 1.60-1.69 (m, 2H, 2 × C*H* piperidine ring), 1.86-1.90 (br d, 2H, 2 × C*H* piperidine ring), 2.18 (br t, 2H, 2 × C*H* piperidine ring), 2.95 (br d, 2H, 2 × C*H* piperidine ring), 3.87 (s, 3H, OC*H₃*), 3.88 (s, 3H, OC*H₃*), 3.92 (s, 2H, C*H₂*-naphthalene), 4.12-4.17 (br m, 1H, C$_4$-*H* piperidine), 7.06 (s, 1H, C$_8$-*H* quinazoline ring), 7.46 (m, 2H, C*H* naphthalene ring), 7.52-7.55 (m, 2H, C*H* naphthalene ring and N*H*), 7.61 (s, 1H, C$_5$-*H* quinazoline ring), 7.84-7.87 (m, 1H, C*H* naphthalene ring), 7.92-7.94 (m, 1H, C*H* naphthalene ring), 7.97-7.99 (d, 1H, C*H* naphthalene ring), 8.37 (d, 1H, C*H* naphthalene ring). MS (ESI) *m/z:* 463 [M + H]$^+$.

2-chloro-6,7-dimethoxy-N-(1-(naphthalen-2-ylmethyl)piperidin-4-yl)quinazolin-4-amine (34). Yield, 95%; mp 135-138 °C. ^{1}H-NMR (400 MHz; DMSO-d_6) δ 1.67-1.75 (m, 2H, 2 × C*H* piperidine ring), 1.92-1.94 (br d, 2H, 2 × C*H* piperidine ring), 2.13-2.34 (br t, 2H, 2 × C*H* piperidine ring), 2.94 (br d, 2H, 2 × C*H* piperidine ring), 3.70 (s, 2H, C*H₂*-naphthalene), 3.88 (s, 3H, OC*H₃*), 3.90 (s, 3H, OC*H₃*), 4.11-4.16 (br m, 1H, C$_4$-*H* piperidine), 7.06 (s, 1H, C$_8$-*H* quinazoline ring), 7.47-7.54 (m, 3H, C*H* naphthalene ring), 7.65 (s, 1H, C$_5$-*H* quinazoline ring), 7.82 (s, 1H, C*H* naphthalene ring), 7.88-7.91 (m, 3H, C*H* naphthalene ring), 8.01-8.03 (br d, 1H, N*H*). MS (ESI) *m/z:* 463 [M + H]$^+$.

N-(1-([1,1'-biphenyl]-4-ylmethyl)piperidin-4-yl)-2-chloro-6,7-dimethoxyquinazolin-4-amine (35). Yield, 89%; mp 181-183 °C. ^{1}H-NMR (400 MHz; DMSO-d_6) δ 1.66-1.74 (m, 2H, 2 × C*H* piperidine ring), 1.92-1.95 (br d, 2H, 2 × C*H* piperidine ring), 2.12-2.15 (br t, 2H, 2 × C*H*

piperidine ring), 2.94 (br d, 2H, 2 × C*H* piperidine ring), 3.57 (s, 2H, NC*H₂*-biphenyl ring), 3.88 (s, 3H, OC*H₃*), 3.90 (s, 3H, OC*H₃*), 4.13 (br m, 1H, C₄-*H* piperidine), 7.07 (s, 1H, C₈-*H* quinazoline ring), 7.36-7.41 (m, 1H, C*H* biphenyl ring), 7.43-7.47 (m, 4H, 3 × C*H* biphenyl ring and N*H*), 7.63-7.68 (m, 5H, 4 × C*H* biphenyl ring and C₅-*H* quinazoline ring), 8.03 (d, 1H, C*H* biphenyl ring). MS (ESI) *m/z:* 489 [M + H]⁺.

N-((1-benzylpiperidin-4-yl)methyl)-2-chloro-6,7-dimethoxyquinazolin-4-amine (**39**). Yield, 85%; mp 181-183 °C. ¹H-NMR (400 MHz; DMSO-*d₆*) δ 1.27-1.37 (m, 2H, 2 × C*H* piperidine ring), 1.71-1.73 (m, 3H, 2 × C*H* piperidine ring and C₄-*H* piperidine), 1.91-1.97 (br m, 2H, 2 × C*H* piperidine ring), 2.68-2.86 (br m, 2H, 2 × C*H* piperidine ring), 3.40 (s, 2H, NC*H₂*-Ph), 3.47-3.48 (m, 2H, NHC*H₂*-piperidine), 3.88 (s, 6H, 2 × OC*H₃*), 7.06 (s, 1H, C₈-*H* quinazoline ring), 7.28-7.32 (m, 5H, C*H* benzene ring)), 7.65 (s, 1H, C₅-*H* quinazoline ring), 8.37 (br t, 1H, N*H*CH₂-piperidine). MS (ESI) *m/z:* 427 [M + H]⁺.

N¹-(2-chloro-6,7-dimethoxyquinazolin-4-yl)-N³-phenylpropane-1,3-diamine (**41**). Yield, 89%; mp 137-139 °C. ¹H-NMR (400 MHz; CDCl₃) δ 2.02-2.10 (m, 2H, CH₂C*H₂*CH₂NHPh), 3.38 (t, *J*=6 Hz, 2H, CH₂CH₂C*H₂*NHPh), 3.75 (s, 3H, OC*H₃*), 3.83-3.87 (m, 2H, NHC*H₂*CH₂CH₂NHPh), 3.97 (s, 3H, OC*H₃*), 4.13-4.17 (br m, 1H, NHCH₂CH₂CH₂N*H*Ph), 6.58 (t, *J*=4 Hz, 1H, N*H*CH₂CH₂CH₂NHPh), 6.72 (s, 1H, C₈-*H* quinazoline ring), 6.76-6.80 (m, 3H, C*H* benzene ring), 7.13 (s, 1H, C₅-*H* quinazoline ring), 7.20-7.24 (m, 2H, C*H* benzene ring). MS (ESI) *m/z:* 373 [M + H]⁺.

N¹-(2-chloro-6,7-dimethoxyquinazolin-4-yl)-N²-(naphthalen-1-yl)ethane-1,2-diamine (**42**). Yield, 71%; mp 150-151 °C. ¹H-NMR (400 MHz; DMSO-*d₆*) δ 3.43-3.48 (m, 2H, NHCH₂C*H₂*NH-naphthalene), 3.68-3.75 (m, 2H, NHC*H₂*CH₂NH-naphthalene), 3.80 (s, 3H, OC*H₃*), 3.82 (s, 3H, OC*H₃*), 6.34 (t, *J*=7 Hz, 1H, NHCH₂CH₂N*H*-naphthalene), 6.80-6.83 (d, 1H,

C*H* naphthalene), 7.06-7.22 (d, 2H, C_8-*H* quinazoline ring and C*H* naphthalene), 7.22-7.31 (m, 3H, C*H* naphthalene), 7.53 (s, 1H, C_5-*H* quinazoline ring), 7.66-7.69 (dd, 1H, C*H* naphthalene ring), 8.03-8.06 (br d, 1H, C*H* naphthalene ring), 8.55 (t, *J*=7 Hz, 1H, N*H*-CH_2CH_2-NH-naphthalene). MS (ESI) *m/z:* 475 $[M + H]^+$.

4.2. Biochemistry.

4.2.1. LSD1-CoREST Binding and Inhibition Assays. Thermal stability, activity on histone H3K4me peptide, and inhibition of human LSD1-CoREST were measured using established protocols [43]. Fluorescence polarization experiments were performed on a CLARIOstar plate reader (BMG LABTECH) in a 384-well format using previously described protocols [75]. Direct binding of the histone H3 *N*-terminal tail peptide to LSD1-CoREST was assayed using protein samples (final concentration, 2 mM) with labeled peptides (constant at a final concentration of 1 nM) followed by serial 1:1 dilutions. For competitive experiments, each well contained LSD1-CoREST (constant at a final concentration of 60 nM) and labeled peptides (fixed at a final concentration of 1 nM) to which decreasing concentrations of the competing inhibitors were added. The shown values are average of 3 replicates ± SD.

4.2.2. G9a Inhibition.

The K_i values for each compound were measured using microfluidic capillary electrophoresis which allows to monitor the methylation status of peptide substrates [45, 52, 76]. Each reaction mixture (15 µL) was set up in 384-well polypropylene shallow microplates and consisted of: 5 µL of each compound dissolved in assay buffer (20 mM Tris-HCl (pH 8), 25 mM NaCl, 0.025%

Tween 20, 2 mM DTT) + 1% DMSO; 5 µL of histone H3 (1-21) peptide substrate in assay buffer; 5 µL of a solution containing G9a (12.5 nM) and SAM (50 µM) in assay buffer.

Each compound was titrated from 80 to 0.3125 µM while the H3 peptide was titrated from 100 to 1.5625 µM; in both cases a 2-fold dilution scheme was followed. A total of 4 grids for each assay time point were set up. The G9a/SAM solution was added to the mixture containing the compound and histone H3 peptide in order to initiate the reactions. Parallel reactions were set up and allowed to proceed for 15, 30, 45, and 60 min at 25°C, after which they were stopped by adding 10 µL of a solution containing Endo-LysC (40 pg/ml), to digest the remaining unmethylated peptide, and UNC0224 (10 µM), to immediately inhibit all further enzyme activity. After 1 h, peptide concentrations over 20 µM were diluted to 20 µM in reaction buffer to avoid saturation of the optics. The plate was read on a Caliper Life Sciences EZR II, using upstream voltage = -500 V, downstream voltage = -1200 V, and pressure = 1.5 psi. Predigested peptide was used as marker. The steady-state velocity was determined by plotting the amount of methylated peptide as a function of time and, applying linear regression, the observed velocities (V_{obs}) were calculated at each peptide concentration to determine Michaelis-Menten kinetics (K_m, k_{cat}) (GraphPad Prism 9.0). This process was repeated for each compound concentration to yield apparent K_m values which were plotted as a function of compound concentration. Linear regression analysis yielded the K_i [76]. The shown values are average of 3 replicates ± SD.

4.2.3. DOT1L, SETD8, EZH2 Complex and PRMT1 Assays. The appropriate methyltransferase substrate (0.05 mg/ml HeLa oligo nucleosomes for DOT1L, 0.05 mg/ml HeLa nucleosomes for SETD8, 0.05 mg/ml chicken core histone for EZH2 complex, and 5 µM chicken histone H4 for PRMT1) was added in freshly prepared reaction buffer (50 mM Tris-HCl (pH 8.5), 5 mM MgCl$_2$, 50 mM NaCl, 1 mM PMSF, 1 mM DTT, 1% DMSO). The MT enzyme was

delivered into the substrate solution and the mixture was mixed gently. Afterwards, the tested compounds dissolved in DMSO were delivered into the enzyme/substrate reaction mixture by using Acoustic Technology (Echo 550, LabCyte Inc. Sunnyvale, CA) in nanoliter range, and 1 μM ^{3}H-SAM was also added into the reaction mixture to initiate the reaction. The reaction mixture was incubated for 1 h at 30 °C and then it was delivered to filter-paper for detection. The data were analyzed using Excel and GraphPad Prism software for IC_{50} curve fits. The shown values are average of 3 replicates ± SD.

4.2.4. Inhibition of Human MAO-A and MAO-B Activity. The synthesized compounds were evaluated against human MAO isoforms by means of a fluorimetric method [77, 78] ($\lambda_{ex/em}$ = 530/585 nm) using the EnzyChromTM Monoamine Oxidase Assay Kit (BioAssay Systems), with the aid of multi detection microplate fluorescence reader (FLX80, Bio-Tek Instruments, Inc., Winooski, VT, USA). The synthesized compounds were assayed in the concentration range from 100 to 0.01 μM (standard solutions were prepared by 10-fold dilution in Assay Buffer) and compared with reference inhibitors: clorgyline (to inhibit MAO A) and pargyline (to inhibit MAO B). In the experimental conditions, MAO A/B catalyzed the oxidation of 1 mM of *p*-tyramine to *p*-hydroxyphenetylacetaldehyde. The results are expressed as *%* of enzymes inhibition.

 4.2.5. Structural Studies. LSD1-CoREST (*N*-terminally deleted Δ123LSD1 and residues 305-485 of CoREST1) crystals were prepared at 20 °C in 100 mM *N*-(2-acetamido)iminodiacetic acid (pH 6.5) and 1.2 M Na/K tartrate using the hanging-drop technique. Soaking was performed by incubating crystals with 0.8 to 5 mM compounds for 1 to 48 h at 20 °C; this was followed by washing in a reservoir solution supplemented with 20% glycerol for cryoprotection and immediate freezing in liquid nitrogen. X-ray diffraction data were collected at a wavelength of

1.000 Å on beamlines X06SA and X06DA at the Swiss Light Source (SLS; Villigen, Switzerland) and at a wavelength of 0.976 Å on beamline ID23EH1 at the European Synchrotron Radiation Facility (ESRF; Grenoble, France). Data processing and scaling were carried out using MOSFLM [79], XDS [80], and AIMLESS [81]. Structure refinement was performed using REFMAC5 [82]. Topologies for the inhibitors were obtained from the PRODRG server [83]. Final data collection and refinement statistics are shown in Table S2. Structural figures were prepared using PyMOL (The PyMOL Molecular Graphics System; Schrödinger LLC; www.pymol.org).

4.3. Cellular Assays.

4.3.1. THP1, MDA-MB231, AHH1 and HME Cell Proliferation Assays. Human commercially available acute monocytic leukemia THP1, breast cancer MDA-MB231, human B lymphocyte AHH1 and human mammary epithelial (HME) cell lines were maintained in RPMI 1640 (EUROCLONE, Milan, IT) medium contained 10% fetal bovine serum (FBS, HyClone, Thermoscientific, South Logan, UT), 2 mM L-glutamine and antibiotics in a humidified atmosphere with 5% CO_2 at 37 °C. For analysis of cell proliferation, cells were treated with 0.1% DMSO as control. After 24 h from seeding, exponentially growing cells were exposed to different drugs for 24-144 h. The inhibitory effect of different drugs was assessed by quantitation of metabolically active cells using CellTiter-Glo Luminescent (Promega, Fitchburg, Wisconsin, USA) for THP1, by MTT (Sigma, St. Louis, MO, USA) colorimetric assays for MDA-MB231, AHH1 and HME cells. The results are reported as "viability of drug-treated cells/viability of untreated cells" × 100 and represent the average ± SD of at least three independent experiments. IC_{50} values were calculated using GraphPad Prism 9.0 software (Biosoft).

4.3.2. MV4-11 Cell Proliferation Assay, Western Blot Analysis of H3K4me2 Levels, and CD86 Induction. RPMI culture media, L-glutamine, FBS and penicillin streptomycin mixture were obtained from EuroClone S.p.A. (Pero, IT). Trypan Blue was purchased from Sigma (St. Louis, US). CD86 primers (Sequence 5' -3', forward CAAGACGCGGCTTTTATCTT; reverse ATCCAAGGAATGTGGTCTGG) and Gfi1-B primers (Sequence 5' -3', forward TCTGGCCTCATGCCCTTA; reverse GGCACTGGTTTGGGAATAGA) were bought from Life Technologies Italia (Monza, IT). Direct-zol RNA MiniPrep was obtained from Zymo Research (Irvine, US). FAST SYBR Green Master Mix was purchased from Applied Biosystems by ThermoFisher (Waltham, US). Anti-H3K4me2 and anti-H3 antibodies were bought from AbCam (Cambridge, UK). Clarity Western ECL substrate was obtained from Biorad (Hercules, US).

4.3.3. Cell Growth Analysis. MV4-11 cells were grown in RPMI supplemented with 10% FBS, 2 mM L-glutamine and antibiotics, treated with increasing concentrations of the indicated compounds (0.2 - 1 - 2.5 µM), and incubated at 37 °C with 5% CO_2. The cells were counted (trypan blue) after 3 days and 6 days of treatment.

4.3.4. Transcriptional Analysis: Quantitative PCR. Total RNA was purified using Direct-zol RNA MiniPrep, quantified, and reverse transcribed. 10 ng of cDNA were used to perform quantitative PCR (qPCR) using FAST SYBR Green Master Mix. Gfi1-B and CD86 mRNA levels were normalized against rPPO mRNA.

4.3.5. Immunoblotting. MV4-11 cells were treated with increasing concentrations of the indicated compounds (**1**, **5**, **7-9**, **21**, **29**, **46**). Whole cell lysates were subjected to SDS-PAGE and then immunoblotted using antibodies against H3K4me2, and against H3 for equal loading.

4.3.6. RD and RH30 RMS and Human Derived Mesenchymal Stem Cells. Cell Culture and Reagents. RD (embryonal FN-RMS) and RH30 (PAX3-FOXO1 expressing alveolar FP-RMS) cell lines were obtained from the American Type Culture Collection (ATCC, Rockville, MD, USA). Human derived Mesenchymal stem cell (MSC) were purchased from Lonza (Walkersville, MD, USA, Cat: PT-2501). RD and RH30 cells were cultured in Dulbecco Modified Eagle Medium (DMEM) high-glucose (Invitrogen, Carlsbad, CA, USA) supplemented with 10% fetal bovine serum (FBS), 1% L-glutamine and 1% penicillin-streptomycin. MSC cells were cultured in Mesenchymal stem cell medium (MSCBM, Lonza, Cat: PT-3238) supplemented with mesenchymal cell growth supplement (MCGS, Lonza, Cat: PT-4105). They were cultured at 37 °C in a humidified atmosphere of 5% CO_2 95% air. All cell lines were routinely tested for Mycoplasma within one or two passages of each experiment.

4.3.7. Cell Proliferation Assay and Determination of the IC_{50} Values. RD and RH30 RMS cells were plated in triplicate on 384-well plates in DMEM high-glucose media containing 10% FBS. After 24 h treatment was added with increasing doses of selected inhibitors. Cells were plated to achieve 20% confluence at time of drug dosing and monitored each 24 h until control (DMSO) wells reached >95% confluence. IC_{50} values (shown as average of 3 replicates ± SD) were calculated for each time point using the GraphPad Prism 9.0. Proliferation rate of adherent cells was determined by quantifying percentage of cell confluence from phase contrast images taken every 24 h using the Celigo image cytometer (Nexcelom Bioscience, Lawrence, MA, USA). At selected time points, cells were stained using Calcein AM (1 mM final concentration, Nexcelom Bioscience, Lawrence, MA, USA) and Propidium Iodide (1 mg/mL final concentration, Sigma Aldrich, St Louis, MO, USA) to highlight live and remnant of dead cells,

respectively. Image capture and analysis were performed using Celigo image cytometer (Nexcelom Bioscience, Lawrence, MA, USA).

4.3.8. Determination of Caspase-3/7 Activity. RD and RH30 cells were seeded into 96-well, black, flat bottom plates at a concentration of 5000 cells per well. For evaluation of apoptosis effects, cells were treated in triplicates. After 24 h, the cells were treated with indicated compound. The measurement of caspase-3/7 has been determined using Caspase-Glo-3/7 (Promega Company, Madison, WI, USA), according to the manufacturer's protocol. The activity of caspase-3/7 was then examined using EnSpire Multimode Plate Reader (PerkinElmer, Waltham, MA, USA).

4.3.9. Western Blot Analysis. Western blotting was performed on whole-cell lysates by homogenizing cells in RIPA lysis buffer (50 mM Tris pH 7.4, 150 mM NaCl, 1% Triton X-100, 1 mM EDTA, 1% sodium deoxycholate, 0.1% SDS), containing the protease inhibitor cocktail (Sigma, St Louis, MO, USA), NaF 1 mM, Na_3VO_4 1mM and PMSF 1 mM. Lysates were incubated on ice for 30 min and centrifuged at 12,000g for 20 min at 4 °C. Supernatants were used as total lysates. Protein concentrations were estimated with the BCA protein assay (Pierce, Rockford, IL, USA), according to the manufacturer's protocol. The proteins (40 μg) were boiled in reducing SDS sample buffer (200 mM Tris–HCl pH 6.8, 40% glycerol, 20% β-mercaptoethanol, 4% sodium dodecyl sulfate, and bromophenol blue), and run on 8% SDS-polyacrylamide gels. Then, the proteins were transferred to Hybond ECL membranes (Amersham, GE HEALTHCARE BioScience Corporate, Piscataway, NJ, USA). Membranes were blocked in 5 % non-fat dried milk in Tris-buffered saline (TBS) for 1 h and incubated overnight with the appropriate primary antibody at 4 °C. After incubation, membranes were washed in TBS and incubated with the appropriate secondary antibody for 1 h at room

temperature. Detection was performed by Pierce ECL Western Blotting Substrate (Thermo Fisher Scientific, Waltham, MA, USA). Antibody against H3K4me2 (Cat. #07-030) was purchased from Millipore (Burlington, MA, USA). Membranes were stripped (ReBlot Plus Mild Antibody Stripping Solution, Millipore, Burlington, MA, USA) and reprobed using antibody against total histone H3 (#4499, Cell Signaling Technology, Danvers, MA, USA) as loading control. Images of blots were acquired through the iBright FL1500 Imaging System (Thermo Fisher Scientific, Waltham, MA, USA).

Accession Codes. Structure factors and coordinates of the LSD1-CoREST complex with **7** were deposited with the Protein Data Bank (PDB, www.rcsb.org/pdb/) under accession code 6TUY. The authors will release the atomic coordinates and experimental data upon article publication.

AUTHOR INFORMATION

Corresponding Authors

*For A.M.: phone, +39 06 49913392; fax, +39 06 49693268; E-mail, antonello.mai@uniroma1.it.

**For D.R.: phone, +39 06 49913237; E-mail, dante.rotili@uniroma1.it.

ORCID

Antonello Mai: 0000-0001-9176-2382

Dante Rotili: 0000-0002-8428-8763

Notes

The authors declare no competing financial interest.

Author Contributions

The manuscript was written through contributions of all authors. All authors have given approval to the final version of the manuscript.

[1]M. Menna and F. Fiorentino contributed equally to this work.

ABBREVIATIONS

AML, acute myeloid leukemia; APL, acute promyelocytic leukemia; CoREST, REST co-repressor 1; DOT1L, Disruptor of telomeric silencing 1-like; DMEM, Dulbecco's modified Eagle's medium; DNMT, DNA methyltransferase; EZH2, Enhancer of zeste homolog 2; FN-RMS, Fusion-negative rhabdomyosarcoma; FBS, Fetal bovine serum; FP-RMS, Fusion-positive rhabdomyosarcoma; GLP, G9a-like protein; HDAC, Histone deacetylase; HME, Human mammary epithelial; HMT, histone methyltransferase; K_D, dissociation constant; KDM, Lysine demethylase; KMT, Lysine methyltransferase; LSD1, Lysine specific demethylase 1; MSC, Mesenchymal stem cell; MSCBM, Mesenchymal stem cell basal medium; MCGS, Mesenchymal cell growth supplement; MTT, 3-(4,5-dimethylthiazol-2-yl)-2,5-diphenyltetrazolium

bromide;PRMT1, Protein arginine methyltransferase 1; RMS, Rhabdomyosarcoma; RTK, Receptor tyrosine kinase; SAH, S-(5'-adenosyl)-L-homocysteine; SAM, S-(5'-adenosyl)-L-methionine; SETD8, SET domain containing (lysine methyltransferase) 8; TBS, Tris-buffered saline; TCP, Tranylcypromine; TNBC, triple negative breast cancer; WB, Western blot;

REFERENCES

[1] K.P. Bhat, H. Umit Kaniskan, J. Jin, O. Gozani, Epigenetics and beyond: targeting writers of protein lysine methylation to treat disease, Nat Rev Drug Discov, (2021).

[2] J. Sterling, S.V. Menezes, R.H. Abbassi, L. Munoz, Histone lysine demethylases and their functions in cancer, Int J Cancer, (2020).

[3] D. Rotili, A. Mai, Targeting Histone Demethylases: A New Avenue for the Fight against Cancer, Genes Cancer, 2 (2011) 663-679.

[4] B. Perillo, A. Tramontano, A. Pezone, A. Migliaccio, LSD1: more than demethylation of histone lysine residues, Exp Mol Med, 52 (2020) 1936-1947.

[5] P. Karakaidos, J. Verigos, A. Magklara, LSD1/KDM1A, a Gate-Keeper of Cancer Stemness and a Promising Therapeutic Target, Cancers (Basel), 11 (2019).

[6] S. Zhang, M. Liu, Y. Yao, B. Yu, H. Liu, Targeting LSD1 for acute myeloid leukemia (AML) treatment, Pharmacol Res, (2020) 105335.

[7] M. Zhou, P.P. Venkata, S. Viswanadhapalli, B. Palacios, S. Alejo, Y. Chen, Y. He, U.P. Pratap, J. Liu, Y. Zou, Z. Lai, T. Suzuki, A.J. Brenner, R.R. Tekmal, R.K. Vadlamudi, G.R. Sareddy, KDM1A inhibition is effective in reducing stemness and treating triple negative breast cancer, Breast Cancer Res Treat, (2020).

[8] T. Etani, T. Naiki, A. Naiki-Ito, T. Suzuki, K. Iida, S. Nozaki, H. Kato, Y. Nagayasu, S. Suzuki, N. Kawai, T. Yasui, S. Takahashi, NCL1, A Highly Selective Lysine-Specific Demethylase 1 Inhibitor, Suppresses Castration-Resistant Prostate Cancer Growth via Regulation of Apoptosis and Autophagy, J Clin Med, 8 (2019).

[9] Y. Jin, D. Ma, T. Gramyk, C. Guo, R. Fang, H. Ji, Y.G. Shi, Kdm1a promotes SCLC progression by transcriptionally silencing the tumor suppressor Rest, Biochem Biophys Res Commun, 515 (2019) 214-221.

[10] S. Ambrosio, C.D. Sacca, S. Amente, S. Paladino, L. Lania, B. Majello, Lysine-specific demethylase LSD1 regulates autophagy in neuroblastoma through SESN2-dependent pathway, Oncogene, 36 (2017) 6701-6711.

[11] C.P. Bailey, M. Figueroa, A. Gangadharan, Y. Yang, M.M. Romero, B.A. Kennis, S. Yadavilli, V. Henry, T. Collier, M. Monje, D.A. Lee, L. Wang, J. Nazarian, V. Gopalakrishnan, W. Zaky, O.J. Becher, J. Chandra, Pharmacologic inhibition of lysine-specific demethylase 1 as a therapeutic and immune-sensitization strategy in pediatric high-grade glioma, Neuro Oncol, 22 (2020) 1302-1314.

[12] C. Lee, V.A. Rudneva, S. Erkek, M. Zapatka, L.Q. Chau, S.K. Tacheva-Grigorova, A. Garancher, J.M. Rusert, O. Aksoy, R. Lea, H.P. Mohammad, J. Wang, W.A. Weiss, H.L. Grimes, S.M. Pfister, P.A. Northcott, R.J. Wechsler-Reya, Lsd1 as a therapeutic target in Gfi1-activated medulloblastoma, Nat Commun, 10 (2019) 332.

[13] I.M. Bennani-Baiti, I. Machado, A. Llombart-Bosch, H. Kovar, Lysine-specific demethylase 1 (LSD1/KDM1A/AOF2/BHC110) is expressed and is an epigenetic drug target in chondrosarcoma, Ewing's sarcoma, osteosarcoma, and rhabdomyosarcoma, Hum Pathol, 43 (2012) 1300-1307.

[14] G.J. Yang, P.M. Lei, S.Y. Wong, D.L. Ma, C.H. Leung, Pharmacological Inhibition of LSD1 for Cancer Treatment, Molecules, 23 (2018).

[15] X.J. Dai, Y. Liu, X.P. Xiong, L.P. Xue, Y.C. Zheng, H.M. Liu, Tranylcypromine Based Lysine-Specific Demethylase 1 Inhibitor: Summary and Perspective, Journal of medicinal chemistry, 63 (2020) 14197-14215.

[16] D.P. Mould, A.E. McGonagle, D.H. Wiseman, E.L. Williams, A.M. Jordan, Reversible inhibitors of LSD1 as therapeutic agents in acute myeloid leukemia: clinical significance and progress to date, Med Res Rev, 35 (2015) 586-618.

[17] G. Stazi, C. Zwergel, S. Valente, A. Mai, LSD1 inhibitors: a patent review (2010-2015), Expert Opin Ther Pat, 26 (2016) 565-580.

[18] C. Binda, S. Valente, M. Romanenghi, S. Pilotto, R. Cirilli, A. Karytinos, G. Ciossani, O.A. Botrugno, F. Forneris, M. Tardugno, D.E. Edmondson, S. Minucci, A. Mattevi, A. Mai, Biochemical, structural, and biological evaluation of tranylcypromine derivatives as inhibitors of histone demethylases LSD1 and LSD2, J Am Chem Soc, 132 (2010) 6827-6833.

[19] S. Valente, V. Rodriguez, C. Mercurio, P. Vianello, B. Saponara, R. Cirilli, G. Ciossani, D. Labella, B. Marrocco, D. Monaldi, G. Ruoppolo, M. Tilset, O.A. Botrugno, P. Dessanti, S. Minucci, A. Mattevi, M. Varasi, A. Mai, Pure enantiomers of benzoylamino-tranylcypromine:

LSD1 inhibition, gene modulation in human leukemia cells and effects on clonogenic potential of murine promyelocytic blasts, Eur J Med Chem, 94 (2015) 163-174.

[20] S. Valente, V. Rodriguez, C. Mercurio, P. Vianello, B. Saponara, R. Cirilli, G. Ciossani, D. Labella, B. Marrocco, G. Ruoppolo, O.A. Botrugno, P. Dessanti, S. Minucci, A. Mattevi, M. Varasi, A. Mai, Pure Diastereomers of a Tranylcypromine-Based LSD1 Inhibitor: Enzyme Selectivity and In-Cell Studies, ACS Med Chem Lett, 6 (2015) 173-177.

[21] V. Rodriguez, S. Valente, S. Rovida, D. Rotili, G. Stazi, A. Lucidi, G. Ciossani, A. Mattevi, O.A. Botrugno, P. Dessanti, C. Mercurio, P. Vianello, S. Minucci, M. Varasi, A. Mai, Pyrrole- and indole-containing tranylcypromine derivatives as novel lysine-specific demethylase 1 inhibitors active on cancer cells, Medchemcomm, 6 (2015) 665-670.

[22] P. Vianello, O.A. Botrugno, A. Cappa, G. Ciossani, P. Dessanti, A. Mai, A. Mattevi, G. Meroni, S. Minucci, F. Thaler, M. Tortorici, P. Trifiro, S. Valente, M. Villa, M. Varasi, C. Mercurio, Synthesis, biological activity and mechanistic insights of 1-substituted cyclopropylamine derivatives: a novel class of irreversible inhibitors of histone demethylase KDM1A, Eur J Med Chem, 86 (2014) 352-363.

[23] P. Vianello, O.A. Botrugno, A. Cappa, R. Dal Zuffo, P. Dessanti, A. Mai, B. Marrocco, A. Mattevi, G. Meroni, S. Minucci, G. Stazi, F. Thaler, P. Trifiro, S. Valente, M. Villa, M. Varasi, C. Mercurio, Discovery of a Novel Inhibitor of Histone Lysine-Specific Demethylase 1A (KDM1A/LSD1) as Orally Active Antitumor Agent, J Med Chem, 59 (2016) 1501-1517.

[24] D. Rotili, S. Tomassi, M. Conte, R. Benedetti, M. Tortorici, G. Ciossani, S. Valente, B. Marrocco, D. Labella, E. Novellino, A. Mattevi, L. Altucci, A. Tumber, C. Yapp, O.N. King, R.J. Hopkinson, A. Kawamura, C.J. Schofield, A. Mai, Pan-histone demethylase inhibitors simultaneously targeting Jumonji C and lysine-specific demethylases display high anticancer activities, Journal of medicinal chemistry, 57 (2014) 42-55.

[25] J.H. Kalin, M. Wu, A.V. Gomez, Y. Song, J. Das, D. Hayward, N. Adejola, M. Wu, I. Panova, H.J. Chung, E. Kim, H.J. Roberts, J.M. Roberts, P. Prusevich, J.R. Jeliazkov, S.S. Roy Burman, L. Fairall, C. Milano, A. Eroglu, C.M. Proby, A.T. Dinkova-Kostova, W.W. Hancock, J.J. Gray, J.E. Bradner, S. Valente, A. Mai, N.M. Anders, M.A. Rudek, Y. Hu, B. Ryu, J.W.R. Schwabe, A. Mattevi, R.M. Alani, P.A. Cole, Targeting the CoREST complex with dual histone deacetylase and demethylase inhibitors, Nat Commun, 9 (2018) 53.

[26] O. Salamero, P. Montesinos, C. Willekens, J.A. Perez-Simon, A. Pigneux, C. Recher, R. Popat, C. Carpio, C. Molinero, C. Mascaro, J. Vila, M.I. Arevalo, T. Maes, C. Buesa, F. Bosch, T.C.P. Somervaille, First-in-Human Phase I Study of Iadademstat (ORY-1001): A First-in-Class Lysine-Specific Histone Demethylase 1A Inhibitor, in Relapsed or Refractory Acute Myeloid Leukemia, J Clin Oncol, 38 (2020) 4260-4273.

[27] K. Pettit, A.T. Gerds, A. Yacoub, J.M. Watts, M. Tartaczuch, T.J. Bradley, J. Shortt, W.S. Stevenson, N.J. Curtin, J.M. Rossetti, K. Burbury, G. Natsoulis, A. Jones, M. Talpaz, J. Peppe,

D.M. Ross, H.Y. Rienhoff, Jr., A Phase 2a Study of the LSD1 Inhibitor Img-7289 (bomedemstat) for the Treatment of Myelofibrosis, Blood, 134 (2019) 556-556.

[28] G. Johnston, H.E. Ramsey, Q. Liu, J. Wang, K.R. Stengel, S. Sampathi, P. Acharya, M. Arrate, M.C. Stubbs, T. Burn, M.R. Savona, S.W. Hiebert, Nascent transcript and single-cell RNA-seq analysis defines the mechanism of action of the LSD1 inhibitor INCB059872 in myeloid leukemia, Gene, 752 (2020) 144758.

[29] H. Mohammad, K. Smitheman, G. van Aller, M. Cusan, S. Kamat, Y. Liu, N. Johnson, C. Hann, S. Armstrong, R. Kruger, 212 Novel anti-tumor activity of targeted LSD1 inhibition by GSK2879552, European Journal of Cancer, 50 (2014) 72.

[30] R. Soldi, T. Ghosh Halder, A. Weston, T. Thode, K. Drenner, R. Lewis, M.R. Kaadige, S. Srivastava, S. Daniel Ampanattu, R. Rodriguez Del Villar, J. Lang, H. Vankayalapati, B. Weissman, J.M. Trent, W.P.D. Hendricks, S. Sharma, The novel reversible LSD1 inhibitor SP-2577 promotes anti-tumor immunity in SWItch/Sucrose-NonFermentable (SWI/SNF) complex mutated ovarian cancer, PLoS One, 15 (2020) e0235705.

[31] A. Hollebecque, S. Salvagni, R. Plummer, N. Isambert, P. Niccoli, J. Capdevila, G. Curigliano, V. Moreno, P. Martin-Romano, E. Baudin, M. Arias, S. Mora, J. de Alvaro, J. Di Martino, J.L. Parra-Palau, T. Sanchez-Perez, I. Aronchik, E.H. Filvaroff, M. Lamba, Z. Nikolova, J.S. de Bono, Phase I Study of Lysine-Specific Demethylase 1 Inhibitor, CC-90011, in Patients with Advanced Solid Tumors and Relapsed/Refractory Non-Hodgkin Lymphoma, Clin Cancer Res, 27 (2021) 438-446.

[32] N. Sacilotto, P. Dessanti, M.M.P. Lufino, A. Ortega, A. Rodríguez-Gimeno, J. Salas, T. Maes, C. Buesa, C. Mascaró, R. Soliva, Comprehensive in Vitro Characterization of the LSD1 Small Molecule Inhibitor Class in Oncology, ACS Pharmacol Transl Sci, 4 (2021) 1818-1834.

[33] T. Maes, C. Mascaró, I. Tirapu, A. Estiarte, F. Ciceri, S. Lunardi, N. Guibourt, A. Perdones, M.M.P. Lufino, T.C.P. Somervaille, D.H. Wiseman, C. Duy, A. Melnick, C. Willekens, A. Ortega, M. Martinell, N. Valls, G. Kurz, M. Fyfe, J.C. Castro-Palomino, C. Buesa, ORY-1001, a Potent and Selective Covalent KDM1A Inhibitor, for the Treatment of Acute Leukemia, Cancer Cell, 33 (2018) 495-511.e412.

[34] V. Sorna, E.R. Theisen, B. Stephens, S.L. Warner, D.J. Bearss, H. Vankayalapati, S. Sharma, High-throughput virtual screening identifies novel N'-(1-phenylethylidene)-benzohydrazides as potent, specific, and reversible LSD1 inhibitors, Journal of medicinal chemistry, 56 (2013) 9496-9508.

[35] J. Chen, B. Levant, C. Jiang, T.M. Keck, A.H. Newman, S. Wang, Tranylcypromine substituted cis-hydroxycyclobutylnaphthamides as potent and selective dopamine D_3 receptor antagonists, Journal of medicinal chemistry, 57 (2014) 4962-4968.

[36] Y. Chang, T. Ganesh, J.R. Horton, A. Spannhoff, J. Liu, A. Sun, X. Zhang, M.T. Bedford, Y. Shinkai, J.P. Snyder, X. Cheng, Adding a lysine mimic in the design of potent inhibitors of histone lysine methyltransferases, J Mol Biol, 400 (2010) 1-7.

[37] V. Speranzini, D. Rotili, G. Ciossani, S. Pilotto, B. Marrocco, M. Forgione, A. Lucidi, F. Forneris, P. Mehdipour, S. Velankar, A. Mai, A. Mattevi, Polymyxins and quinazolines are LSD1/KDM1A inhibitors with unusual structural features, Sci Adv, 2 (2016) e1601017.

[38] J.T. Lynch, M.J. Cockerill, J.R. Hitchin, D.H. Wiseman, T.C. Somervaille, CD86 expression as a surrogate cellular biomarker for pharmacological inhibition of the histone demethylase lysine-specific demethylase 1, Anal Biochem, 442 (2013) 104-106.

[39] A. Bouchut, D. Rotili, C. Pierrot, S. Valente, S. Lafitte, J. Schultz, U. Hoglund, R. Mazzone, A. Lucidi, G. Fabrizi, D. Pechalrieu, P.B. Arimondo, T.S. Skinner-Adams, M.J. Chua, K.T. Andrews, A. Mai, J. Khalife, Identification of novel quinazoline derivatives as potent antiplasmodial agents, European journal of medicinal chemistry, 161 (2019) 277-291.

[40] F. Liu, X. Chen, A. Allali-Hassani, A.M. Quinn, G.A. Wasney, A. Dong, D. Barsyte, I. Kozieradzki, G. Senisterra, I. Chau, A. Siarheyeva, D.B. Kireev, A. Jadhav, J.M. Herold, S.V. Frye, C.H. Arrowsmith, P.J. Brown, A. Simeonov, M. Vedadi, J. Jin, Discovery of a 2,4-diamino-7-aminoalkoxyquinazoline as a potent and selective inhibitor of histone lysine methyltransferase G9a, J Med Chem, 52 (2009) 7950-7953.

[41] S. Sundriyal, N.A. Malmquist, J. Caron, S. Blundell, F. Liu, X. Chen, N. Srimongkolpithak, J. Jin, S.A. Charman, A. Scherf, M.J. Fuchter, Development of diaminoquinazoline histone lysine methyltransferase inhibitors as potent blood-stage antimalarial compounds, ChemMedChem, 9 (2014) 2360-2373.

[42] S. Sundriyal, P.B. Chen, A.S. Lubin, G.A. Lueg, F. Li, A.J.P. White, N.A. Malmquist, M. Vedadi, A. Scherf, M.J. Fuchter, Histone lysine methyltransferase structure activity relationships that allow for segregation of G9a inhibition and anti-Plasmodium activity, Medchemcomm, 8 (2017) 1069-1092.

[43] F. Forneris, R. Orru, D. Bonivento, L.R. Chiarelli, A. Mattevi, ThermoFAD, a Thermofluor-adapted flavin ad hoc detection system for protein folding and ligand binding, FEBS J, 276 (2009) 2833-2840.

[44] J.R. Hitchin, J. Blagg, R. Burke, S. Burns, M.J. Cockerill, E.E. Fairweather, C. Hutton, A.M. Jordan, C. McAndrew, A. Mirza, D. Mould, G.J. Thomson, I. Waddell, D.J. Ogilvie, Development and evaluation of selective, reversible LSD1 inhibitors derived from fragments, Medchemcomm, 4 (2013) 1513-1522.

[45] M. Vedadi, D. Barsyte-Lovejoy, F. Liu, S. Rival-Gervier, A. Allali-Hassani, V. Labrie, T.J. Wigle, P.A. Dimaggio, G.A. Wasney, A. Siarheyeva, A. Dong, W. Tempel, S.C. Wang, X. Chen, I. Chau, T.J. Mangano, X.P. Huang, C.D. Simpson, S.G. Pattenden, J.L. Norris, D.B. Kireev, A. Tripathy, A. Edwards, B.L. Roth, W.P. Janzen, B.A. Garcia, A. Petronis, J. Ellis, P.J. Brown,

S.V. Frye, C.H. Arrowsmith, J. Jin, A chemical probe selectively inhibits G9a and GLP methyltransferase activity in cells, Nat Chem Biol, 7 (2011) 566-574.

[46] G. Blum, G. Ibanez, X. Rao, D. Shum, C. Radu, H. Djaballah, J.C. Rice, M. Luo, Small-molecule inhibitors of SETD8 with cellular activity, ACS Chem Biol, 9 (2014) 2471-2478.

[47] S.X. Skapek, A. Ferrari, A.A. Gupta, P.J. Lupo, E. Butler, J. Shipley, F.G. Barr, D.S. Hawkins, Rhabdomyosarcoma, Nat Rev Dis Primers, 5 (2019) 1.

[48] S. Rodriguez-Perales, A. Martinez-Ramirez, S.A. de Andres, L. Valle, M. Urioste, J. Benitez, J.C. Cigudosa, Molecular cytogenetic characterization of rhabdomyosarcoma cell lines, Cancer Genet Cytogenet, 148 (2004) 35-43.

[49] M. Cassandri, S. Pomella, A. Rossetti, F. Petragnano, L. Milazzo, F. Vulcano, S. Camero, S. Codenotti, F. Cicchetti, R. Maggio, C. Festuccia, G.L. Gravina, A. Fanzani, F. Megiorni, M. Catanoso, C. Marchese, V. Tombolini, F. Locatelli, R. Rota, F. Marampon, MS-275 (Entinostat) Promotes Radio-Sensitivity in PAX3-FOXO1 Rhabdomyosarcoma Cells, Int J Mol Sci, 22 (2021).

[50] S. Kubicek, R.J. O'Sullivan, E.M. August, E.R. Hickey, Q. Zhang, M.L. Teodoro, S. Rea, K. Mechtler, J.A. Kowalski, C.A. Homon, T.A. Kelly, T. Jenuwein, Reversal of H3K9me2 by a small-molecule inhibitor for the G9a histone methyltransferase, Mol Cell, 25 (2007) 473-481.

[51] F. Liu, D. Barsyte-Lovejoy, A. Allali-Hassani, Y. He, J.M. Herold, X. Chen, C.M. Yates, S.V. Frye, P.J. Brown, J. Huang, M. Vedadi, C.H. Arrowsmith, J. Jin, Optimization of cellular activity of G9a inhibitors 7-aminoalkoxy-quinazolines, Journal of medicinal chemistry, 54 (2011) 6139-6150.

[52] F. Liu, X. Chen, A. Allali-Hassani, A.M. Quinn, T.J. Wigle, G.A. Wasney, A. Dong, G. Senisterra, I. Chau, A. Siarheyeva, J.L. Norris, D.B. Kireev, A. Jadhav, J.M. Herold, W.P. Janzen, C.H. Arrowsmith, S.V. Frye, P.J. Brown, A. Simeonov, M. Vedadi, J. Jin, Protein lysine methyltransferase G9a inhibitors: design, synthesis, and structure activity relationships of 2,4-diamino-7-aminoalkoxy-quinazolines, Journal of medicinal chemistry, 53 (2010) 5844-5857.

[53] Y. Xiong, F. Li, N. Babault, A. Dong, H. Zeng, H. Wu, X. Chen, C.H. Arrowsmith, P.J. Brown, J. Liu, M. Vedadi, J. Jin, Discovery of Potent and Selective Inhibitors for G9a-Like Protein (GLP) Lysine Methyltransferase, J Med Chem, 60 (2017) 1876-1891.

[54] A. Ma, W. Yu, F. Li, R.M. Bleich, J.M. Herold, K.V. Butler, J.L. Norris, V. Korboukh, A. Tripathy, W.P. Janzen, C.H. Arrowsmith, S.V. Frye, M. Vedadi, P.J. Brown, J. Jin, Discovery of a selective, substrate-competitive inhibitor of the lysine methyltransferase SETD8, J Med Chem, 57 (2014) 6822-6833.

[55] K.V. Butler, A. Ma, W. Yu, F. Li, W. Tempel, N. Babault, F. Pittella-Silva, J. Shao, J. Wang, M. Luo, M. Vedadi, P.J. Brown, C.H. Arrowsmith, J. Jin, Structure-Based Design of a

Covalent Inhibitor of the SET Domain-Containing Protein 8 (SETD8) Lysine Methyltransferase, J Med Chem, 59 (2016) 9881-9889.

[56] C. Scheufler, H. Mobitz, C. Gaul, C. Ragot, C. Be, C. Fernandez, K.S. Beyer, R. Tiedt, F. Stauffer, Optimization of a Fragment-Based Screening Hit toward Potent DOT1L Inhibitors Interacting in an Induced Binding Pocket, ACS Med Chem Lett, 7 (2016) 730-734.

[57] A.K. Upadhyay, D. Rotili, J.W. Han, R. Hu, Y. Chang, D. Labella, X. Zhang, Y.S. Yoon, A. Mai, X. Cheng, An analog of BIX-01294 selectively inhibits a family of histone H3 lysine 9 Jumonji demethylases, J Mol Biol, 416 (2012) 319-327.

[58] L. Halby, Y. Menon, E. Rilova, D. Pechalrieu, V. Masson, C. Faux, M.A. Bouhlel, M.H. David-Cordonnier, N. Novosad, Y. Aussagues, A. Samson, L. Lacroix, F. Ausseil, L. Fleury, D. Guianvarc'h, C. Ferroud, P.B. Arimondo, Rational Design of Bisubstrate-Type Analogues as Inhibitors of DNA Methyltransferases in Cancer Cells, J Med Chem, 60 (2017) 4665-4679.

[59] D. Rotili, D. Tarantino, B. Marrocco, C. Gros, V. Masson, V. Poughon, F. Ausseil, Y. Chang, D. Labella, S. Cosconati, S. Di Maro, E. Novellino, M. Schnekenburger, C. Grandjenette, C. Bouvy, M. Diederich, X. Cheng, P.B. Arimondo, A. Mai, Properly substituted analogues of BIX-01294 lose inhibition of G9a histone methyltransferase and gain selective anti-DNA methyltransferase 3A activity, PLoS One, 9 (2014) e96941.

[60] Z. Lin, K.S. Bishop, H. Sutherland, G. Marlow, P. Murray, W.A. Denny, L.R. Ferguson, A quinazoline-based HDAC inhibitor affects gene expression pathways involved in cholesterol biosynthesis and mevalonate in prostate cancer cells, Mol Biosyst, 12 (2016) 839-849.

[61] Z. Lin, P.M. Murray, Y. Ding, W.A. Denny, L.R. Ferguson, Quinazolines as novel anti-inflammatory histone deacetylase inhibitors, Mutat Res, 690 (2010) 81-88.

[62] Z. Yang, T. Wang, F. Wang, T. Niu, Z. Liu, X. Chen, C. Long, M. Tang, D. Cao, X. Wang, W. Xiang, Y. Yi, L. Ma, J. You, L. Chen, Discovery of Selective Histone Deacetylase 6 Inhibitors Using the Quinazoline as the Cap for the Treatment of Cancer, J Med Chem, 59 (2016) 1455-1470.

[63] C.W. Yu, P.T. Chang, L.W. Hsin, J.W. Chern, Quinazolin-4-one derivatives as selective histone deacetylase-6 inhibitors for the treatment of Alzheimer's disease, J Med Chem, 56 (2013) 6775-6791.

[64] C.W. Yu, P.Y. Hung, H.T. Yang, Y.H. Ho, H.Y. Lai, Y.S. Cheng, J.W. Chern, Quinazolin-2,4-dione-Based Hydroxamic Acids as Selective Histone Deacetylase-6 Inhibitors for Treatment of Non-Small Cell Lung Cancer, J Med Chem, 62 (2019) 857-874.

[65] T. Noguchi-Yachide, BET Bromodomain as a Target of Epigenetic Therapy, Chem Pharm Bull (Tokyo), 64 (2016) 540-547.

[66] S. Picaud, D. Da Costa, A. Thanasopoulou, P. Filippakopoulos, P.V. Fish, M. Philpott, O. Fedorov, P. Brennan, M.E. Bunnage, D.R. Owen, J.E. Bradner, P. Taniere, B. O'Sullivan, S. Muller, J. Schwaller, T. Stankovic, S. Knapp, PFI-1, a highly selective protein interaction inhibitor, targeting BET Bromodomains, Cancer Res, 73 (2013) 3336-3346.

[67] S. Picaud, C. Wells, I. Felletar, D. Brotherton, S. Martin, P. Savitsky, B. Diez-Dacal, M. Philpott, C. Bountra, H. Lingard, O. Fedorov, S. Muller, P.E. Brennan, S. Knapp, P. Filippakopoulos, RVX-208, an inhibitor of BET transcriptional regulators with selectivity for the second bromodomain, Proc Natl Acad Sci U S A, 110 (2013) 19754-19759.

[68] D. Robaa, T. Wagner, C. Luise, L. Carlino, J. McMillan, R. Flaig, R. Schule, M. Jung, W. Sippl, Identification and Structure-Activity Relationship Studies of Small-Molecule Inhibitors of the Methyllysine Reader Protein Spindlin1, ChemMedChem, 11 (2016) 2327-2338.

[69] E. Curry, I. Green, N. Chapman-Rothe, E. Shamsaei, S. Kandil, F.L. Cherblanc, L. Payne, E. Bell, T. Ganesh, N. Srimongkolpithak, J. Caron, F. Li, A.G. Uren, J.P. Snyder, M. Vedadi, M.J. Fuchter, R. Brown, Dual EZH2 and EHMT2 histone methyltransferase inhibition increases biological efficacy in breast cancer cells, Clin Epigenetics, 7 (2015) 84.

[70] E. San Jose-Eneriz, X. Agirre, O. Rabal, A. Vilas-Zornoza, J.A. Sanchez-Arias, E. Miranda, A. Ugarte, S. Roa, B. Paiva, A. Estella-Hermoso de Mendoza, R.M. Alvarez, N. Casares, V. Segura, J.I. Martin-Subero, F.X. Ogi, P. Soule, C.M. Santiveri, R. Campos-Olivas, G. Castellano, M.G.F. de Barrena, J.R. Rodriguez-Madoz, M.J. Garcia-Barchino, J.J. Lasarte, M.A. Avila, J.A. Martinez-Climent, J. Oyarzabal, F. Prosper, Discovery of first-in-class reversible dual small molecule inhibitors against G9a and DNMTs in hematological malignancies, Nat Commun, 8 (2017) 15424.

[71] O. Rabal, E. San Jose-Eneriz, X. Agirre, J.A. Sanchez-Arias, A. Vilas-Zornoza, A. Ugarte, I. de Miguel, E. Miranda, L. Garate, M. Fraga, P. Santamarina, R. Fernandez Perez, R. Ordonez, E. Saez, S. Roa, M.J. Garcia-Barchino, J.A. Martinez-Climent, Y. Liu, W. Wu, M. Xu, F. Prosper, J. Oyarzabal, Discovery of Reversible DNA Methyltransferase and Lysine Methyltransferase G9a Inhibitors with Antitumoral in Vivo Efficacy, J Med Chem, 61 (2018) 6518-6545.

[72] O. Rabal, J.A. Sanchez-Arias, E. San Jose-Eneriz, X. Agirre, I. de Miguel, L. Garate, E. Miranda, E. Saez, S. Roa, J.A. Martinez-Climent, Y. Liu, W. Wu, M. Xu, F. Prosper, J. Oyarzabal, Detailed Exploration around 4-Aminoquinolines Chemical Space to Navigate the Lysine Methyltransferase G9a and DNA Methyltransferase Biological Spaces, J Med Chem, 61 (2018) 6546-6573.

[73] L. Zang, S.M. Kondengaden, Q. Zhang, X. Li, D.K. Sigalapalli, S.M. Kondengadan, K. Huang, K.K. Li, S. Li, Z. Xiao, L. Wen, H. Zhu, B.N. Babu, L. Wang, F. Che, P.G. Wang, Structure based design, synthesis and activity studies of small hybrid molecules as HDAC and G9a dual inhibitors, Oncotarget, 8 (2017) 63187-63207.

[74] M.E. Ourailidou, A. Lenoci, C. Zwergel, D. Rotili, A. Mai, F.J. Dekker, Towards the development of activity-based probes for detection of lysine-specific demethylase-1 activity, Bioorg Med Chem, 25 (2017) 847-856.

[75] S. Pilotto, V. Speranzini, M. Tortorici, D. Durand, A. Fish, S. Valente, F. Forneris, A. Mai, T.K. Sixma, P. Vachette, A. Mattevi, Interplay among nucleosomal DNA, histone tails, and corepressor CoREST underlies LSD1-mediated H3 demethylation, Proc Natl Acad Sci U S A, 112 (2015) 2752-2757.

[76] T.J. Wigle, L.M. Provencher, J.L. Norris, J. Jin, P.J. Brown, S.V. Frye, W.P. Janzen, Accessing protein methyltransferase and demethylase enzymology using microfluidic capillary electrophoresis, Chem Biol, 17 (2010) 695-704.

[77] O. Suzuki, E. Noguchi, K. Yagi, A simple fluorometric assay for type B monoamine oxidase activity in rat tissues, J Biochem, 79 (1976) 1297-1299.

[78] M. Mladenović, A. Patsilinakos, A. Pirolli, M. Sabatino, R. Ragno, Understanding the Molecular Determinant of Reversible Human Monoamine Oxidase B Inhibitors Containing 2H-Chromen-2-One Core: Structure-Based and Ligand-Based Derived Three-Dimensional Quantitative Structure-Activity Relationships Predictive Models, J Chem Inf Model, 57 (2017) 787-814.

[79] A.G. Leslie, Integration of macromolecular diffraction data, Acta Crystallogr D Biol Crystallogr, 55 (1999) 1696-1702.

[80] W. Kabsch, Xds, Acta Crystallogr D Biol Crystallogr, 66 (2010) 125-132.

[81] N. Collaborative Computational Project, The CCP4 suite: programs for protein crystallography, Acta Crystallogr D Biol Crystallogr, 50 (1994) 760-763.

[82] G.N. Murshudov, A.A. Vagin, E.J. Dodson, Refinement of macromolecular structures by the maximum-likelihood method, Acta Crystallogr D Biol Crystallogr, 53 (1997) 240-255.

[83] A.W. Schuttelkopf, D.M. van Aalten, PRODRG: a tool for high-throughput crystallography of protein-ligand complexes, Acta Crystallogr D Biol Crystallogr, 60 (2004) 1355-1363.
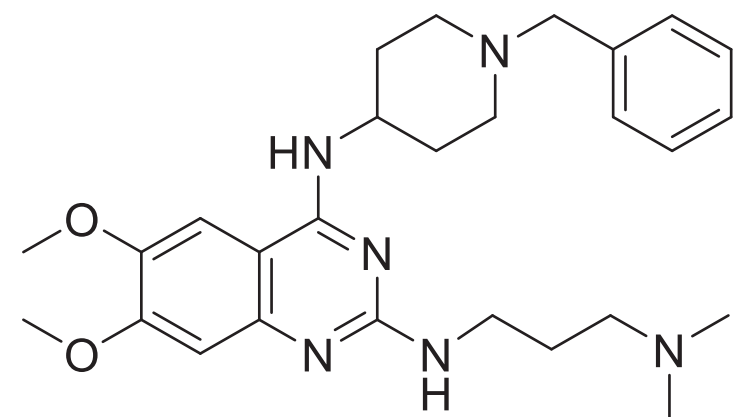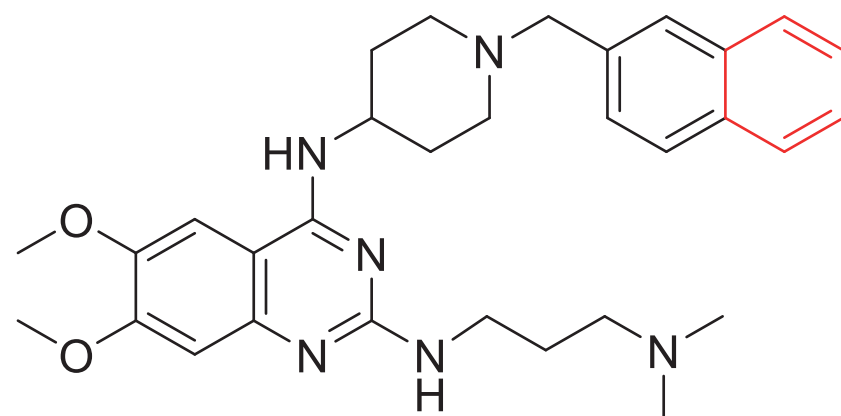
1
Dual LSD1/G9a inhibitor

LSD1 K_i = 0.44 μM
G9a K_i = 0.68 μM

Med Chem Optimization
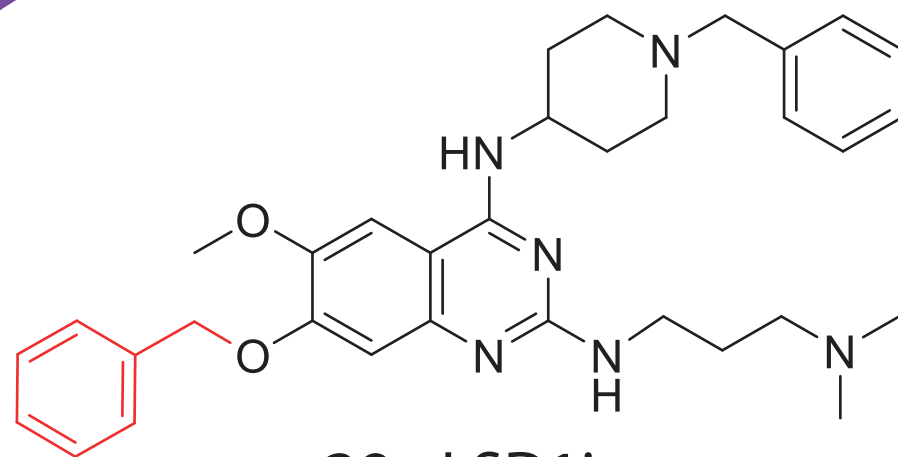
7 - LSD1i
LSD1 K_i = 0.16 μM
G9a K_i = 2.93 μM

29 - LSD1i
LSD1 K_i = 0.11 μM
G9a K_i = 39.4 μM

↑ Antiproliferative activity **vs**

Acute Myeloid Leukemia
Breast Cancer
Rhabdomyosarcoma